

Newcastle
University

The Influence of Intercellular Connections on Beta Cell Function

Thesis submitted in fulfilment of the requirements for the Degree of Doctor of
Philosophy

Deborah Cornell

Institute of Cellular Medicine

Faculty of Medical Sciences

Newcastle University

2020

Abstract

Background

Pancreatic beta cells cultured in 2D systems display similar characteristics to dysfunctional beta cells of patients with diabetes. This thesis explores the impact of cell connectivity on functional and metabolic characteristics of insulin secreting beta cells.

Methods

The MIN6 mouse beta cell line was cultured as 2D monolayers and 3D structures named pseudoislets. The insulin secretion response and metabolic function of 2D and 3D MIN6 cultures, along with islets from human donors were compared. Roles for cell-cell interactions in regulating metabolic changes were explored with focus on the gap junctional protein, connexin36, using an inducible knockdown MIN6 cell line.

Results

MIN6 pseudoislets displayed improved functional responses compared to monolayers with 7.4-fold and 1.5-fold increases in glucose-induced insulin secretion respectively. XFe24 Seahorse bioanalyser data showed the improved glucose-stimulated pseudoislet response was fuelled by large increases in glycolytic flux and a more moderate increase in oxidative phosphorylation. Basal insulin secretion and basal oxidative phosphorylation were both higher in monolayers but there were no differences in basal glycolysis. Human islets displayed a similar phenotype to pseudoislets with high contributions of glycolysis to glucose-induced ATP production. Pseudoislets indicated some hypoxia through trends towards increased lactate dehydrogenase and phosphoinositide-dependent kinase-1 expression and increased glycolytic activity of phosphofruktokinase-1 and glyceraldehyde 3-phosphate

dehydrogenase but superior glucose sensing through decreased hexokinase I and increased GLUT2 expression and more active mitochondrial activities of pyruvate carboxylase, citrate synthase, α -ketoglutarate dehydrogenase, and malate dehydrogenase. Knockdown of connexin36 did not alter glucose-stimulated insulin secretion or metabolic flux. However, there was a trend towards increased basal insulin secretion and basal oxidative phosphorylation indicating a possible role for this connection in regulating basal metabolic flux.

Conclusions

The improved glucose-stimulated secretion conferred by pseudoislet configuration was accompanied by an increase in ATP production suggesting a role for alteration in metabolic flux in the improved functionality. Improved functional responses of beta cells in 3D structures was accompanied by a small increase in oxidative phosphorylation but a large increase in glycolysis that cannot be fully explained by hypoxia. Connexin36 may play a role in regulating the basal response but other connections are involved in regulating the glucose-stimulated response.

Declaration

I declare that no portion of the work compiled in this thesis has been submitted in support of any other degree or qualification at Newcastle University or any other University or institute of learning. The work has been carried out by myself unless otherwise stated. All sources of information have been acknowledged by means of reference.

Published Abstracts

Understanding the Mechanisms Involved in the Improved Insulin Secretory Response of Pseudoislets.

Poster presentation, Diabetes UK conference, 2017

Presentations

Understanding the Role of Cell Connectivity in Preserving the Pancreatic Beta Cell Phenotype

User presentation, Agilent Seahorse Seminar and Workshop, 2017

Paper in Preparation

Improved glucose sensitivity of MIN6 pseudoislets is dependent on upregulation of glycolytic flux.

Cornell D, Miwa S, Honkanen-Scott M, Shaw JAM, Arden C.

Target journal: Diabetologia

Acknowledgements

This thesis would not have been possible without the support of my supervisor, Dr Catherine Arden. She has provided a great deal of guidance and encouragement to me, which I will never forget. I must also thank Professor Lorraine Agius for her wealth of knowledge. Also, to the members of their lab groups, Dr Francesco Zummo, Dr Tabassum Moonira, Dr Brian Ford, Dr Shruti Chachra, and Dr Ahmed Alshawi for the assistance they've provided around the lab, as well as being friendly faces and a pleasure to work with.

Thank you to the donors and their families for making the difficult decision to donate organs for the purpose of research. Also, to Dr Minna Honkanen-Scott for her dedication to ensuring maximum research potential from each organ, her care taken in isolating the islets, and her long hours of hard work.

I am grateful to Dr Satomi Miwa for all her advice and guidance on the use of the Seahorse bionalyser, and her friendship through difficult times.

Thank you to my family. To my parents who raised me with the determination and ambition needed to complete this PhD. I'd like to give special thanks to my siblings who have always been on the other end of the phone to support me, and to Heather for correcting my clumsy prose. To Nana and my grandparents for all their support, and to my Auntie Margaret who sent me care packages.

To my loving partner, soon to be Dr Thomas Werner. You have been incredible in your unwavering belief and optimism. I could not have completed this without your emotional and practical support. And to his family for all the good times and food they've provided throughout my write up period.

I gratefully acknowledge the funding received towards my PhD from the Medical Research Council (MRC). My secondary supervisor, Professor James Shaw, and all other lab members who have been happy to share reagents and advice.

CONTENTS

Chapter 1. Introduction.....	17
1.1. Regulation of Blood Glucose	17
1.2. Islet Architecture.....	17
1.3. Diabetes Mellitus	18
1.3.1. Type 1 Diabetes.....	18
1.3.2. Type 2 Diabetes.....	19
1.3.3. Complications Associated with Diabetes	20
1.4. Current Treatments for T1DM	20
1.4.1. Exogenous Insulin.....	20
1.3.2. Islet Transplantation	21
1.3.3. Islet Isolation	22
1.3.4. Limitations of Islet Transplantation	23
1.5. Pancreatic B-cell Physiology.....	24
1.5.1. Regulation of Insulin Secretion	24
1.5.2. Metabolic Phenotype	26
1.6. Cell Connectivity.....	33
1.6.1. Cell Connectivity is Essential for GSIS.....	33
1.6.2. Pseudoislet Culture	34
1.6.3. Cell-Cell Interactions	36
1.7. Hypothesis.....	39
1.8. Aims.....	40
Chapter 2. Methods	41
2.1. Reagents.....	41
2.2. Cell Culture	41
2.2.1. MIN6.....	41
2.2.2. Human Islets.....	42
2.3. Generation of Stable Inducible MIN6 Cx36 Knockdown Cell Line.....	43
2.3.1. Lentiviral Promotor Selection.....	43
2.3.2. Transduction of Lentiviral Particles.....	43
2.3.3. Maintenance of Stable Cell Line.....	44
2.4. Islet Equivalent Counts.....	44
2.5. Propidium Iodide Viability Staining.....	45
2.6. Enzyme Activity Assays.....	45
2.6.1. Glycolytic Enzyme Activity Assays	46

i	Hexokinase/GlucoKinase	46
ii	Phosphoglucoisomerase	47
iii	Phosphofructokinase.....	47
iv	Aldolase	48
v	Glyceraldehyde 3-phosphate dehydrogenase (GAPDH)	48
vi	Pyruvate Kinase	49
vii	Lactate Dehydrogenase.....	49
2.6.2.	Mitochondrial Enzyme Activity Assays.....	50
viii	Pyruvate Carboxylase	50
ix	Citrate Synthase	50
x	Isocitrate Dehydrogenase (NADP linked).....	50
xi	α -ketoglutarate Dehydrogenase	51
xii	Malate Dehydrogenase	51
2.7.	Western Blotting	51
2.8.	Glucose Stimulated Insulin Secretion Enzyme-Linked Immunosorbent Assay (GSIS ELISA) 52	
2.9.	Protein Quantification using the Bradford Method.....	53
2.10.	Metabolic Analysis	53
2.10.1.	Seahorse XFe96 Analyser	53
2.10.2.	Seahorse XFe24 Analyser	54
2.11.	RT-PCR.....	55
2.12.	Statistical Analysis	56
Chapter 3.	Optimisation of Pseudoislet Formation	57
3.1.	Introduction	57
3.2.	Aims.....	58
Objectives.....		58
3.3.	Selection of optimal surface for MIN6 pseudoislet formation	60
3.4.	Selection of seeding density for optimal pseudoislet diameter	61
3.5.	Comparison of static or stirred suspension culture methods for Pseudoislet formation	65
3.6.	Impact of pseudoislet formation on insulin secretion	68
3.6.1.	Optimisation of GSIS measurements for Pseudoislets.....	68
3.6.2.	Effect of Seeding Density on Insulin Secretion.....	69
3.6.3.	Effect of cell passage on insulin secretion	71
3.6.4.	comparing glucose induced insulin secretion in 2D vs 3D Structures.....	73
3.7.	Conclusion	75
3.7.1.	Pseudoislet Formation	75
3.7.2.	Passage Number Influences Insulin Secretion	76

3.7.3. Pseudoislet Formation Appears to Improve Insulin Secretion Response	77
Chapter 4. Analysis of Metabolic Function in 2D Vs 3D Structures	79
4.1. Introduction	79
4.1.2. Aims.....	81
Objectives.....	81
4.2. XFe96 Bioanalyser Optimisation	84
4.2.1. Selection of oligomycin and FCCP concentrations for seahorse analyser	84
4.2.2. OCR and ECAR Measurements of 2D vs 3D Structures	88
4.3. Seahorse XFe24 analyser optimisation	94
4.4. Comparison of Metabolic Function for monolayer and pseudoislet MIN6	98
4.4.1. OCR Measurements	98
4.4.2. ECAR Measurements.....	100
4.4.3. Contribution of oxidative phosphorylation and glycolysis to ATP Production in MIN6 monolayers and pseudoislets.....	102
4.5. Analysis of Metabolic Function in Human Islets Stimulated by Glucose or Pyruvate....	104
4.6. Contribution of oxidative phosphorylation and glycolysis to ATP Production in Human Islets	107
4.7. Conclusion	110
4.7.1. Seahorse Bioanalyser Optimisation	110
4.7.2. Total ATP Production in Response to Glucose is Greater in 3D Structures.....	112
4.7.3. Increased Basal ATP Production in 2D Beta Cells is caused by an Increase in Oxidative Phosphorylation	113
4.7.4. Pancreatic Beta Cells Display Improved ATP Production Responsiveness When Cultured as 3D Structures due to Increased Glycolysis.....	114
4.7.5. Beta Cells in 2D Structures Show Some Response to Pyruvate Stimulation.....	116
Chapter 5. Comparison of beta cell Metabolic Activity in 2D Vs 3D Structures	117
5.1. Introduction	117
5.2. Aims.....	119
5.3. Comparison of Glycolytic Enzyme Activities in 3D vs 2D Structures.....	120
5.4. Comparison of Mitochondrial Enzyme Activities in 2D vs 3D Structures.....	123
5.5. Assessment of Hypoxia in Monolayer Vs Pseudoislets	125
5.6. Investigation into increased Basal ATP Production in 2D structures	126
5.7. UK5099 Inhibition.....	129
5.8. MCT1 Inhibition.....	132
5.9. Conclusion	133
5.9.1. Increased Glycolytic Contribution in Pseudoislets	133
5.9.2. Increased Basal Insulin Secretion	135

5.9.3. MPC inhibition.....	135
Chapter 6. Influence of Cx36 Knockdown on beta cell function.....	137
6.1. Introduction	137
6.2. Aims.....	139
6.3. MIN6 cell Connexin 36 Knockdown model Development.....	139
6.3.1. Optimisation of Transduction Conditions	141
6.3.2. Selection of optimal Promotor for MIN6 Transduction	142
6.3.3. Analysis of Doxycycline induced Connexin 36 knockdown in transduced MIN6	143
6.4. Influence of Connexin 36 Knockdown on the Insulin Secretion Response of MIN6 Pseudoislets.....	145
6.5. Influence of Connexin 36 Knockdown on ATP Production.....	146
6.6. Conclusion	151
6.6.1. Development of Cx36 Knockdown Model.....	151
6.6.2. Increased functional activity at Basal Glucose in Cx36 Knockdown	152
6.6.3. Reduced Insulin Secretion Response in Cx36 Knockdown.....	153
Chapter 7. Final Discussions.....	155
7.1. Effects of 3D structure on beta cell function	155
7.1.1. Improved Function of Beta Cells in 3D Structures	155
7.1.2. Beta Cell Response to Pyruvate	156
7.1.3. Possible Amino Acid Stimulated ATP Production.....	157
7.1.4. Role of Cx36 in the Metabolic Phenotype of the 3D Structure.....	158
7.1.5. Comparison of Function with Human Islets	159
7.2. In vitro Limitations	160
7.2.1. Possible Hypoxia in 3D structures	160
7.2.2. Influence of Passage number on Results	161
7.3. Long Term Significance of findings.....	161
7.4. Future Directions.....	162
7.4.1. Short term	162
7.4.2. Long term	162
8. References.....	164

List of Figures

Figure 1. Diagram showing the architecture of rodent and primate islets [4].	18
Figure 2. Image depicting process of islet isolation and transplantation from donor to recipients' hepatic portal vein [29]	21
Figure 3. Rate of insulin independence after islet infusion as reported by the Collaborative Islet Transplantation Registry. Image taken from [35]	22
Figure 4. B-cell insulin secretion mechanism in response to glucose stimulus [42]	25
Figure 5. Schematic showing the steps involved in glycolysis leading to the generation of pyruvate from glucose [50]	27
Figure 6. Schematics showing enzymes and intermediates involved in the TCA cycle taken from [30]	28
Figure 7. Diagram showing G3P shuttle and electron transfer chain. [59]	31
Figure 8. Diagram showing malate/aspartate shuttle [58]	31
Figure 9. EphA-Ephrin-A bidirectional signalling between two β -cells [89]	37
Figure 10 – Pseudoislet preparation methods described in current literature	58
Figure 11. Images of Monolayer and Pseudoislet Formation on Various Surfaces	61
Figure 12 - IEQ counts of MIN6 cultured for 5 days in low attachment petri dishes at three different densities. N=1	63
Figure 13. Viability Images of Pseudoislets	63
Figure 14 – Image Processing using Cell Profiler	64
Figure 15. Seeding Density influence on Pseudoislet Viability	65
Figure 16 - IEQ counts of MIN6 cultured for five days in either stirred suspension (stirred) or in low attachment petri dishes (static). N=1	66
Figure 17. Pseudoislet Viability Images of Static Vs Stirred Culture	67
Figure 18. Pseudoislet Viability in Static Vs Stirred Culture Methods	67
Figure 19. Initial GSIS Measurements	68
Figure 20. Optimising Glucose Concentration for GSIS.	69
Figure 21. Optimisation of Seeding Density for GSIS	70
Figure 22. MIN6 Monolayer Insulin Secretion at High and Low Passage	72
Figure 23. Monolayer Basal Insulin Increase with Passage Number	72
Figure 24. MIN6 Pseudoislet Insulin Secretion at High and Low Passage	73
Figure 25. GSIS Response in Monolayer Vs Pseudoislet MIN6	74
Figure 26. Seahorse Bioanalyser Parameters [94]	83
Figure 27. ECAR Response to Oligomycin Titrations	85
Figure 28. ECAR Increase After Oligomycin Injections	86
Figure 29. OCR Response to FCCP Titrations	87
Figure 30. OCR Increase after FCCP Injections	87
Figure 31. Monolayer OCR Response in XFe96 Analyser	89
Figure 32. Monolayer ECAR Response in XFe96 Analyser	90
Figure 33. Pseudoislet OCR Response in XFe96 Analyser	92
Figure 34. Pseudoislet ECAR Response in XFe96 Analyser	93
Figure 35. Light Microscope Image of Pseudoislets in Islet Capture Plate	94

Figure 36. Monolayer Density and FCCP Optimisation	95
Figure 37. Pseudoislet Seahorse Plating Optimisation.....	96
Figure 38. MIN6 Monolayer and Pseudoislet Response to Oligomycin	97
Figure 39. OCR of Monolayer MIN6	99
Figure 40. OCR of Pseudoislet MIN6	100
Figure 41. ECAR of Monolayer MIN6.....	101
Figure 42. ECAR of Pseudoislet MIN6.....	101
Figure 43. Total ATP Production in Monolayers and Pseudoislets.....	103
Figure 44. ATP Production from Oxidative Phosphorylation in Monolayers and Pseudoislets.....	103
Figure 45. ATP Production from Glycolysis in Monolayers and Pseudoislets	104
Figure 46. OCR of Human Islets	106
Figure 47. ECAR of Human Islets	107
Figure 48. Total ATP Production in Human Islets	108
Figure 49. ATP Production from Oxidative Phosphorylation in Human Islets	109
Figure 50. ATP Production from Glycolysis in Human Islets	110
Figure 51. Phosphoglucokinase Isomerase Activity in Monolayers and Pseudoislets .	120
Figure 52. Phosphofruktokinase 1 Activity in Monolayers and Pseudoislets.....	121
Figure 53. Aldolase Activity in Monolayer and Pseudoislets.....	121
Figure 54. GAPDH Activity in Monolayers and Pseudoislets	121
Figure 55. Pyruvate Kinase Activity in Monolayers and Pseudoislets.....	122
Figure 56. Lactate Dehydrogenase Activity in Monolayers and Pseudoislets.....	122
Figure 57. Pyruvate Carboxylase Activity in Monolayers and Pseudoislets	123
Figure 58. Citrate Synthase Activity in Monolayers and Pseudoislets	124
Figure 59. Isocitrate Dehydrogenase Activity in Monolayers and Pseudoislets	124
Figure 60. α -Ketoglutarate Dehydrogenase Activity in Monolayers and Pseudoislets	124
Figure 61. Malate Dehydrogenase Activity in Monolayers and Pseudoislets	125
Figure 62. PCR Analysis of Hypoxic Markers in Monolayers and Pseudoislets	126
Figure 63. Western Blot Analysis of GLUT2 Expression.....	127
Figure 64. Hexokinase Expression in Monolayers and Pseudoislets.....	128
Figure 65. Glucokinase Expression in Monolayers and Pseudoislets.....	128
Figure 66. Western Blot Analysis of Hexokinase I Expression in Monolayers and Pseudoislets.....	129
Figure 67. Monolayer OCR Reduction with UK5099	130
Figure 68. Pseudoislet OCR Reduction with UK5099	131
Figure 69.OCR Reduction with UK5099	131
Figure 70. Western Blot Analysis of MCT1 Expression.....	132
Figure 71. SMARTvector Inducible Lentiviral shRNA Vector	140
Figure 72. Plate Format for Transduction Optimisation	142
Figure 73. Fluorescence Microscopy Images of SMARTchoice Promotoers	143
Figure 74. Western Blot Analysis of Cx36 KD	144
Figure 75. GSIS of MIN6 Pseudoislets with Cx36 KD	145
Figure 76. OCR of Pseudoislets with Cx36 KD	147
Figure 77. ECAR of Pseudoislets with Cx36 KD	148
Figure 78. ATP Production in Pseudoislets with Cx36 KD.....	149

Figure 79. ATP Production from Oxidative Phosphorylation in Pseudoislets with Cx36KD	150
Figure 80. ATP Production from Glycolysis in Pseudoislets with Cx36 KD	151

List of Tables

Table 1. Metabolic phenotype for optimal insulin secretion	29
Table 2. Islet Donor Information	43
Table 3. SMARTvector shRNA Lentiviral Constructs.....	43
Table 4. Primer Sequences for RT-PCR	56
Table 5. Pseudoislet Production Methods	59
Table 6. shRNA Construct Elements	140

List of Acronyms and Abbreviations

2-DG	2-deoxy-D-glucose
Acyl CoA	Acetyl Coenzyme A
ADP	Adenosine di-phosphate
α-KG	α -ketoglutarate
AMPK	Adenosine monophosphate activated protein kinase
APS	Ammonium persulfate
ATP	Adenosine triphosphate
CAM	Cell adhesion molecule
CCK	Cholecystokinin
CITR	Collaborative islet transplant registry
CMRL	Connaught Medical Research Laboratories
Cx36	Connexin 36
DBD	Donor after brain death
DCD	Donor after cardiac death
DMEM	Dulbecco's modified eagle medium
DTT	Dithiothreitol
ECAR	Extracellular acidification rate
EDTA	Ethylenediamine tetraacetic acid
EIHI	Exercise induced hyperinsulinemic hypoglycaemia
ELISA	Enzyme-linked immunosorbent assay
FAD	Flavin adenine dinucleotide
FBS	Foetal bovine serum
FCCP	Trifluoromethoxy)phenylhydrazone
FRAP	Fluorescence recovery after photobleaching
G3P	Glycerol-3-phosphate
GA	18-a-glycyrrhetic acid
GAPDH	Glyceraldehyde 3-phosphate dehydrogenase

GDH	Glutamate dehydrogenase
GFP	Green fluorescence protein
GIP	Glucose dependent insulinotropic poly peptide
GJD2	Gap junction delta 2
GLP1	Glucagon like peptide-1
GLUT1/2	Glucose transporter 1/2
GSIS	Glucose stimulated insulin secretion
HIF	Hypoxia inducible factors
ICD	Isocitrate dehydrogenase
IEQ	Islet equivalent count
INS-1	Rat insulinoma cell line
KD	Knockdown
LDH	Lactate dehydrogenase
MCT	Monocarboxylate transporter
MDH	Malate dehydrogenase
MIN6	Mouse insulinoma cell line
MOI	Multiplicity of infections
MPC	Mitochondrial pyruvate carrier
NADP	Nicotinamide adenine dinucleotide phosphate
OCR	Oxygen consumption rate
PBS	Phosphate buffered saline
PC	Pyruvate carboxylase
PDK1	Phosphoinositide-dependent kinase-1
PEG	Polyethylene glycol
PEP	Phospho(enol)pyruvic acid
PFK	Phosphofructokinase
PGI	Phosphoglucoisomerase
PI	Propidium iodide
PK	Pyruvate kinase
PYY	Peptide yy

mRNA	Messenger ribonucleic acid
RT-PCR	Reverse transcription polymer chain reaction
shRNA	Short hairpin ribonucleic acid
SUR1	Sulfonylurea receptor
T1DM	Type 1 diabetes mellitus
T2DM	Type 2 diabetes mellitus
TCA	Tricarboxylic acid
TPP	Thiamine Pyrophosphate

CHAPTER 1. INTRODUCTION

1.1. Regulation of Blood Glucose

Blood glucose levels are maintained within strict boundaries between 4mmol/l and 7.8mmol/l to maintain blood glucose homeostasis and avoid detrimental effects of hyperglycaemia. Islets of Langerhans are essential for blood glucose homeostasis, these are regions of endocrine tissue contained within the pancreas. Cells within these islets monitor glucose levels and respond to low and high glucose by synthesising and releasing glucagon and insulin [1]. Following a rise in blood glucose, such as after a meal, insulin released by beta cells binds to receptors on cells of insulin sensitive tissues to initiate three key responses that counteract the rise of glucose. Uptake of glucose into muscle, fat and liver cells is increased; storage of glucose as glycogen in the liver through glycogenesis is upregulated; and the production of glucose through gluconeogenesis is inhibited. When blood glucose levels begin to drop due to exercise or lack of food, glucagon triggers the conversion of glycogen back to glucose and the production of glucose through gluconeogenesis restoring the homeostatic balance. The ability of beta cells to regulate blood glucose via insulin can be compromised; the conditions where this occurs are collectively termed diabetes mellitus [2].

1.2. Islet Architecture

Islets of Langerhans consist of three main cell types, insulin producing beta cells, glucagon producing alpha cells, and somatostatin producing delta cells. Due to the high availability, relatively low costs, and ease of genetic selection, rodent islets are often used experimentally to further understanding of islet biology and further develop therapeutic options for patients with diabetes [3]. Figure 1 shows the structures of rodent and primate islets. Both consist mostly of beta cells along with alpha cells, delta cells and blood vessels that provide the islet with oxygen and metabolic cues [4]. The beta cells of rodent islets are located mostly in the core and surrounded by alpha and delta cells, while primate islets have a more heterogeneous distribution of cell types. A

small proportion of the islet, <5%, is made up of cells not pictured in figure 1. These include pancreatic polypeptide producing PP cells and ghrelin producing epsilon cells and are randomly distributed throughout primate islets and found mostly around the beta cell core of rodent islets [5]. The primate islet contains a lower proportion of beta cells than the rodent islet, 65% compared to 80% respectively. Despite some differences in the islet architecture, both rodent and primate islets display a robust insulin secretion response stimulated through similar metabolic pathways meaning rodent islets are often used in islet studies [6-16].

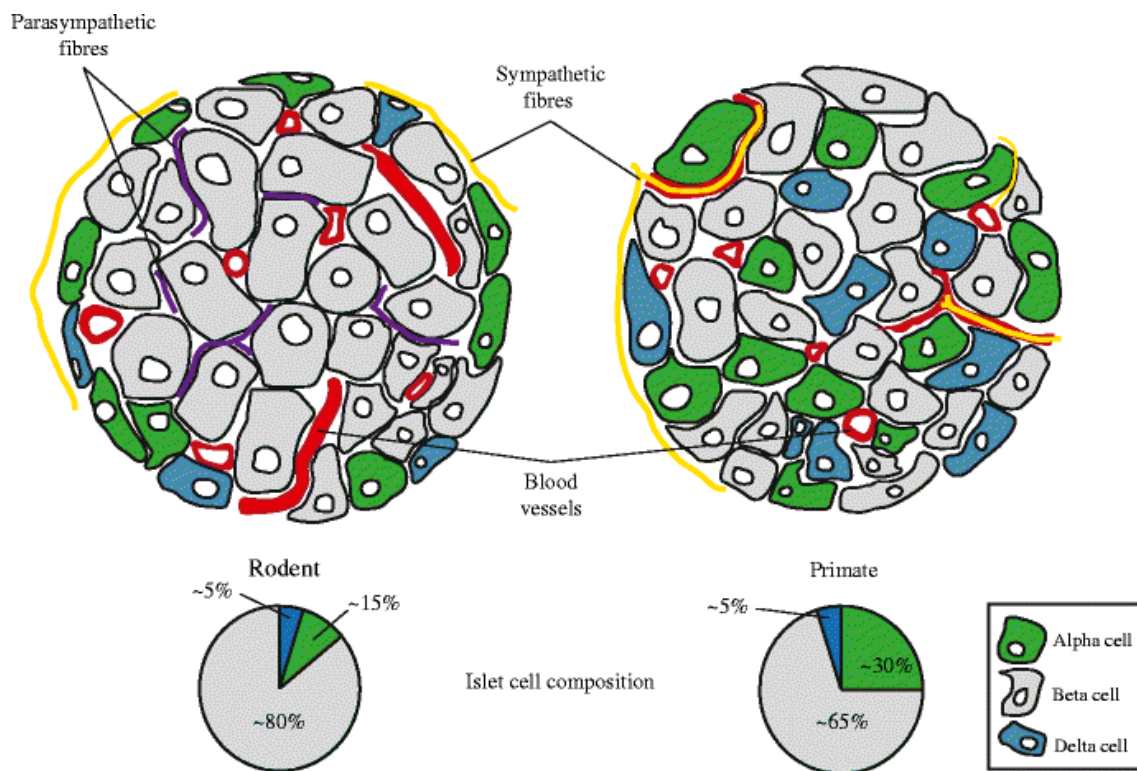


Figure 1. Diagram showing the architecture of rodent and primate islets [4].

1.3. Diabetes Mellitus

1.3.1. Type 1 Diabetes

Type 1 diabetes mellitus (T1DM) accounts for 5-10% of people diagnosed with diabetes. It is a chronic disease characterised by autoimmune destruction of insulin-producing beta cells, leading to absolute insulin deficiency [17]. The cause is the combination of a genetic predisposition and one or more environmental triggers, which are currently

poorly defined but are thought to include viral infections, stress and diet [18]. Presentation of the disease typically occurs between the ages of 5 and 7 years although it can present later in life and the onset can be variable, often slower in adults [19]. Symptoms develop over several weeks or days and typically begin at 90-95% β -cell loss. They can range from severe hyperglycaemia and ketoacidosis, to excessive thirst, urination, tiredness and weight loss [17].

1.3.2. Type 2 Diabetes

As opposed to T1DM, patients with Type 2 diabetes mellitus (T2DM) do not suffer from absolute insulin deficiency, but experience a relative insulin decrease as well as peripheral insulin resistance [20]. There are five stages in the progression of beta cell dysfunction towards T2DM described by Weir in 2004 [21]. First is compensation where the rate of insulin secretion increases to compensate for increasing insulin resistance. The second is stable adaptation characterised by fasting blood glucose levels between 5.0 and 7.3mmol/l, blood glucose levels in this stage can be maintained at these levels for years with the right diet and exercise regimen. Beta cells in stage two display impeded GSIS. Stage three is known as unstable early decompensation, this is a relatively short phase in which beta cells reach a critical stage due to loss of beta cell mass and/or increases in insulin resistance leading in a rapid increase in blood glucose levels until they stabilise in stage four at \sim 16–20mmol/l. Patients in stage four, stable decompensation, retain enough insulin secretion to avoid diabetic ketoacidosis and will often remain in this stage for the remainder of their lives. Patients reaching stage five, severe decompensation, are reliant on exogenous insulin to maintain blood glucose levels but it is rare for T2DM patients to progress to this stage [21]. The primary cause of T2DM is obesity; other risk factors include genetics, lack of physical activity, and increasing age. The incidence of T2DM correlates with the increase in life expectancy, world population, and levels of obesity. It is estimated that the prevalence of diabetes mellitus will increase from 2.8% of the world population in 2000, to 4.4% by 2030 [22]. T2DM can take years to diagnose as the symptoms are less obvious. However, if

untreated the high glucose levels can cause damage to the microvascular and macrovascular systems [23].

1.3.3. Complications Associated with Diabetes

Hypoglycaemic attacks more typically associated with T1DM, range in severity. Mild hypoglycaemia can be recognised by symptoms such as blurred vision, confusion, and shaking. During a severe hypoglycaemic attack, the availability of glucose to the brain is reduced and can result in a diabetic coma, which if untreated can lead to death. Hyperglycaemia leads to microvascular complications such as nephropathy, retinopathy, and neuropathy and macrovascular complications such as cardiovascular disease [24, 25]. Complications caused by hyperglycaemia affect most patients with diabetes and can seriously impact on the patients' quality of life and life expectancy. Around 60% of T2DM patients' deaths are caused by cardiovascular disease [26] and more than 10% of annual healthcare spending in developed countries is currently spent on diabetes and its related conditions [27]. Tight control of blood glucose levels can help reduce the impact of these complications making the development of effective treatments essential.

1.4. Current Treatments for T1DM

1.4.1. Exogenous Insulin

The current standard treatment for T1DM is injection with exogenous insulin, administered through multiple daily injections or continuous subcutaneous insulin infusions. These infusions consist of a combination of rapid or short acting insulin around mealtimes and long or medium acting insulins to provide background insulin throughout the day. Continual insulin therapy with regular blood glucose testing has the capability to dramatically increase quality of life [25]. Unfortunately the treatment for T1DM is an expensive one meaning that there are many patients, primarily in developing countries who are not able to access the necessary treatments and hence have a very poor prognosis [28]. For those able to access it, exogenous insulin is not a perfect treatment as it is not able to mimic the actions of endogenous insulin completely. The dosage

required varies depending on food eaten and physical activity. This means it can be difficult to calculate, especially in the early stages of diagnosis, leading to large fluctuations in blood glucose [25].

1.3.2. Islet Transplantation

Islet transplantation is a current treatment option for patients with T1DM, who are unable to regulate their blood glucose levels through exogenous insulin therapies and have reduced hypoglycaemia awareness. These patients are at high risk of microvascular and macrovascular diseases. Islets are isolated from a donor pancreas and infused into the patient's liver through the portal vein as shown in Figure 2 [29].

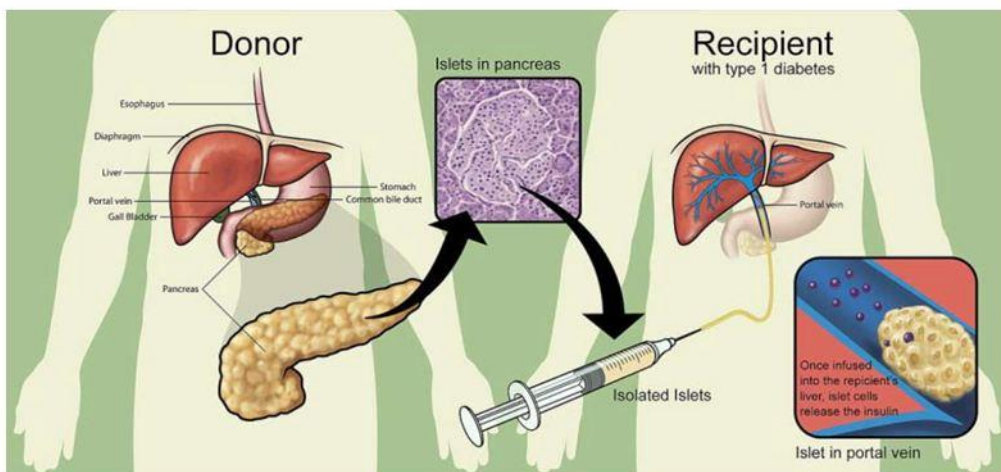


Figure 2. Image depicting process of islet isolation and transplantation from donor to recipients' hepatic portal vein [29]

Of the patients who received transplants between 2007 and 2010, 44% were insulin independent after 3 years (Figure 3 [30]). Partial function of the graft can provide protection from severe hypoglycaemia and hypoglycaemic unawareness. By 2017, more than 1500 patients had received islet transplantations [31]. The Collaborative Islet transplant Registry (CITR) reported that by 2012 44% of patients were free of severe hypoglycaemic events four years post-transplant and the most recent CITR report states that around 20% of recipients are insulin independent at five years post-transplant [32].

1.3.3. Islet Isolation

Before transplantation, islets must first be isolated from the surrounding exocrine tissue of the donor pancreas by enzymatic digestion, as was first described in 1965 [33]. Lacy and Kostianovsky used these enzymatic digestion techniques, along with gradient purification, to successfully isolate metabolically active islets from the pancreas of rodents [34]. The islets were transplanted into diabetic rats, resulting in some recovery of glucose control [34]. Isolation and purification techniques continued to improve, and human islet transplantation trials began in the mid 1980's. Subsequent studies showed that long term insulin independence could be achieved in humans through islet transplants, but with a limited success rate (16-18). Between 1990 and 2001, 267 islet transplants were recorded in the Islet Transplant Registry but only 8.2% of these achieved insulin independence for over one year [35] [36].

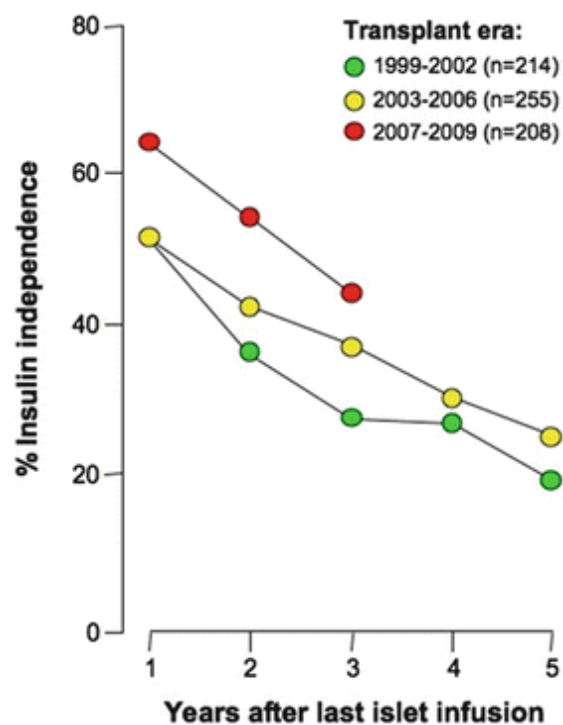


Figure 3. Rate of insulin independence after islet infusion as reported by the Collaborative Islet Transplantation Registry. Image taken from [36]

The success rates of islet transplantations improved following the publication of a study by the Edmonton group, who reported insulin independence in all seven recipients at one-year post-transplant. The key changes introduced in the Edmonton protocol include

an increase in the number of islets transplanted and a steroid-free immunosuppressive regime [37]. Although the outcomes of islet transplants have improved, the treatment still has limitations which prevent it from being a widely available option for patients.

1.3.4. Limitations of Islet Transplantation

The long-term success of islet transplantation is highly variable between patients. A low donor availability along with other limiting factors mean that the treatment is not widely available. Careful selection of donors and recipients has resulted in a steady improvement in patient outcome over the last few years [38].

The isolation and processing techniques used to prepare the islets for transplantation also influence patient outcome. During isolation the beta cells within the islets begin to lose some function, causing them to become less responsive to stimuli such as glucose. Patients often require multiple infusions from different donors so understanding why function is lost and how to maintain it could lower the number of infusions needed allowing more patients to benefit from the same number of donors [39]. Improvements have been made in the enzymatic isolation and purification methods of islets from the pancreas. The use of enzyme blends containing class I collagenase and class II collagenase, along with varying concentrations of non-collagenolytic enzymes, allows digestion to be tailored to the requirements of each pancreas [12, 40]. Careful control over digestion is necessary as too much can cause islets to fragment and disintegrate reducing viability and yield.

A clearer understanding of mechanisms involved in the loss of function in transplanted beta cells could lead to improved isolation and preparation of pancreas endocrine tissue before transplantation and hence improved treatment of T1DM. Optimising the culture conditions beta cells are exposed to between extraction and implantation is a necessary step towards retaining greater beta cell function.

1.5. Pancreatic B-cell Physiology

1.5.1. Regulation of Insulin Secretion

Glucose metabolism within beta cells provides the primary stimulus for the secretion of insulin. Amino and fatty acid metabolism also contribute to signals resulting in release of insulin. Glucose is transported into the beta cell through glucose transporters; GLUT1 in human and GLUT2 in rodent cells, [41] causing a rapid increase in intracellular glucose levels [30] [42]. The glucose is then phosphorylated by glucokinase in the rate limiting step of glycolysis. The glycolytic pathway leads to the production of pyruvate. During aerobic metabolism the pyruvate is oxidised to form one of two metabolites that can be transported into the mitochondria for further metabolism and optimum energy production. The metabolism of glucose through glycolytic and mitochondrial metabolism results in an increase in the ATP to ADP ratio which causes ATP sensitive potassium (K_{ATP}) channels situated in the plasma membrane to close and the membrane to depolarise. The K_{ATP} channels are composed of a core made of Kir6.2 and a regulatory subunit made of sulfonylurea receptor 1 (SUR1). Voltage gated Ca^{2+} channels open in response to the depolarised membrane allowing influx of Ca^{2+} ions into the cell. An increase in intracellular Ca^{2+} is essential for the activation of exocytosis of insulin containing granules (Figure 4). The importance of K_{ATP} channels in the insulin secretion pathway has been demonstrated through the addition of pharmacological agents such as sulfonylureas that bind to and induce closure of K_{ATP} channels depolarising the membrane and triggering insulin release. Agents such as diazoxide that interact with SUR1 to open K_{ATP} channels have been shown to inhibit glucose stimulated insulin secretion (GSIS) [43].

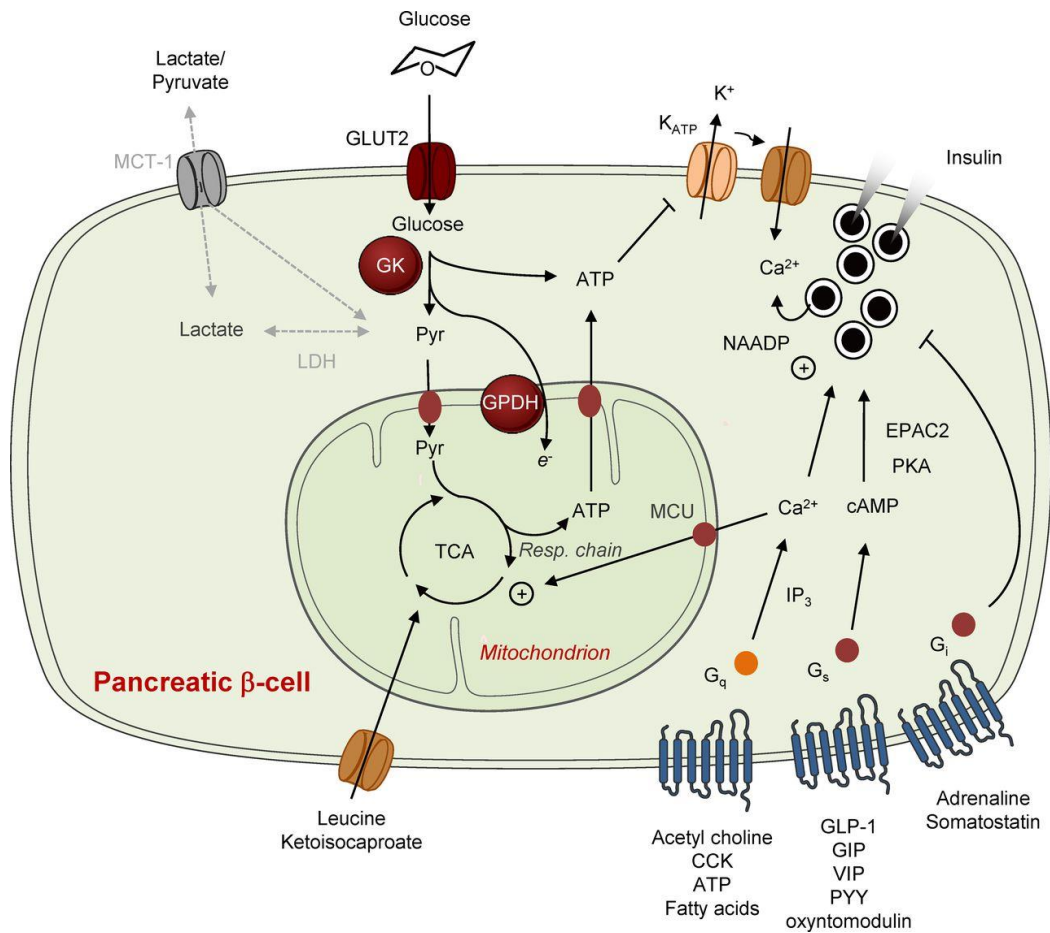


Figure 4. Beta-cell insulin secretion mechanism in response to glucose stimulus. Abbreviations: monocarboxylate transporter 1 (MCT-1), lactate dehydrogenase (LDH), glucose transporter (GLUT2), glucokinase (GK), pyruvate (Pyr), tricarboxylic acid cycle (TCA), glyceraldehyde 3-phosphate dehydrogenase (GAPDH), adenosine triphosphate (ATP), mitochondrial calcium uniporter (MCU), nicotinic acid adenine dinucleotide phosphate (NAADP), exchange protein directly activated by cAMP (EPAC2), protein kinase A (PKA), cholecystikinin (CCK), glucagon-like peptide 1 (GLP-1), glucose dependent insulinotropic polypeptide (GIP), vasoactive intestinal peptide (VIP), and peptide YY (PYY). [44]

In addition to glucose-stimulated secretion, secretagogues such as gut-derived incretins amplify the insulin release under high glucose conditions [45]. These include glucagon-like peptide-1 (GLP-1), glucose dependent insulinotropic polypeptide (GIP), cholecystikinin (CCK), peptide YY (PYY), and oxyntomodulin which are released in response to food transit [46]. These incretins trigger an increase in intracellular cAMP through the activation of G protein-coupled receptors [44]. Insulin secretion can also be inhibited by activation of inhibitory G protein-coupled receptors by adrenaline or somatostatin [10].

An alternative mechanism for GSIS that is not reliant on Ca^{2+} oscillations was discovered by blocking the K_{ATP} channels using sulfonylurea [47], this is known as the K_{ATP} channel independent pathway. This pathway has been shown to function in the absence of extracellular Ca^{2+} and to a higher extent when the intracellular Ca^{2+} concentration is consistently high [48]. The mechanism for this pathway is still unclear but is thought to involve coupling factors such as NAD(P)H, glutamate, Acyl CoA, reactive oxygen species, and / or AMP activated protein kinase (AMPK) [44].

GSIS is biphasic. This is possibly due to two distinct pools of insulin granules, one docked to the plasma membrane ready for release, and one that requires trafficking to the membrane [49]. It is proposed that the initial pulse is caused by the release of docked insulin granules responding to the Ca^{2+} increase driven by glucose metabolism and the second pulse of insulin is triggered by subsequent oscillations in Ca^{2+} [50]. The Ca^{2+} oscillations are thought to be regulated in part by the positive product feedback of glycolytic enzyme phosphofructokinase (PFK).

1.5.2. Metabolic Phenotype

For optimal insulin secretion in response to glucose it is important that glycolytic and mitochondrial metabolism are tightly coupled to produce the maximum amount of ATP with oxidative phosphorylation being the main source of ATP. It is estimated that mitochondrial metabolism generates 98% of beta cell ATP production [51]. The conversion of glucose to pyruvate through glycolysis is shown in figure 5 [52] then, once the pyruvate has been shuttled into the mitochondria, it is metabolised through the steps of the tricarboxylic acid (TCA) cycle (figure 6) [30]

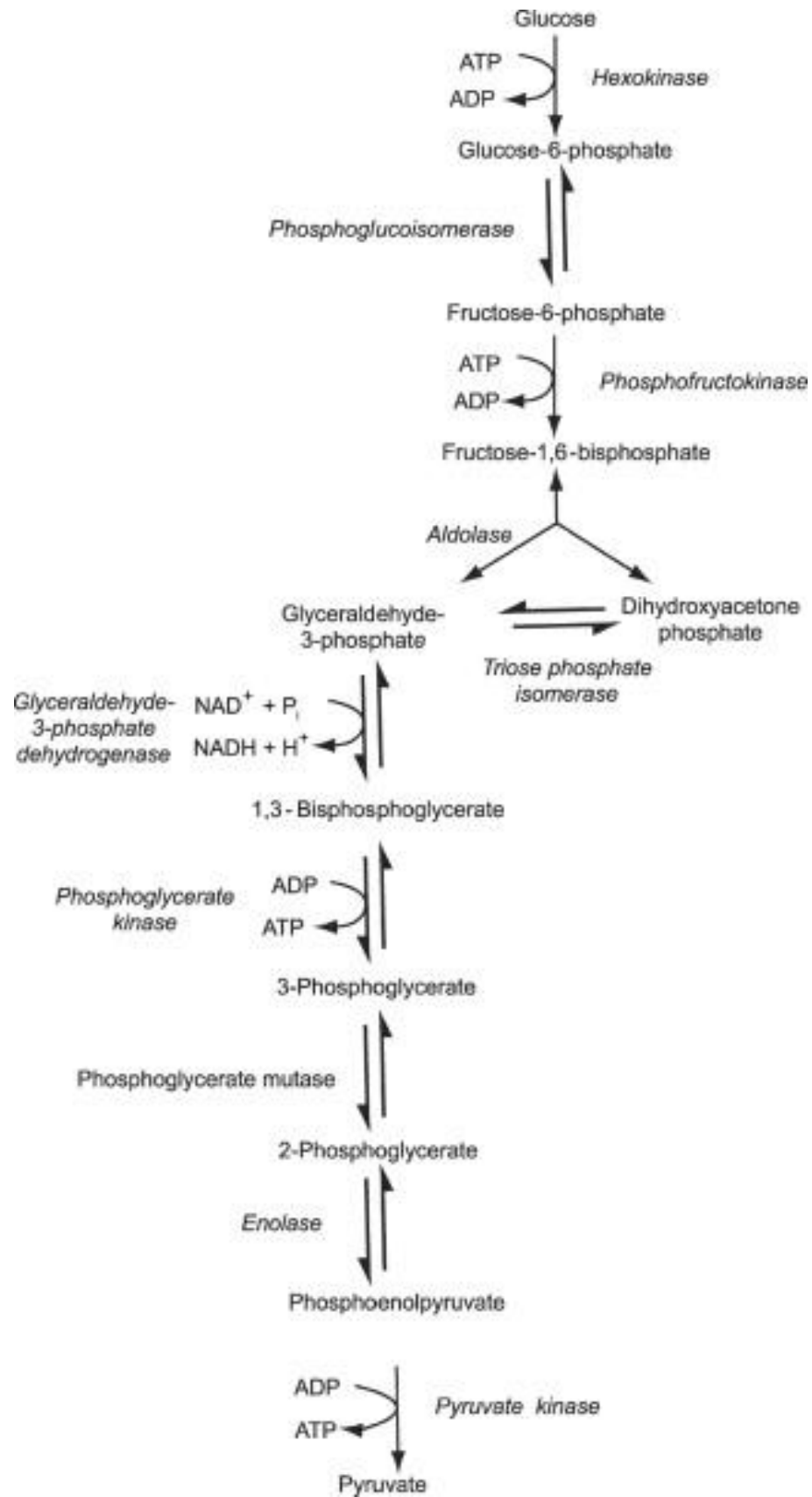


Figure 5. Schematic showing the steps involved in glycolysis leading to the generation of pyruvate from glucose [51]

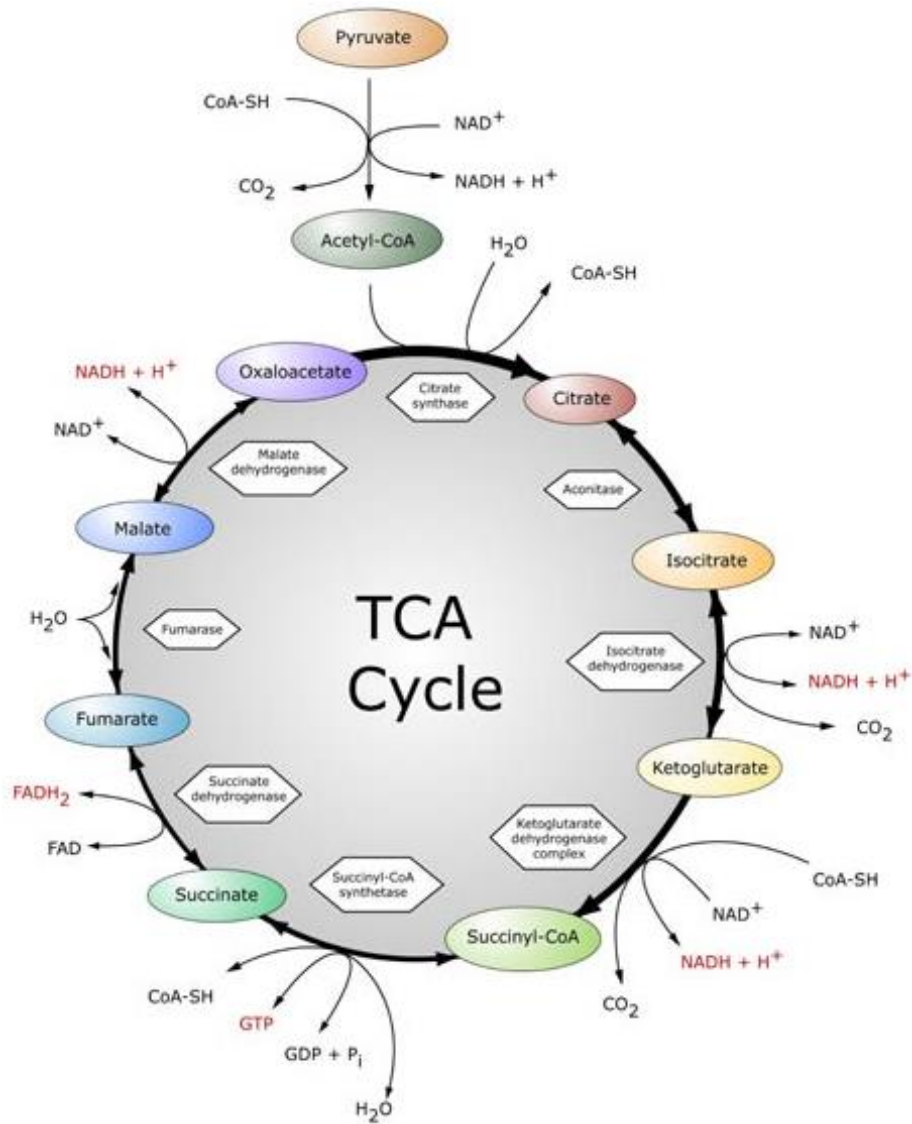


Figure 6. Schematics showing enzymes and intermediates involved in the TCA cycle taken from [42]

Tight coupling between glycolysis and mitochondrial metabolism relies on a number of characteristics of the beta cell such as the expression of glycerol-3-phosphate and malate/aspartate shuttles that transfer glycolytic derivatives into the mitochondria for ATP generation, and low hexokinase-1 [53], lactate dehydrogenase (LDH), and monocarboxylate transporter (MCT) expression [54, 55], as well as the presence of anaplerotic reactions [56]. To achieve these metabolic characteristics, the beta cell relies on a specific metabolic phenotype comprising several allowed and disallowed genes. expression These genes are listed in table 1.

Optimal Insulin Secretion	
High Expression	Low Expression
<ul style="list-style-type: none"> • GLUT1/GLUT2 • Glucokinase • Glycerol-3-phosphate shuttle • Malate/aspartate shuttle • Anaplerotic reactions 	<ul style="list-style-type: none"> • Hexokinase-1 • Lactate Dehydrogenase • Monocarboxylate Transporter

Table 1. Metabolic phenotype for optimal insulin secretion

The expression of either GLUT1 or GLUT2 ensures that rapid equilibrium between the extracellular and intracellular glucose concentrations is achieved. This enables the beta cell to respond quickly to small changes in blood glucose concentration.

Glucokinase is the rate limiting step for GSIS due to its high $S_{0.5}$ for glucose ensuring that it is most active at physiological glucose concentrations. Due to this it is deemed the glucose sensor for GSIS and ensures low rates of insulin secretion [57]. This step relies on exclusive expression of glucokinase with minimal expression of low K_m hexokinase isoforms [58]. The utilisation of glucose-6-phosphate in other pathways such as glycogen synthesis and the pentose-phosphate pathway is low enabling most of the glucose to enter the glycolytic pathway [59]. The cytosolic NADPH/NADP⁺ ratio increases in response to increased pyruvate/malate shuttle activity resulting in further inhibition of the pentose-phosphate pathway.

A high NAD:NADH ratio is required by the beta cell to sustain glycolytic flux. However, the low LDH activity in the beta cell means NAD⁺ cannot be regenerated through the production of lactate as it is in other cell types. High expression of the G3P and malate aspartate shuttles are therefore necessary for the transfer of reducing equivalents into the mitochondrial matrix and the regeneration of NAD⁺ in the cytosol. The G3P shuttle

(Figure 7) converts dihydroxyacetone phosphate to glycerol-3-phosphate in the cytosol in a NADH reduction coupled reaction and then converts glycerol-3-phosphate back to dihydroxyacetone phosphate in a reaction coupled to the oxidation of FAD to form FADH₂ [60, 61]. The Malate/aspartate shuttle (Figure 8) is made up of two antiporters, the malate/ α -ketoglutarate antiporter and the glutamate/aspartate antiporter [61, 62]. In the cytosol, aspartate is converted to malate via oxaloacetate resulting in the oxidation of NADH to NAD⁺, the malate can then be transported across the mitochondrial membrane by the malate/ α -ketoglutarate antiporter. Once in the mitochondrial matrix the malate is converted back to aspartate via oxaloacetate and NAD⁺ is reduced to generate NADH, the aspartate is transported back to the cytosol by the glutamate/aspartate antiporter [60]. These mechanisms have the overall effect of transporting electrons in the form of NADH or FADH₂ into the mitochondrial space to enter the electron transfer chain as shown on the inner mitochondrial membrane in Figure 7 and thereby increasing the potential ATP generation from glycolysis [57]. Inhibition of both G3P and malate/aspartate shuttles in rodent beta cells severely decreases the glucose stimulated insulin secretion response [63] and decreased activity of either shuttle is associated with T2DM [64].

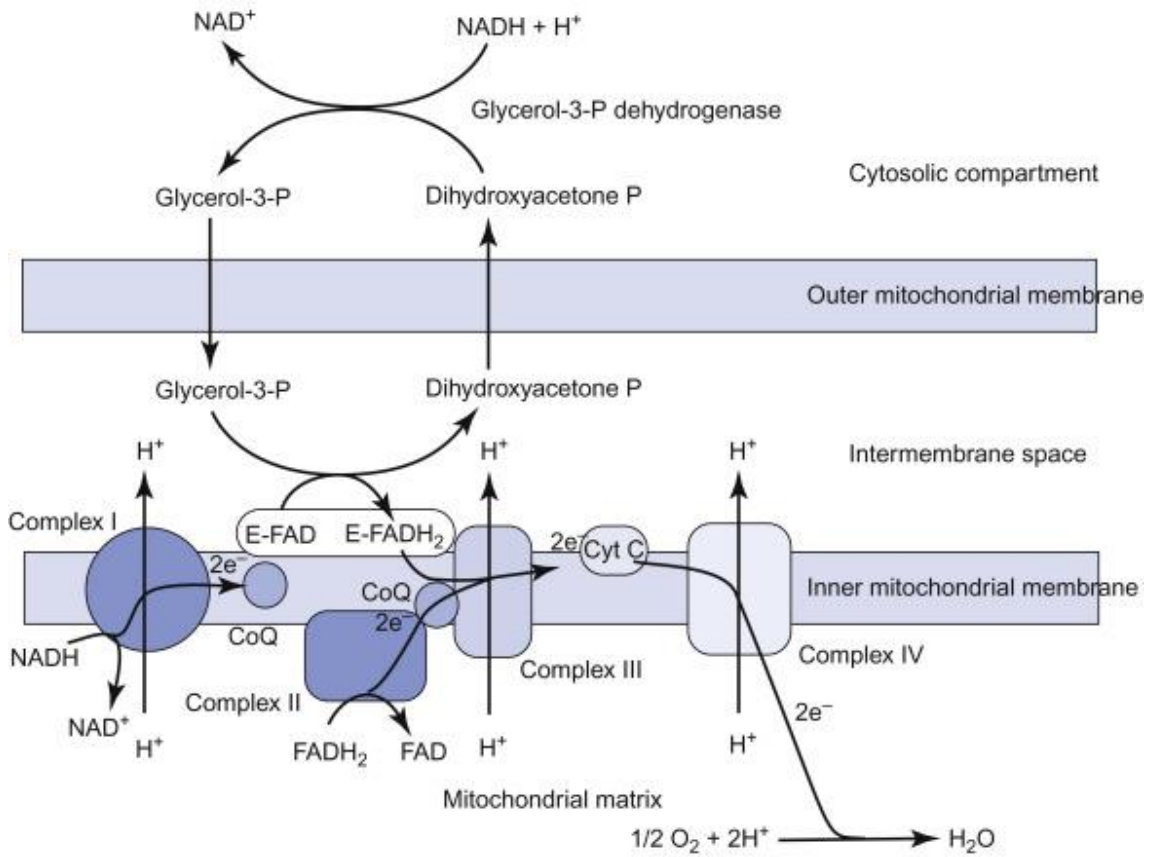


Figure 7. Diagram showing G3P shuttle and electron transfer chain. [61]

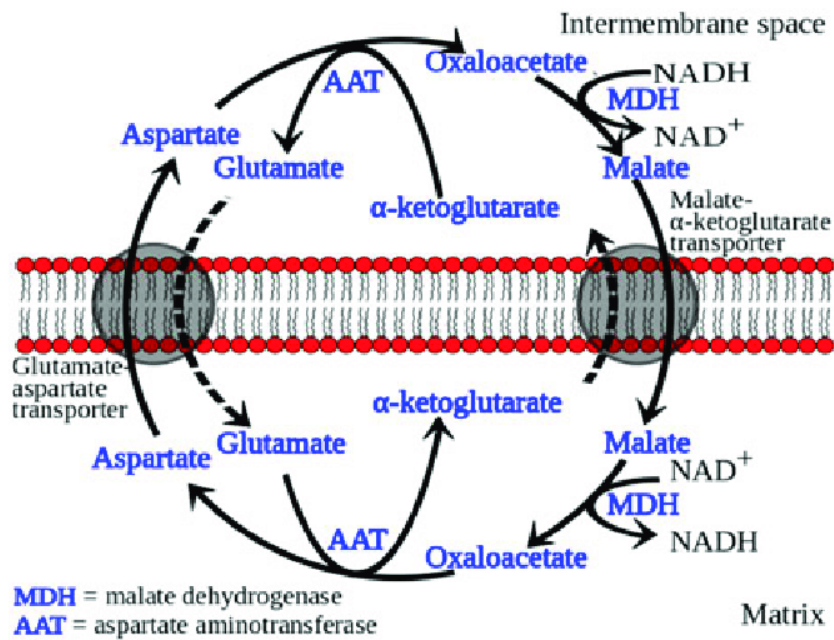


Figure 8. Diagram showing malate/aspartate shuttle [60]

Anaplerosis is the process by which the intermediates in the TCA cycle are replenished and is necessary for the transfer of glucose derivatives through the TCA cycle. One of the most important anaplerotic reactions involves the conversion of pyruvate to oxaloacetate by pyruvate carboxylase (PC). Around 60% of glucose in beta cells is oxidised by pyruvate dehydrogenase to produce acetyl CoA whilst around 40% is carboxylated by PC [55]. Together these intermediates produce citrate which can enter the TCA cycle. PC activity is higher in beta cells than in most other tissues and its inhibition through either the addition of the inhibitor phenylacetic acid or small interfering RNA knockdown has been shown to inhibit GSIS [56, 65]. Mutations in the PC gene do not lead to a clinically detectable decrease in GSIS but its activity correlates with the glucose concentration beta cells are exposed to and the consequent insulin release [65]. At higher extracellular glucose concentrations PC is more active as the rates of metabolism increase and intermediates must be replenished at a higher rate [66].

In most mammalian cells, pyruvate can also be metabolised by LDH to produce lactate which is transported across the plasma membrane by MCT but the expression of LDH and MCT in beta cells can interfere with glucose sensing. When LDH was overexpressed in INS-1 cells, insulin secretion could be stimulated at low lactate concentrations and MCT overexpression resulted in a 3.7-fold increase in lactate transport activity [54]. An increase in LDH activity would indicate a shift towards anaerobic metabolism meaning a loss in the tight coupling between glycolytic and mitochondrial metabolism required for maximal ATP production [54, 59, 67]. Uptake of lactate into the beta cell from the blood via MCT can stimulate inappropriate insulin release leading to hypoglycaemia. The expression of LDH and MCT genes in beta cells is repressed during early postnatal islet maturation [55, 68] and Sekine et al reported that LDH activity was 100 fold lower in beta cells than in other cell types investigated in the same study such as lymphocytes, macrophages, heart tissue, and brain cortex [52, 69].

1.6. Cell Connectivity

1.6.1. Cell Connectivity is Essential for GSIS

Insulin secretion from beta cells is dependent on connections with adjacent cells. When islets are dispersed into individual beta cells, the insulin secretion response to nutrient stimulation is reduced. When beta cells are allowed to reaggregate they can form islet-like structures known as pseudoislets that mimic the 3D architecture seen in the primary islets [70]. The insulin content does not differ between monolayer and 3D culture [71]. However, there is a greatly enhanced insulin secretory response in the pseudoislets [72]. Beta cell lines are often grown in monolayer culture which prevents the formation of the 3D architecture of islets seen *in vivo* but pseudoislets provide an ideal model for investigating the effect of homotypic connections on insulin secretion. The insulin secretion response is also higher in islets than in monolayer cultures when other stimulus is applied such as sulphonylureas, the K_{ATP} receptor stimuli carbachol or tolbutamide, and protein kinase activators [71]. The integrated insulin secretion response of the islet is greater than the sum of the responses of the individual beta cells suggesting that the 3D arrangement is necessary for an efficient insulin secretion response. If culture conditions are favourable beta cells will begin to reaggregate into 3D structures over time in culture, if not, beta cells can adhere to plastic and outgrow.

The improved insulin secretion response of islets is thought to be due to synchronisation of calcium oscillations. Beta cells within primary islets display synchronised oscillations in cytoplasmic Ca^{2+} concentration [73, 74]. The response of individual beta cells can vary greatly in the threshold for stimulation, the change in calcium concentration and the magnitude of the insulin secretion response [75]. If 3D structures begin to form, the insulin secretion response can be restored and the synchronisation of the amplitude and frequency of the cytoplasmic Ca^{2+} oscillations is regained [76, 77]. The cytoplasmic Ca^{2+} oscillations in beta cells that occur in response to glucose have been shown to be synchronised within islets whilst isolated beta cells do not display this synchronisation and have a much larger variability in the threshold for stimulation.

It has been reported that the decrease in insulin secretion response is immediate when islet or pseudoislets are dispersed. This shows that it is a result of short-term intracellular interactions rather than a change in the beta cell phenotype. However, it has also been demonstrated that connections between beta cells result in chronic changes to the cell proteome. Chowdhury et al used mass spectrometry and immunometric-based approaches to show that pathways involved in glycolysis, the TCA cycle, and oxidative phosphorylation were enhanced in beta cells cultured as pseudoislets when compared to those cultured in monolayer [78]. Phosphofructokinase (PFK) and pyruvate kinase were two of the proteins upregulated and showed a 2-fold and 4-fold increase in protein expression respectively in pseudoislets compared to monolayers. Both of these enzymes are involved in the glycolytic pathway with PFK being one of the key regulatory enzymes. PFK is also involved in the generation of rhythmic insulin oscillations [79]. All enzymes of the TCA cycle investigated were upregulated in pseudoislets, particularly citrate synthase, isocitrate dehydrogenase (ICD), and succinate dehydrogenase. Of the proteins involved in the oxidative phosphorylation pathway, 19 out of 22 were upregulated in pseudoislets. The enhancement of this pathway is supported by another study in which expression of 84 genes involved in oxidative phosphorylation was quantified in monolayers and pseudoislets [80]. It was found that 76% of the genes showed at least a 1.4-fold increase in expression but the effect these changes have on glucose metabolism and insulin secretion was not investigated. The increased intercellular connectivity within pseudoislets was demonstrated by the increase in expression of proteins involved in gap junctions, tight junctions and adherent junctions.

1.6.2. Pseudoislet Culture

Due to the difficulty in retaining function in primary rodent beta cells and the scarce availability of human islets for use in research, most of the studies mentioned have used rodent derived insulinoma beta cell lines such as INS1, MIN6, RINm5F, and BRIN BD11. These cell lines have been shown to retain an insulin secretory response to glucose over prolonged culture periods. Three insulin secreting human beta cell lines have recently

been generated, but are still in the early stages of characterisation [81, 82]. The human cell line EndoC- β H1 shows improved GSIS when configured as pseudoislets [83].

The preparation of pseudoislets requires culture on a surface with low negative charge to prevent adhesion of the cells to the surface. Ideal surfaces that have been shown to allow pseudoislet formation include ultralow adhesion plates [84], gelatine coated plates [77], agarose gels [85] and PEG wells produced by contact photolithography [86]. Functioning pseudoislets produced by these methods have been used to generate valuable data but the consistency in islet size can be low and larger islets are prone to formation of necrotic cores. In an attempt to improve the quality of the pseudoislets, stirred suspension methods have been used by culturing the beta cells on an orbital shaker [86] or in a spinner flask [87]. This minimises the formation of pseudoislets that are too large and improves flow of nutrients to the cells, thereby preventing the formation of necrotic cores. Pseudoislets that have been produced in stirred suspension have been shown to have enhanced cell survival, propagation, and insulin secretion when compared to pseudoislets from static culture over a ten day culture period [88]. Pseudoislets can also be produced using a hanging drop method which involves the seeding of single drops containing a specified number of beta cells onto a culture dish which is then inverted for five to eight days [13]. The size of the pseudoislet can be controlled by changing the number of cells in the drop. The outcome was similar to that of the stirred suspension methods with smaller and more consistent pseudoislets. The hanging drop method is labour intensive but can be considered as a cheaper alternative to stirred suspension cultures when only small numbers of pseudoislets are required.

Communication within islets occurs through autocrine and paracrine actions of hormones such as insulin, glucagon and somatostatin. Beta cells in islets are also linked directly by intracellular junctions, integrins, receptors, and cell adhesion molecules. Many of these connections have been implicated in the regulation of insulin secretion in response to glucose [89].

1.6.3. Cell-Cell Interactions

i. Cell Adhesion Molecules

The cell adhesion molecule (CAM), N-CAM acts to maintain cell-cell interactions and may be involved in regulating beta cell proliferation [90]. The transmembrane CAM E-Cadherin is present in the beta cell plasma membrane and forms calcium dependent homodimers with cadherins on neighbouring cells [1]. E-cadherin plays an important role in the formation of pseudoislets as shown by the culture of MIN6 in the presence of an E-cadherin antibody which inhibits the formation of pseudoislet structures [77]. The aggregation of beta cells is calcium dependent and can be reversed through culture in Ca^{2+} free media. The intracellular region of the E-Cadherin interacts with the actin cytoskeleton of the beta cell and contributes to the regulation of beta cell function and proliferation through coupling to the β -catenin/Wnt signalling pathway [77]. The aggregation of beta cells facilitated by E-cadherins enables other cell-cell interactions to form such as through connexins and EphA/Ephrin-As.

ii. EphA-Ephrin-A system.

EphA receptor tyrosine kinases and their Ephrin-A ligands are located on the plasma membrane of beta cells and are classified into A and B subclasses [91]. Most EphAs bind to Ephrin-As and most EphBs bind to Ephrin-Bs activating either a forward or a reverse signalling pathway. When Ephrin-A-Fc-fusion proteins bind to EphAs the forward signalling pathway is activated resulting in inhibition of basal insulin secretion. The reverse signalling is activated when EphA-Fc-fusion proteins bind to Ephrin-As. This pathway is predominant in the presence of glucose and enhances glucose stimulated insulin secretion [1]. When beta cells are arranged in pseudoislets the ephAs and Ephrin-As can interact with those of adjacent cells as shown in Figure 9.

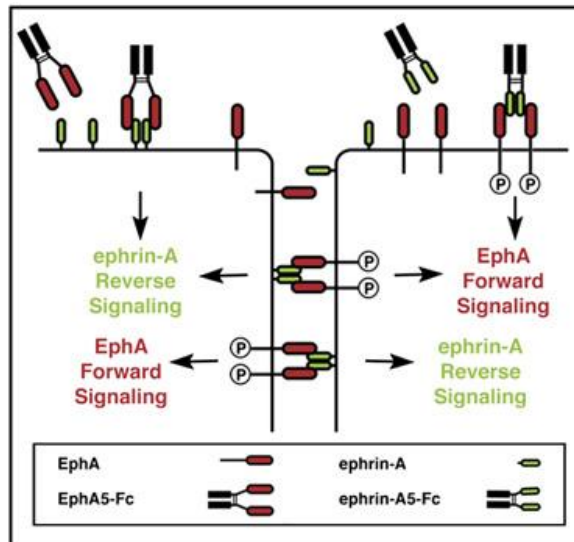


Figure 9. EphA-Ephrin-A bidirectional signalling between two β -cells [91]

Konstantinova et al discovered that EphAs are concentrated on insulin granules and are incorporated into the plasma membrane of beta cells during insulin secretion. The EphAs are then either phosphorylated at low glucose concentrations resulting in further inhibition of insulin secretion in a negative feedback mechanism or they are dephosphorylated under high glucose conditions favouring the reverse signalling pathway and increasing insulin secretion. It is proposed that the coexpression of EphA and Ephrin-A in β -cells is important for the regulation of the insulin secretion response [91]. A study by Jain et al showed that insulin secretion at high glucose concentrations could be further increased by the addition of small molecular weight Eph inhibitors [6].

iii. Connexins

A gap junction is formed when a connexon in the plasma membrane of a cell docks to a connexon of a neighbouring cell to form a channel that permits the transfer of small molecules up to 900 Da between cells. So far, 21 different connexin isoforms have been identified; these are expressed in varying proportions throughout different tissues in the body [92]. Connexons can dock with a connexon of the same isoform to form homomeric channels or with one made from different connexins to form heterotypic channels, this allows a large diversity of possible channels with varying properties. Connexin

hemichannels are involved in paracrine signalling, ATP, glutamate, NAD⁺, and prostaglandins. In neurons, connexins can increase rates of synaptic transmission and enable cells within excitable tissue to coordinate a synchronised response [93]. They also play a role in proliferation and apoptosis, and homeostasis in non-excitabile tissue [92].

The principal connexin isoform expressed in pancreatic beta cells, as well as neurons within the central nervous system, is connexin 36. Deletion of Cx36 in mouse models results in impaired function of neuronal and retinal cells and an increase in basal insulin secretion in the beta cells [94]. Evidence of other connexins within the islet has also been reported. Cx43 and Cx45 in mice, and Cx30.3, Cx31, Cx31.1, Cx31.9, Cx37, and Cx45 in human models. It is possible that these connexins form heterotypic channels with the Cx36 in beta cells aiding communication between the beta cells and vasculature or exocrine tissue [95].

The synchronisation of the beta cell insulin response relies largely on connexin 36 (Cx36) gap junctions that provide electrical and metabolic coupling between cells. In the case of beta cells, the alignment of connexons relies on E-Cadherins. Gating of the Cx36 is controlled through a variety of environmental factors such as pH, the voltage across the channel, or the intracellular Ca²⁺.

The importance of Cx36 in beta cells was first investigated by comparing monolayer and islet cultures since intercellular connexin channels cannot form between the isolated cells in monolayer. It was documented that beta cells that lack the intercellular connections displayed irregular Ca²⁺ oscillations that were not synchronised between beta cells and reduced overall GSIS indicating that the connections are essential for the optimal functioning of the beta cells [89]. This has since been confirmed in multiple studies both *in vitro* and *in vivo* through genetic Cx36 knockdown and reversibly blocking channels using lipophilic drugs [96]. Some studies have reported lower basal insulin secretion in beta cells connected by Cx36 channels than in isolated cells, this could be explained by the diffusion of Ca²⁺ ions throughout the beta cells allowing the less active

beta cells to prevent the more active cells from initiating an insulin secretion response at low glucose. However, the change in basal insulin secretion was not consistent in all studies with some reporting no increase in Cx36 deficient islets [95].

It has been shown that it is not necessary for all beta cells within the islet to be interconnected by Cx36 channels with an improvement in function detected when only two or three beta cells are connected and (fluorescence recovery after photobleaching) FRAP images have shown that not all neighbouring beta cells are connected but that connection patterns occur over long distances [97]. Overexpression of Cx36 may provide some protection against ER and oxidative stress and pro-inflammatory cytokines.

Work by Squires et al suggests that intercellular communication via gap junctions is not solely responsible for the synchronisation of Ca^{2+} oscillations or the increase in insulin response [98]. MIN6 cells were cultured as monolayers or pseudoislets and gap junctions were blocked with the addition of either heptanol or 18- α -glycyrrhetic acid (GA). The addition of heptanol at low concentrations resulted in a decrease in frequency of Ca^{2+} oscillations but the synchronisation of the oscillations between beta cells was not affected. Addition of GA, which has a higher potency in the uncoupling of gap junctions, decreased the amplitude of the Ca^{2+} oscillations. However, like the heptanol, GA did not interrupt the synchronisation of the oscillations between the β -cells or the initiation of insulin secretion.

1.7. Hypothesis

Evidence suggests that efficient glucose stimulated insulin secretion in beta cells is dependent on both tight coupling between glycolysis and mitochondrial metabolism and through the maintenance of intercellular connectivity present in islets or pseudoislets. However, it is not clear if the cell connectivity influences the metabolic phenotype of the beta cell. The hypothesis of this study is that cell connectivity within islet structures

maintains the tight coupling between glycolysis and mitochondrial metabolism which is essential for appropriate GSIS.

1.8. Aims

This thesis aims to explore the impact of cell connectivity on the metabolic characteristics of beta cells and determine the consequent impact on GSIS in both mouse and human models. The three main objectives are:

1. To compare effects of 2D vs 3D culture on the metabolic function of beta cells.
2. To determine whether any changes in function correlate with changes in the metabolic phenotype of the beta cells.
3. To explore a role for cell-cell interactions in regulating these metabolic changes.

CHAPTER 2. METHODS

2.1. Reagents

All reagents were obtained from Sigma Aldrich unless otherwise stated. High range rat insulin ELISA kits were obtained from Mercodia (Uppsala, Sweden). Dulbecco's modified eagle medium (DMEM), foetal bovine serum (FBS), penicillin-streptomycin, trypsin-EDTA, sodium pyruvate, and Hepes buffer were obtained from Thermo Scientific (Paisley, UK). Magnesium chloride, glucose, Triton-X 100, sodium hydroxide, triethanolamine buffer, and EDTA were obtained from BDH Laboratory Supplies (Poole, Dorset, UK). MIN6 cells were kindly provided by Prof. J.-I. Miyazaki (University of Tokyo, Japan).

2.2. Cell Culture

2.2.1. MIN6

i. MIN6 Maintenance

Mouse insulinoma MIN6 cells (between passages 21 to 29) were cultured in 25cm² and 75cm² cell culture flasks (Greiner Bio-one Ltd) in Dulbecco's modified Eagle's Medium (DMEM) containing 25mM glucose and 25mM HEPES and supplemented with 100mM pyruvate, 15% foetal bovine serum (FBS), 5µl/l β-mercaptoethanol, 75mg/l penicillin, 50mg/l streptomycin and cultured in a humidified incubator at 37°C in 5% CO₂. Media was replaced every 2 to 3 days and the cells were passaged when confluent using trypsin-EDTA.

ii. MIN6 counting

For counting, media was removed, and cells were washed twice with PBS, then 0.5ml trypsin-EDTA was added to a 25cm³ flask of confluent cells and incubated at room temperature for three to five minutes. Once cells had detached the suspension was transferred to a universal containing 5ml of media. A stock solution was prepared by

adding 5µl cell suspension to 45µl PBS. A glass coverslip was placed on a haemocytometer and 10µl of the diluted cell suspension was added to the coverslip. Cells were counted in the four corner squares and the centre squares and the number of cells was calculated using Equation 1.

$$\text{Total Cells/ml} = \text{cells counted} \frac{\text{dilution factor}}{\text{no. squares}} 10,000$$

Equation 1. calculation for total number of cells per ml

iii. MIN6 Experimental Culture

The monolayer cultures were prepared by culturing MIN6 on either 6 or 24 well plates for five days. The seeding density used reflected the density used in the pseudoislet culture ranging from 5×10^3 to 5×10^5 cells/cm².

Pseudoislets were initially prepared by culturing MIN6 on 1% (wt) gelatin coated 6 well plates and petri dishes at seeding densities of 2.5×10^4 , 2.5×10^5 and 2.5×10^6 cells/ml. To compare seeding densities MIN6 were then cultured in petri dishes at densities of 2.5×10^4 , 2.5×10^5 and 2.5×10^6 cells/ml or 3×10^3 , 3×10^4 , and 3×10^5 cells/cm² respectively. All further pseudoislets were cultured on petri dishes for five to six days with an initial seeding density of either 4.3×10^5 cells/cm² or 2.8×10^5 cells/ml. The media was replaced by carefully transferring the pseudoislets into a Falcon® 15mL polystyrene conical centrifuge tube, allowing the pseudoislets to form a pellet by gravity so that the media could be aspirated and replaced. The petri dishes were washed with (phosphate buffered saline) PBS and the pseudoislets in the fresh media replaced.

2.2.2. Human Islets

Human islets (LDIS247, LDIS248, and LDIS256) were isolated from three donors without diabetes at NHS Blood and Transplant, Barrack road, UK, with appropriate ethical approval. Table 2 shows Islet donor information. Islets were maintained in CMRL media

supplemented with 0.5% human albumin serum, 50µg/ml streptomycin and 50µg/ml penicillin. On receipt, Islets were given one day to recover from transportation before being used for experiments.

Code	Age	Gender	BMI	Donor Type	Purity
LDIS247	48	F	32.49	DBD	80%
LDIS248	49	F	26.63	DCD	82.5%
LDIS246	53	M	25	DBD	80%

Table 2. Islet Donor Information

DBD = donor after brain death, DCD – donor after cardiac death

2.3. Generation of Stable Inducible MIN6 Cx36 Knockdown Cell Line

2.3.1. Lentiviral Promotor Selection

The optimal promotor for transduction of MIN6 was selected using a SMARTchoice promotor selection kit. This kit allowed transduction of MIN6 with seven different promotors, hCMV, mCMV, hEF1 α , mEF1 α , PGK, and UBC. The most active promotor could be selected through assessment of visual intensity (SP-001000-01, Dharmacon).

2.3.2. Transduction of Lentiviral Particles

Three SMARTvector shRNA lentiviral constructs listed in table 3 were ordered containing the mCMV promotor and targeting Cx36 expression along with a non-targeting control (VSC6570).

KD	Catalogue Code	Antisense Sequence	Target
1	V3SM7672-232247995	CGTAATCCCTCTAGCTTG	3' UTR
2	V3SM7672-233160478	TAGAGTACCGGCGTTCTCG	ORF
3	V3SM7672-235462855	TTGATGCAGGGGTAACGGT	ORF

Table 3. SMARTvector shRNA Lentiviral Constructs

On day one of transduction, a 96 well plate was seeded with P25 MIN6 cells at a density of 30,000 cells/well. On day two cells were transduced with the three constructs and the

control with anticipated functional titres of 2.5×10^6 TU/ml for the targeting constructs and an anticipated functional titre of 3×10^6 TU/ml for the control. The MIN6 and shRNA constructs were incubated with $8 \mu\text{g/ml}$ polybrene in FBS free media for six hours. After six hours the transduction medium was replaced with MIN6 culture medium. On day four $1 \mu\text{g/ml}$ puromycin was added for at least three days to select transduced cells. The shRNA expression was induced by addition of 1mg/ml doxycycline for 48 hours and transduction was confirmed by checking TurboGFP expression using fluorescence microscopy and through western blot analysis.

2.3.3. Maintenance of Stable Cell Line

The stable MIN6 cell line with inducible Cx36 knockdown along with another cell line transfected with a scrambled control were cultured in the same conditions as the MIN6 with $1 \mu\text{g/ml}$ puromycin added. Pseudoislets were generated by culturing the cells on petri dishes for five days. Puromycin was removed during pseudoislet formation. The knockdown was induced over the final 48 hours of the pseudoislet formation by the addition of $1 \mu\text{g/ml}$ doxycycline on day three of pseudoislet culture.

2.4. Islet Equivalent Counts

Islet equivalent quotients (IEQ) were calculated where one islet equivalent is equal to an islet with a diameter of $150 \mu\text{m}$. The volume of media in each petri dish containing pseudoislets was measured and recorded as the pool volume. The pseudoislets were mixed by inverting and $100 \mu\text{l}$ samples were transferred to a six well plate for counting. Counting was performed at 10x magnification on a microscope with a measuring grid in the eyepiece. The islets were measured and classified according to size and the totals were multiplied by an islet equivalent conversion factor. The total number of free islet equivalents was defined as the sum of all islet equivalents \times pool volume/sample size [99].

2.5. Propidium Iodide Viability Staining

A viability stain was prepared by adding 10 μ l of propidium iodide dye (P1304MP, Thermo Fisher) and 1 μ l 10mM H33342 to 1ml of media. A sample of 100 pseudoislets (P21 to P25) was incubated in 500 μ l of the PI stain for 10 minutes at room temperature then the stain was replaced with fresh media. The pseudoislets were transferred to a 24 well plate and imaged using light microscopy and fluorescence microscopy on a Nikon Eclipse TE2000-S. Images were analysed using CellProfiler software to calculate the percentage viability of each islet.

2.6. Enzyme Activity Assays

Enzyme activity assays were performed at 37°C in 96 well plates using the Spectramax plate reader (Molecular Devices) and analysed using Softmax pro software. Absorbance was read at 340nm every minute for 20 minutes unless otherwise specified. The enzyme activity is expressed as mU/mg protein.

For each sample 500 μ l of extraction buffer was added to either one well of a 6 well plate for monolayer culture or 800 pseudoislets. The extraction buffer was prepared with 150mM KCl, 3mM Hepes, 1mM dithiothreitol (DTT), 1mM Benzamidine, and 10 μ l PIC (P8340 Sigma Aldrich). Supernatant and cell pellet fractions were then separated by transferring half of each sample to a separate 1.5ml Eppendorf and centrifuged at 9000 rpm (Harrier 18/80R) for five minutes. The supernatant was removed and saved, and the remaining pellet was resuspended in 400 μ l of the extraction buffer. The total cell homogenate, pellet and supernatant were then assayed individually. Enzyme concentrations were calculated on Microsoft excel using equation 2.

$$c = \frac{\frac{A}{(\epsilon \times l)} \times DF \times V}{P} \quad \text{Equation 2}$$

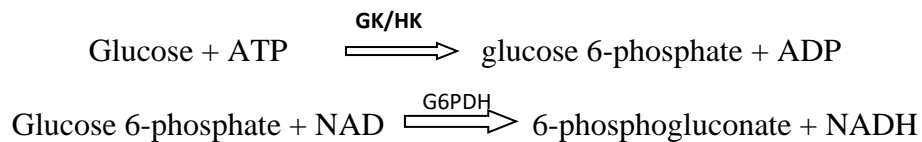
Equation 1. Equation based on the beer lambert law used to calculate the enzyme concentration (mU/mg). c =enzyme activity concentration, A =absorbance, ϵ =molar extinction coefficient (NADH=6.22 and DTNB=13.6), l =path length (0.45 for 200 μ l sample, and 0.36 for 160 μ l sample), v =volume of initial cell suspension, DF =dilution factor, and P =protein concentration.

Originally all enzyme activity assays were completed using earlier passage, P21 to P25 MIN6. When data showed a trend towards changes in activity but did not reach statistical significance, these assays were repeated using higher passage MIN6, P26 to P29.

2.6.1. Glycolytic Enzyme Activity Assays

i Hexokinase/Glucokinase

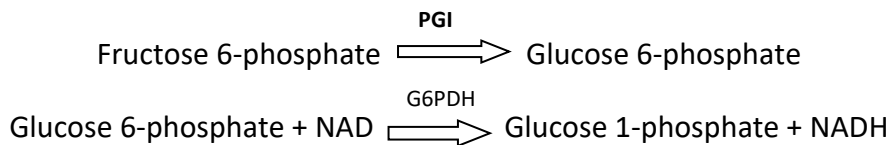
Hexokinase (HK) and glucokinase (GK) activities were assayed by measuring the NADH production in the following reaction.



Each sample was centrifuged at 9000 rpm (Harrier 18/80) in a 1.5ml Eppendorf and the supernatant transferred to a new Eppendorf. 80 μ l of each supernatant was pipetted into wells of a 96 well with 80 μ l of the main reagent containing 50mM Hepes (pH 7.8), 100mM KCl, 2mM MgCl₂, 6mM ATP/Mg²⁺, 1mM NAD, 2mM DTT, and 1.5U/ml glucose 6-P dehydrogenase. A glucose concentration of 0.5mM was used to measure low K_m HK activity and 50mM glucose to measure total HK activity. GK activity was calculated by the difference in activity between these two conditions.

ii Phosphoglucoisomerase

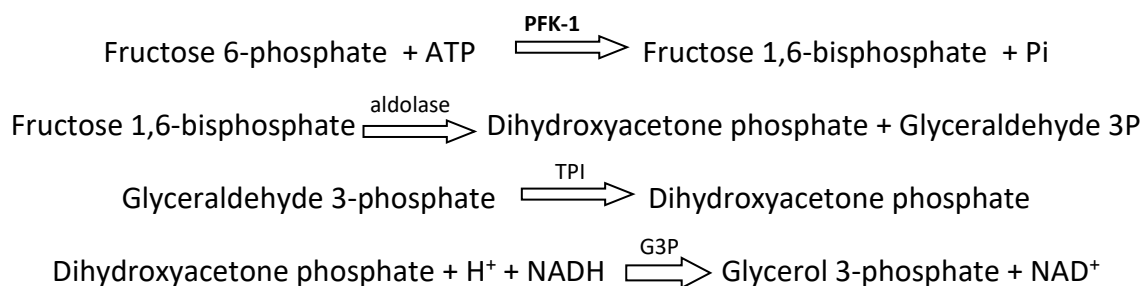
Phosphoglucoisomerase (PGI) activity was measured by recording the NADH production in the following reaction.



Each sample was diluted 1:5 with the extraction buffer described above then 20 μ l was pipetted into a 96 well plate with 180 μ l of the main reagent containing 50mM HEPES, 1mM MgCl₂, 0.5mM NAD, 2mM fructose 6-phosphate, 1mM DTT, and 2.5U/ml glucose 6-P dehydrogenase.

iii Phosphofructokinase

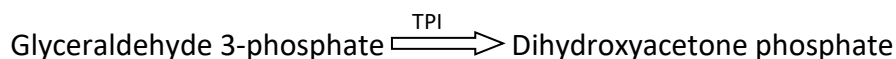
PFK1 activity was measured by recording the rate of oxidation of NADH in the following reactions.



For each sample, 20 μ l of the total cell homogenate was pipetted into a 96 well plate with 180 μ l of the main reagent containing, 20mM Tris, 100mM KCl, 2mM NH₄Cl₂, 3mM MgCl₂, 1mM ATP/MgCl₂, 0.16mM NADH, 2mM AMP, 10mM fructose 6-phosphate, 12 μ l α -glycerophosphate dehydrogenase-triosephosphate isomerase from rabbit muscle (sigma Aldrich, G1881), and 24 μ l aldolase.

iv Aldolase

Aldolase activity was recorded by measuring the oxidation of NADH in during the following reactions:



For each sample, 20 μ l of the total cell homogenate was pipetted into a 96 well plate with 180 μ l of the main reagent containing, 20mM Tris, 100mM KCl, 0.32mM NADH, 10mM fructose 1,6-bisphosphate, and 12 μ l α -glycerophosphate dehydrogenase-triosephosphate isomerase from rabbit muscle (G6755, Sigma Aldrich).

v Glyceraldehyde 3-phosphate dehydrogenase (GAPDH)

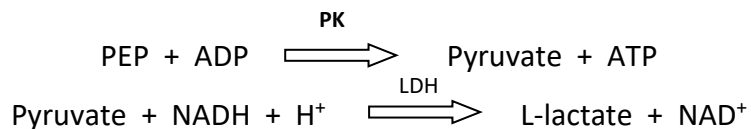
GAPDH activity was measured by recording the rate of oxidation of NADH during the following reactions:



For each sample 20 μ l of the sample to a 96 well plate with 180 μ l of main reagent containing, 0.1M triethanolamine (pH 8), 6mM glycerate 3-phosphate, 0.18mM EDTA, 1.12mM ATP, 0.4mM NADH, 5mM MgSO₄, and 5 μ l Phosphoglycerokinase (E6126, Sigma Aldrich).

vi Pyruvate Kinase

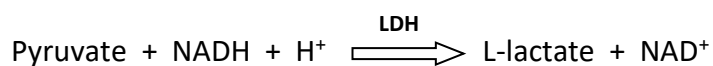
Pyruvate kinase activity was measured by recording the rate of oxidation of NADH during the following reactions:



Each sample was diluted 1 in 5 with the extraction buffer and 20 μ l of the total cell homogenate was pipetted into a 96 well plate with 180 μ l of the main reagent containing, 0.1M triethanolamine, 4mM phospho(enol)pyruvic acid (PEP), 4mM ADP, 0.4mM NADH, 5mM MgSO₄, and 5 μ l 25mg/ml LDH.

vii Lactate Dehydrogenase

LDH activity was measured by recording the rate of oxidation of NADH during the following reaction:

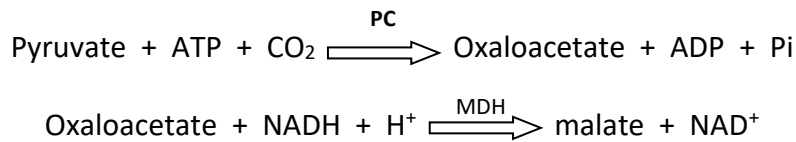


For each sample, 50 μ l of the total cell homogenate was pipetted into a 96 well plate with 150 μ l of the main reagent containing 0.2M KPi, 0.2mM NADH, and 2.8mM pyruvate.

2.6.2. Mitochondrial Enzyme Activity Assays

viii Pyruvate Carboxylase

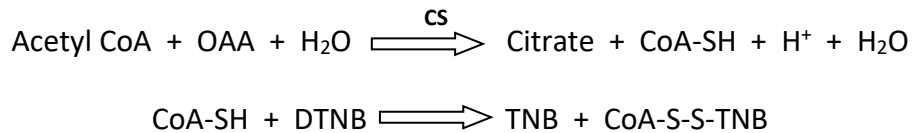
PC activity was measured by recording the rate of oxidation of NADH during the following reactions:



Samples were assayed by adding 20µl of the sample to a 96 well plate with 180µl of main reagent containing 80mM Tris, 2mM ATP, 16mM Sodium pyruvate, 22mM KHCO₃, 9mM MgSO₄, 0.32mM acetyl CoA, 0.16mM NADH, and 10µl malate dehydrogenase L(MDH-RO, Roche)

ix Citrate Synthase

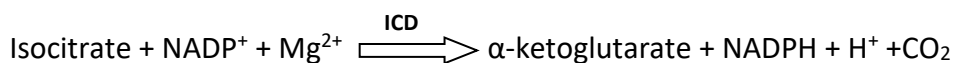
Citrate Synthase activity was measured by recording the rate of TNB production during the following reaction:



Samples were assayed by adding 20µl of the sample to a 96 well plate with 180µl of main reagent containing 50mM Tris (pH8), 0.3mM Acetyl CoA, 0.24mM oxaloacetate, and 0.2mM DTNB. Absorbance was read at 412nm every minute for 20 minutes.

x Isocitrate Dehydrogenase (NADP linked)

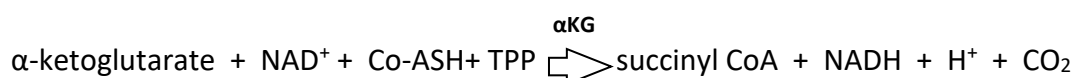
ICD activity was measured by recording the rate of NADP reduction in the following reaction:



Samples were assayed by adding 20µl of the sample to a 96 well plate with 180µl of main reagent containing 50mM KPi (pH 7.4), 10mM MgCl₂, 2.5mM isocitrate, and 0.25mM NADP (94596).

xi α-ketoglutarate Dehydrogenase

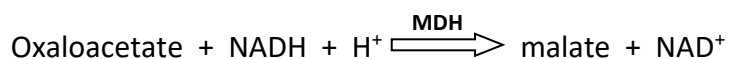
α-ketoglutarate Dehydrogenase activity was measured by recording the rate of NAD reduction in the following reaction:



Samples were assayed by adding 40µl of the sample to a 96 well plate with 160µl of main reagent containing 100mM Tris (pH 8), 0.5mM NAD, 3mM MgCl₂, 0.2mM Thiamine Pyrophosphate (TPP), 0.04mM Coenzyme A, 0.0025mM rotenone, and 5mM α-ketoglutarate.

xii Malate Dehydrogenase

Malate dehydrogenase activity was measured by recording the rate of NAD reduction in the following reaction:



Each sample was diluted 1:5 with the extraction buffer then 20µl of the sample to a 96 well plate with 180µl of main reagent containing, 0.2M KPi, 0.2mM NADH, and 2.78mM oxaloacetate.

2.7. Western Blotting

MIN6 cells (P26 - P29) from each well of a confluent 6 well plate were extracted in 2ml of extraction buffer comprising of 100mM Tris-HCL pH 7.4, 100mm NaCl, 2mM EDTA, 25mM NaF, 0.1% Triton X-100, 0.1mM Na₃VO₄, 1mM Benzamidine, 1:1000 dilution Protease Inhibitor Cocktail (Sigma Aldrich, P8340). Samples were mixed 1:4 with loading

buffer (121.4 mM Tris (pH6.8), 1.94% SDS, 10% glycerol, 0.04% bromophenol blue, 4% mercaptoethanol) and heated to 100°C for five mins and 10-40µg of protein were loaded in the gels. The gels were either made from 10% resolution gel (10% acrylamide, 39mM Tris (pH 8.8), 0.1% SDS, 1mM Temed, 1.7mM APS) and stacking gel (3% acrylamide, 0.217mM Tris pH 6.8), 0.05% SDS, 1.7mM Temed and 2.6mM APS) or readymade gels were used (4-12% SDS-PAGE gels (Bio-Rad, Hertfordshire, UK). Gels were run at 90V while samples moved through the stacking gel then 180V for 45-60 mins.

Proteins were then electro-transferred at 15V and 0.8 Amps from the gels to PVDF paper that had been pre-soaked in methanol. The Blot was then blocked in 5% milk for 1 hour then washed in TBST, TBST was composed of 25mM Tris (pH7.4), 144mM NaCl, 5ml/L Tween-20 (P1379, Sigma Aldrich). Blots were incubated with primary antibodies prepared in 0.5% milk overnight at 4°C, 1:200 (GLUT2 (NBP2-22218SS), 1:100 anti-monocarboxylic acid transporter 1 (ab90582), 1:200 connexin 36/GJA9 (QG219843), 1:200 anti-hexokinase 1 (sc-46695). The blot was then washed in TBST and incubated with the secondary antibody in a 1:2500 dilution with 0.5% milk for 1 hour at room temperature (ant-rabbit HRP (P0448) and anti-mouse HRP (P0260)). Bands were detected using enhanced chemiluminescence and quantified using image J.

2.8. Glucose Stimulated Insulin Secretion Enzyme-Linked Immunosorbent Assay (GSIS ELISA)

MIN6 (P21 – P29) were cultured for five days in 24 well plates for monolayer cultures and petri dishes for pseudoislet culture. On day five the monolayers and pseudoislets were washed in Krebs-Hepes buffer containing 119mM NaCl, 4.74mM KCl, 2.54mM CaCl₂, 1.19mM MgCl₂, 1.19mM KH₂PO₄, 25mM NaHCO₃, 10mM Hepes (pH 7.4), and 0.5% bovine serum albumin (BSA). The petri dish was washed in phosphate buffered saline and the pseudoislets were replaced in 7ml of the Krebs-Hepes buffer with 0.5mM glucose. Both the pseudoislets and the monolayers were incubated in the 0.5mM buffer for 30 minutes at 37°C then washed twice in the glucose free buffer. Approximately 200 pseudoislets were transferred to each well of a 24 well plate and incubated along with

corresponding monolayers for a further hour in Krebs-Hepes buffer containing either 5mM glucose or 25mM glucose. The supernatant was removed, and the insulin content measured using a high range rat insulin ELISA kit. The remaining cells were washed in PBS and extracted into 0.05% Triton-X 100 so that the protein concentration could be calculated through a Bradford assay and used to normalise the insulin activity.

2.9. Protein Quantification using the Bradford Method

Cells extracted for western blotting, enzyme activity analysis and GSIS ELISAs were diluted in 0.05% Triton X-100 solutions and sonicated for 20 seconds. The protein content was calculated using the Bradford method. 200µl of 1:5 v/v Biorad reagent (#5000006, Biorad) was added to 10µl of each sample as well as to 10µl samples of protein standards at 25, 50, 100, 150, 200, 300, and 500µg/ml in a 96 well plate. The plate was assayed on a plate reader using end point assay at 595nm. The concentrations of samples were calculated against the standard curve using Microsoft excel.

2.10. Metabolic Analysis

2.10.1. Seahorse XFe96 Analyser

The seahorse bioanalyser requires a microplate in which cells or 3D structures are plated and a cartridge in which drugs and compounds to be injected into the plate are loaded [100]. The cartridge contains wells for four different injections to be preloaded and injected over the course of the experiment into each well. It also has a probe which sits above the samples with two sensors, one to measure pH and one to measure O₂ concentration.

MIN6 monolayers (P26 – P29) were seeded onto plates five days before the assay. Pseudoislets were formed over five days in a petri dish then transferred to a spheroid microplate. Monolayers were seeded at a density of 1×10^4 cells/well onto a XF96 cell

culture microplate the day before testing. The pseudoislets were placed in XFe96 spheroid microplates. The wells of the spheroid plate were first coated with cell-takTM (Corning) in 0.093mM NaHCO₃ pH8 and incubated at 37°C for 20 minutes before washing in distilled water. One pseudoislet was then placed in the centre of each well with 180µl culture media and the plate was centrifuged at 200g for one minute to aid attachment.

On the day before the assay, the cartridge was hydrated by filling each well of the utility plate with 200µl of XF calibrant (100840-000, Agilent) ensuring each sensor of the cartridge is submerged then incubated in a non-CO₂ incubator overnight. On the day of the assay, the media on the assay plates was replaced with either mitochondrial stress test base media (103015-100, Agilent) containing 10mM Glucose, 1mM sodium pyruvate and 2mM L-glutamine or glycolysis stress test medium (103020-100, Agilent) containing 0.5mM glucose and 2mM L-Glutamine and the plate was incubated for one hour in a non-CO₂ incubator. During the incubation, the injections were prepared and loaded into the cartridge. For measurement of the extracellular acidification rate (ECAR), injections were 200mM glucose, 20µM oligomycin then 500mM 2-DG. For measurement of the oxygen consumption rate (OCR), the injections prepared were 20µM oligomycin, 5µM FCCP, then 5µM rotenone and antimycin A. These solutions are 10 times the final concentrations achieved once the compounds are injected into the well.

2.10.2. Seahorse XFe24 Analyser

Monolayer plates were set up as they were for the XFe96 but using 24-well plates instead of 96-well plates. Initially seeding densities of 60,000, 80,000, and 100,000 cells per well were used then 80,000 cells per well were plated in each subsequent experiment. Around 300 pseudoislets were placed in the centre of each well (excluding blanks) of a seahorse islet capture plate and an islet capture screen was placed on top of each sample. Plates were incubated in the seahorse base described in the previous step for one hour prior to incubation. Compounds injected for both OCR and ECAR measurements were glucose, oligomycin, FCCP, and antimycin A. Protein was then extracted in 0.05% Triton-X 100 so that the protein concentration could be calculated through a Bradford assay and used to normalise readings. ATP from oxidative

phosphorylation = $OCR_{\text{basal}} - OCR_{\text{oligo}}$ where OCR_{basal} is the OCR measured after the respiration of the MIN6 has reached equilibrium after addition of glucose and OCR_{oligo} is the minimum OCR after addition of oligomycin. ATP from glycolysis = $ECAR_{\text{tot}}/BP - (10^{(pH-pK1)} / (1+10^{(pH-pK1)}))(\max H^+/O_2)(OCR_{\text{tot}} - OCR_{\text{AA}})$ where $ECAR_{\text{tot}}/BP$ is the total cellular ECAR divided by the buffering capacity of the media and $OCR_{\text{tot}} - OCR_{\text{AA}}$ is the remaining OCR after mitochondrial metabolism is blocked by the addition of the complex III inhibitor, antimycin A. (1)

2.11. RT-PCR

RNA was extracted from MIN6 samples (P26 – P29) using a High Pure RNA Isolation kit (Roche, 11828665001). To quantify the RNA, 2 μ l of each sample of the sample was added to 100 μ l of distilled water and RNA standards were prepared at 5, 10, 20, 40, and 50 μ g/ml. The samples and standards were pipetted in 100 μ l volumes onto a UV microtitre plate and absorbance was measured at 260nm by a spectramax plate-reader. Then cDNA was synthesised from 0.5 μ g RNA made up to 9 μ l with distilled water and treated with 2 μ l of 50 μ M random hexamers and incubated for 10 minutes at 70°C. the RT mix was prepared containing 4 μ l MMLV buffer, 0.5 μ l MMLV, 0.5 μ l 10mM dNTP mix and 4 μ l water per sample. From this mix, 9 μ l were added to each sample and this was incubated at 37°C for 50 minutes followed by 70°C for 15 minutes.

Taqman based real time RT-PCR was performed using 18 μ l of taqman mix with 2 μ l of either H₂O blank, RNA control, cDNA standard or sample. Primer sequences are listed in 4. Relative mRNA levels were calculated from Δ cycle thresholds and corrected for the Rplp0 gene.

Gene	Gene Symbol	Species	Transcript detected
Lactate Dehydrogenase A	LDHa	Mouse, Human	Mm01612132_g1 Hs01378790_g1
Glucose Transporter Protein 1	Slc2a1	Mouse, Human	Mm00441480_m1 Hs00892681_m1
Ribosomal Protein Lateral Stalk Subunit P0	RPLP0	Mouse, Human	Mm00725448_s1 Hs99999902_m1

Table 4. Primer Sequences for RT-PCR

2.12. Statistical Analysis

All statistical analysis was carried out on GraphPad Prism 6 software. The mean and standard error mean were calculated in each case and means were compared using a paired t test to test for significance at $P < 0.05$, n numbers are representative of number of experiments.

CHAPTER 3. OPTIMISATION OF PSEUDOISLET FORMATION

3.1. Introduction

Loss of functional beta cell mass is central to the development of both type 1 and type 2 diabetes. One indicator of good beta cell function is the insulin secretion response under basal and stimulating levels of glucose. Many independent investigations have shown that increasing cell-cell contacts improved glucose stimulated insulin secretion (GSIS) from beta cells in human and rodent models, in both primary cells and cell-lines [14, 76-78, 83, 88, 89, 101-103]. However, the specific pathways that lead to the improved response are unknown. From further studies, it is known that appropriate GSIS relies on ATP production in response to nutrients, particularly glucose [11, 43, 51, 67]. However, whether improved cell-cell interactions alter metabolic flux and/or ATP production by beta cells has not been examined. In this study the influence of cell to cell connections on metabolic function in the MIN6 pancreatic beta cell line will be assessed.

One way to introduce intracellular connections between beta cells is to allow the cells to aggregate in solution to form 3D structures known as pseudoislets as described in section 1.5.2. A variety of culture methods have been used to allow the pseudoislets to form (Figure 10), they have been grouped into four different methods. The culture duration, seeding density used, cell passage number, and resulting islet size for some studies utilising these methods are collated in table 5 where available. The most common method used is static culture on surfaces which prevent attachment either by applying a coating with a low static charge or using pre-treated wells that are commercially available [77, 84-86, 104]. Stirred suspension methods are also common, this involves agitating the cells throughout the culture to maintain them in suspension [88, 105]. It has been suggested that these stirred suspension techniques result in smaller, more consistent, islets forming. Smaller islets may be advantageous as this could reduce the occurrence of necrotic cores within the pseudoislets as nutrients have a smaller distance to travel as they diffuse to the innermost cells. Other methods include

the “hanging drop” technique and co culture with other cells such as endothelial cells. Since the hanging drop technique is labour intensive and will not produce the number of islets needed for this study, this method will not be investigated further [106].

Once the pseudoislets have formed, the function of the beta cells in the pseudoislet structure in response to glucose can be assessed by investigating the amount of insulin secreted in response to glucose stimulation. This is known as the glucose stimulated insulin secretion (GSIS) response. The comparison of the GSIS of MIN6 pseudoislets to the GSIS of MIN6 cultured as monolayers can give an indication of how the formation of the 3D structure influences beta cell function in response to glucose.

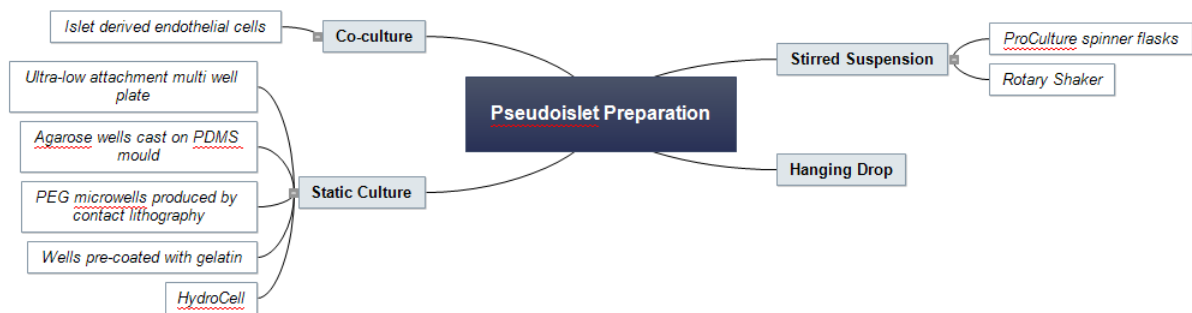


Figure 10 – Pseudoislet preparation methods described in current literature

3.2. Aims

The aim of this chapter was to optimise a method for pseudoislet formation, a combination of static and stirred suspension culture technique were used. The viability, size and function of the resulting pseudoislets was recorded by a variety of methods.

Objectives

1. Determine the optimal conditions for culture of MIN6 as pseudoislet structures.
2. Compare static vs stirred culture of pseudoislets.
3. Assess the impact of pseudoislet formation on beta cell function compared to monolayer culture.

Method	Culture duration	Cell Type	Seeding density	Passage	Islet size	Comments
Gelatin coated wells [107]	6-8 days	MIN6		43-54	3,000-5,000 MIN6/PI	
Agarose microwell [108]	7 days	Primary human islets	Microwell – 10,25,50,100,250, 500 Control - 1×10^5 cells		Microwell $93\mu\text{m} \pm 16$ Control $88\mu\text{m} \pm 49$	Aggregates containing 1000 cells were unstable.
PEG microwell [109]	5 days	MIN6	3×10^6 cells/mL (x2)			Incubated on an orbital shaker for at least 2 hours
Ultra-low attachment wells 2010 [110]	7 days	MIN6 $\alpha\text{TC1.9}$ TGP52	2×10^5 cells per well on 6 well plate.		4000 ± 379 cells per pseudoislet	
Ultra-low attachment 2015 [104]		1.1B4 Cells	1×10^5 per well on 6 well plate	25-35		
ProCulture spinner flask [87]	2 weeks (PIs in static didn't grow after 8 days)	MIN6	$2-5 \times 10^4$ cells/ml	25-40	100-200 μm	
Shaking culture [88]	10 days	RIN5F				reciprocal shaker at 70rpm for up to 10 days

Table 5. Pseudoislet Production Methods

Table showing how pseudoislet production methods vary between studies using different culture methods. Pseudoislets are produced from the MIN6 mouse pancreatic beta cell line unless otherwise specified.

3.3. Selection of optimal surface for MIN6 pseudoislet formation

First, the ideal seeding density and culture surface for the formation of pseudoislets was determined, initial densities investigated were based on the ranges of densities used previously as reported in table 3. A culture period of five days was selected as preliminary data in the lab deemed five days to be optimal to achieve an improvement in GSIS without development of a necrotic core and this culture period had been used in previous studies [78, 86]. MIN6 were cultured at seeding densities of 2.5×10^4 , 2.5×10^5 and 2.5×10^6 cells/ml on standard tissue culture 6 well plates, 6 well plates coated with (1% Wt/Vol) gelatin, and low adhesion petri dishes for five days. Images in Figure 11 show that cells on the standard 6 well plate formed a monolayer particularly at the higher seeding density. Cells in the gelatin coated wells formed pseudoislets with the most consistently sized islets forming at the middle density. However, the pseudoislets began to attach to the gelatin coated wells making extraction of intact pseudoislets difficult and the pseudoislets at the higher density began to fragment. Free floating pseudoislets formed in the petri dish and the middle density also seemed to produce the most consistent islets. The islets at the higher density varied greatly in size and the larger islets had darkened centres indicating the possibility of necrotic cores.

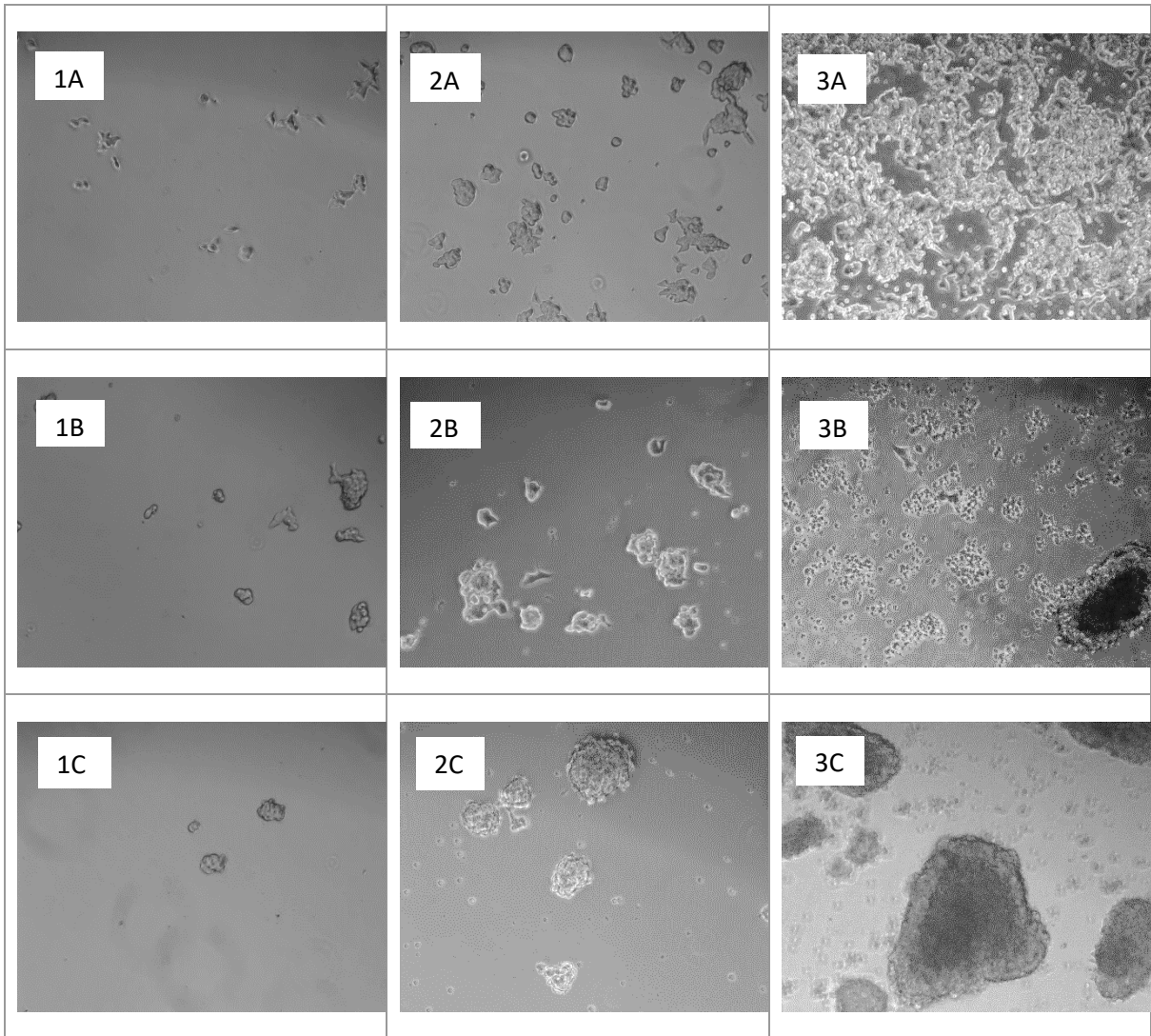


Figure 11. Images of Monolayer and Pseudoislet Formation on Various Surfaces

Light microscope images at 10x magnification of MIN6 cultured for 5 days on A) a 6 well plate, B) a gelatin coated 6 well plate and C) a low attachment petri dish each at densities of 1) 2.5×10^4 cells/ml, 2) 2.5×10^5 cells/ml and 3) 2.5×10^6 cells/ml. Representative of 1 experiment.

3.4. Selection of seeding density for optimal pseudoislet diameter

As the MIN6 seeded in the petri dish seemed to form the best islets in the initial culture all future pseudoislets were cultured in petri dishes. To further investigate the optimal seeding density, MIN6 were cultured for five days in petri dishes at seeding densities of, 1.4×10^5 , 2.9×10^5 , and 4.3×10^5 cells/ml. Islets can vary in size and shape so islet equivalent counts (IEQs) provide a method of standardising measurement of these islets relative to a standard islet of $150 \mu\text{m}$. Islets around the standard islet measurement are preferable

as islets smaller than this are likely to be fragments of islets that haven't formed properly and as islet size increases above 150µm the risks of necrotic cores increases. The IEQ counts show that as the seeding density increased the diameters of the pseudoislets became more varied with islets over 251µm in diameter being formed at the highest density (Figure 12).

Next the viability of the pseudoislets at the three seeding densities was determined. A propidium iodide stain was used to identify dead cells (red) and a Hoechst 33342 stain to identify all cells (blue) (Figure 13). For each image the percentage area covered by red or blue was calculated using CellProfiler so that the percentage viability for pseudoislets at each density could be calculated (Figure 14). The highest percentage viability was seen in the islets cultured at an initial seeding density of 2.9×10^5 cells/ml (Figure 15). At densities higher than this, the viability began to decrease and the variability between viability of islets began to increase. A seeding density to be used to produce pseudoislets in this study was selected based on the highest percentage viability and most desirable range of islet size, between 100 and 200µm. The seeding density of 2.9×10^5 cells/ml with a percentage viability of 84% was selected. Due to the limitations of fluorescence microscopy, calculations were made based only on signal from surface of the islet and does not include cells in the core of the islet.

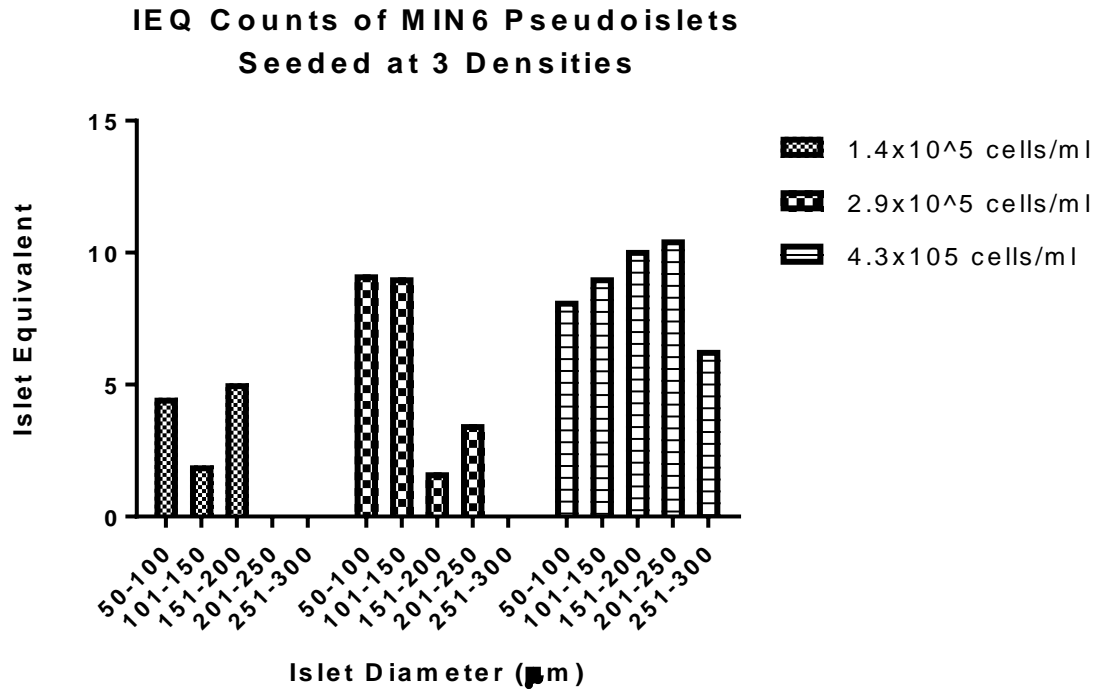


Figure 12 - IEQ counts of MIN6 cultured for 5 days in low attachment petri dishes at three different densities. N=1

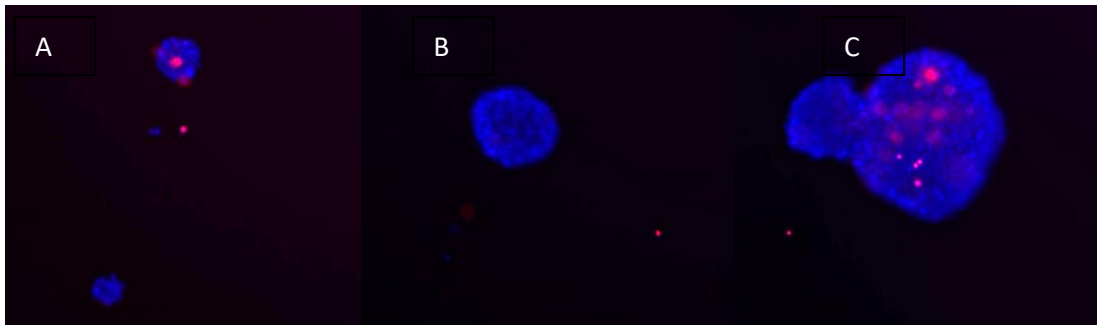


Figure 13. Viability Images of Pseudoislets

Images at 10x magnification of pseudoislets after five days of culture and stained with Propidium iodide (red) and Hoechst stain (blue). Cultures were prepared with an initial seeding density of a) 1.4×10^5 cells/ml b) 2.9×10^5 cells/ml and c) 4.3×10^5

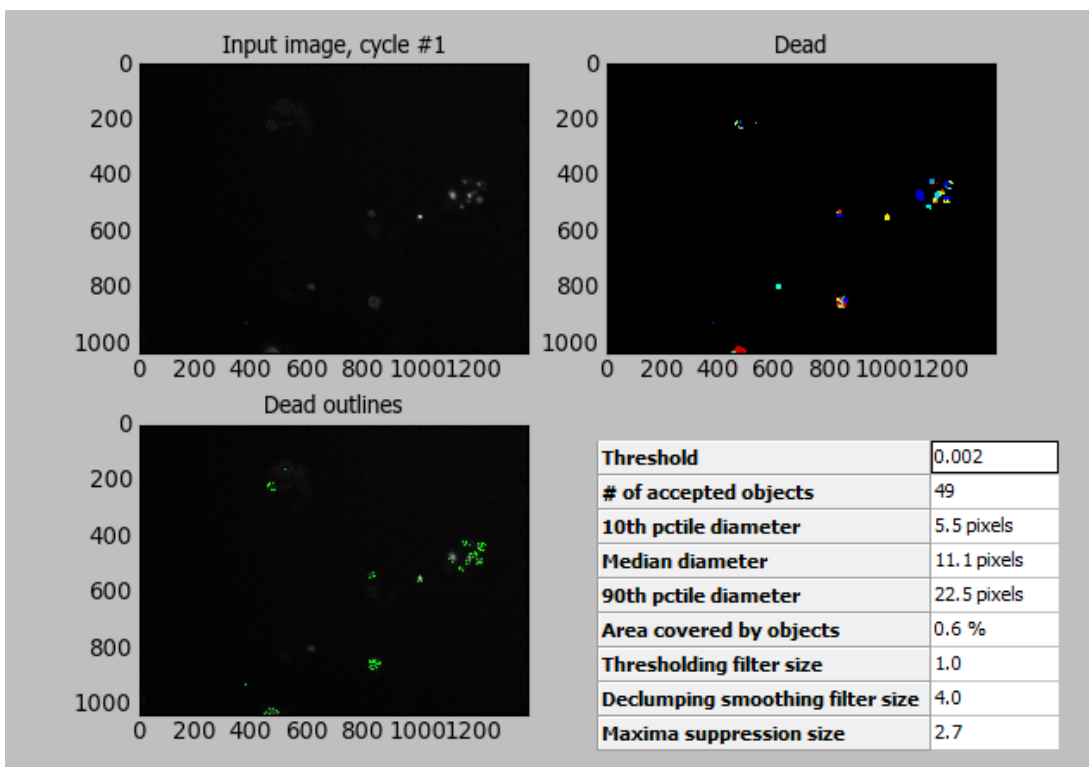
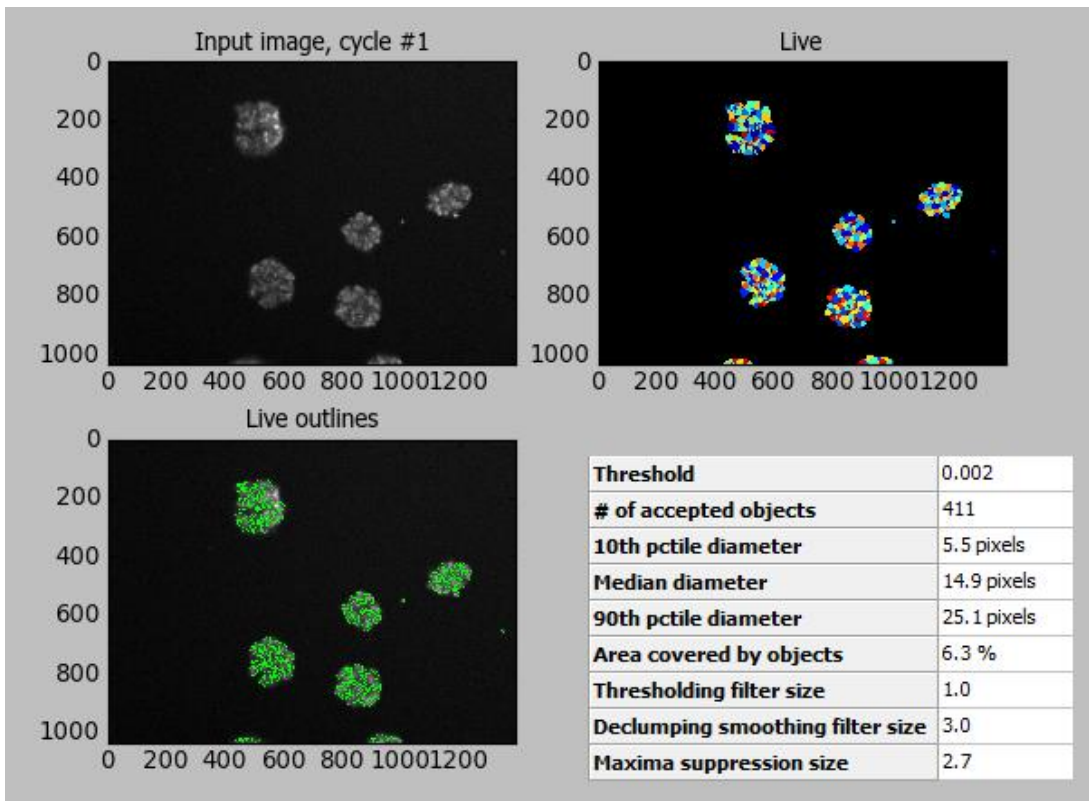


Figure 14 – Image Processing using Cell Profiler

Example of Image processing steps used to calculate percentage viability of pseudoislets using cell profiler. First calculating the % area covered by live cells shown using a Hoescht stain then the percentage area covered by dead cells using a propidium iodide stain.

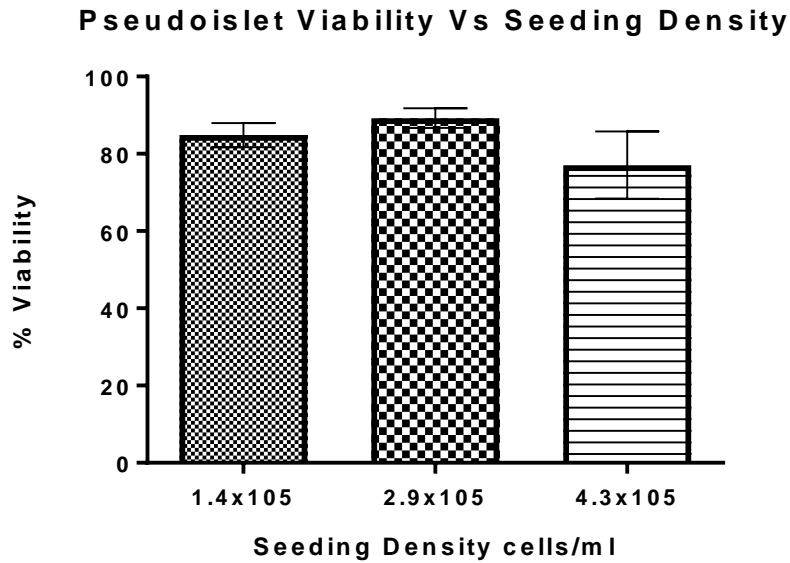


Figure 15. Seeding Density influence on Pseudoislet Viability

Percentage viability of pseudoislets cultured for five days at 3 different initial seeding densities. Calculated using a propidium iodide stain to identify dead cells and a Hoechst stain to identify viable cells. Mean ± SEM N=5

3.5. Comparison of static or stirred suspension culture methods for Pseudoislet formation

Previous studies have reported that pseudoislets cultured in stirred suspension display improved viability and consistency in size to those cultured in a static system [88, 105]. Preliminary data in the laboratory deemed five days to be optimal to achieve an improvement in GSIS without development of a necrotic core, this culture period has also been used elsewhere [80]. To compare pseudoislets formed in each culture system and to determine whether a stirred suspension culture system would be beneficial, MIN6 were cultured for either five days on static culture or two days of static followed by three days of stirred suspension on an orbital shaker. The IEQ counts show that in this case the pseudoislets that formed in static culture were smaller and more consistent in size than those in stirred suspension (Figure 16). The viability of pseudoislets was then compared with a propidium iodide and Hoechst stain (Figure 17). The islets produced through just static culture were mostly between 100 and 200µm in diameter which is accepted in this study as the optimal size (Figure 16). The viability of islets from both

culture systems was similar with a high proportion of viable cells. Stirred culture offered no improvement in viability and unfortunately did not produce consistently sized pseudoislets so static culture was used for the formation of pseudoislets for the remainder of the study.

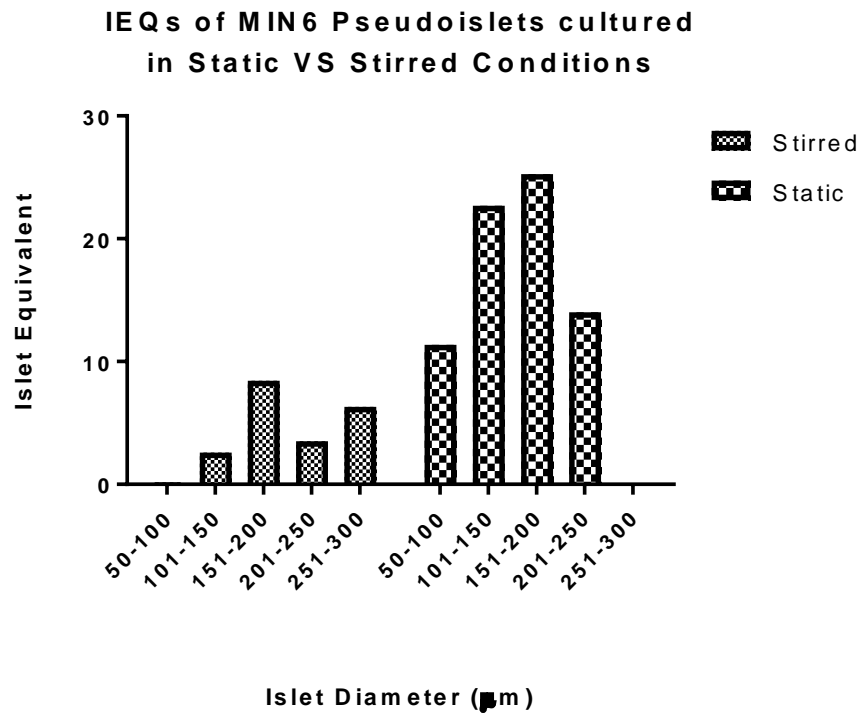


Figure 16 - IEQ counts of MIN6 cultured for five days in either stirred suspension (stirred) or in low attachment petri dishes (static). N=1

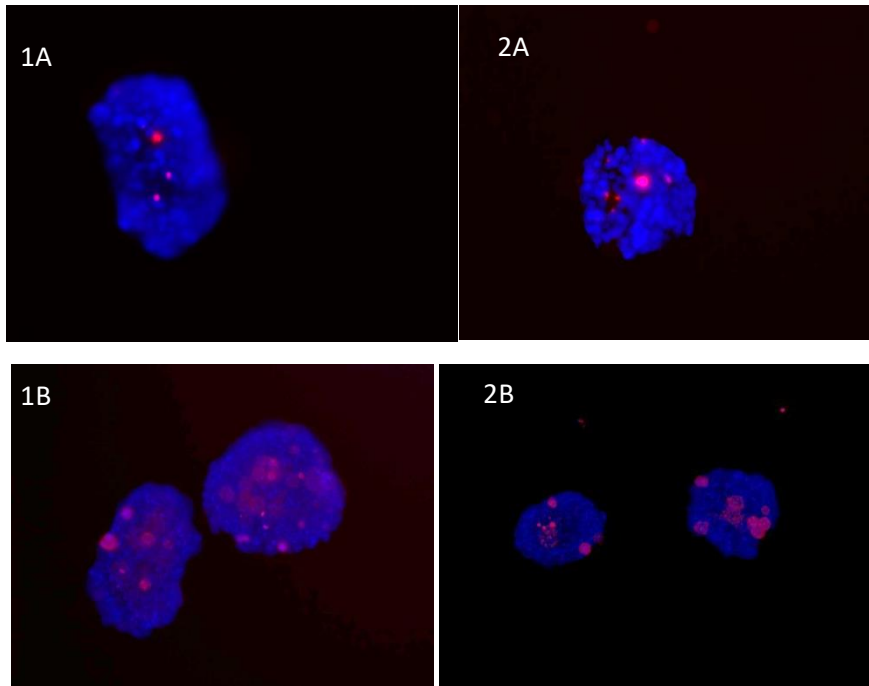


Figure 17. Pseudoislet Viability Images of Static Vs Stirred Culture

Propidium iodide (red) and Hoechst stain (blue) to show viability of pseudoislets cultured in A) static culture and B) stirred suspension for five days. Images are taken at 1) 10x and 2) 20x magnification.

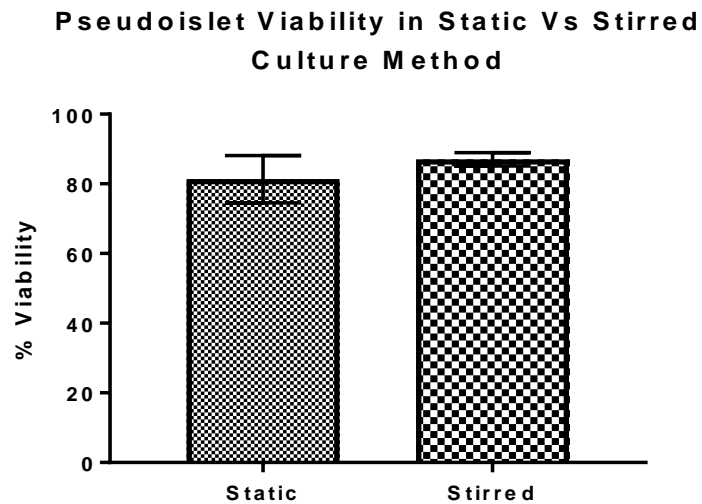


Figure 18. Pseudoislet Viability in Static Vs Stirred Culture Methods

Percentage viability of pseudoislets cultured for either five days in static culture or 4 days in static plus one day in a stirred suspension. Calculated using a propidium iodide stain to identify dead cells and a Hoechst stain to identify viable cells. Based on one experiment, error bars based on technical replicates.

3.6. Impact of pseudoislet formation on insulin secretion

3.6.1. Optimisation of GSIS measurements for Pseudoislets

To confirm that pseudoislet formation increased the glucose stimulated insulin secretion response as described in previous studies [65], insulin secretion was measured at 3mM glucose and 16.7mM glucose. To test this, we incubated pseudoislets and monolayers in media without glucose for 30 minutes and then stimulated with 3mM versus 16.7mM glucose for 1 hour. However, the results showed that the insulin secretion was higher at 3mM glucose than at 16.7mM glucose, particularly in the pseudoislet cultures (Figure 19). This may be because the cells at the lower glucose concentration were releasing insulin under stress, to avoid this the glucose concentrations used were altered.

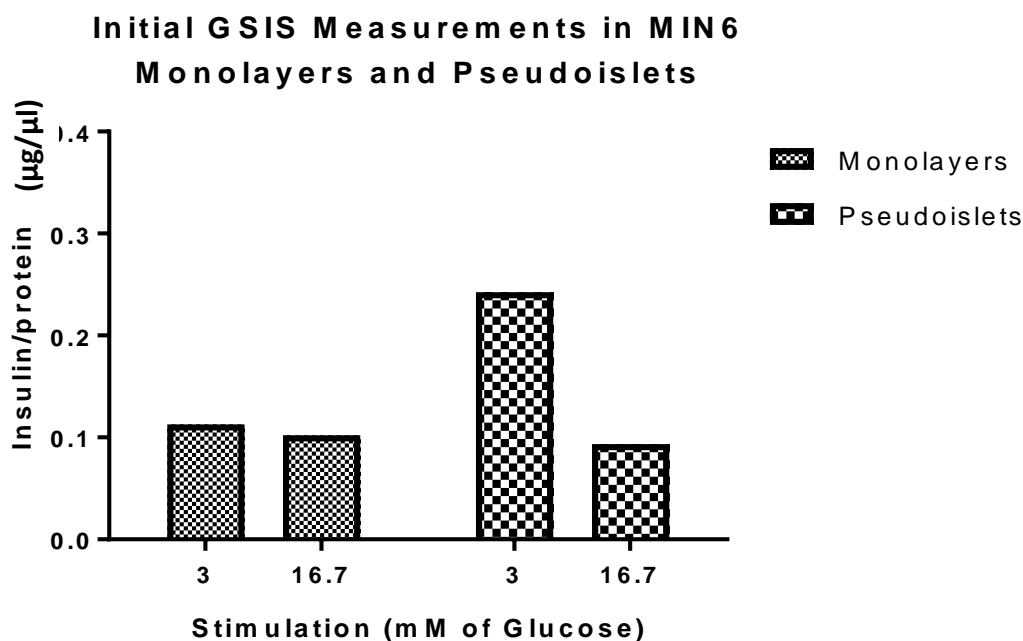


Figure 19. Initial GSIS Measurements

Insulin secretion response of MIN6 (P21-P25) cultured as either monolayers or pseudoislets for 5 days and incubated for 30 minutes in glucose free media then 1 hour at either 3mM glucose or 16.7mM glucose. N=1

Instead of starving the MIN6 before glucose stimulation, samples were incubated in either 0.5mM or 3mM glucose for 30 minutes. The insulin secretion response was

stimulated by one hour of incubation at either 3mM, 5mM, 16.7mM, or 25mM glucose (Figure 20). There was no difference between samples incubated at the initial concentration of 0.5mM or 3mM glucose. The basal insulin secretion was lower at 5mM glucose than at 3mM glucose. Incubation at both 16.7mM and 25mM glucose increased insulin secretion with the 25mM glucose concentration stimulating the highest secretion. In future assays, islets will be preincubated at 0.5mM glucose and 5mM and 25mM glucose concentrations will be used to compare non-stimulating and stimulating conditions.

Optimising Glucose Concentration for GSIS

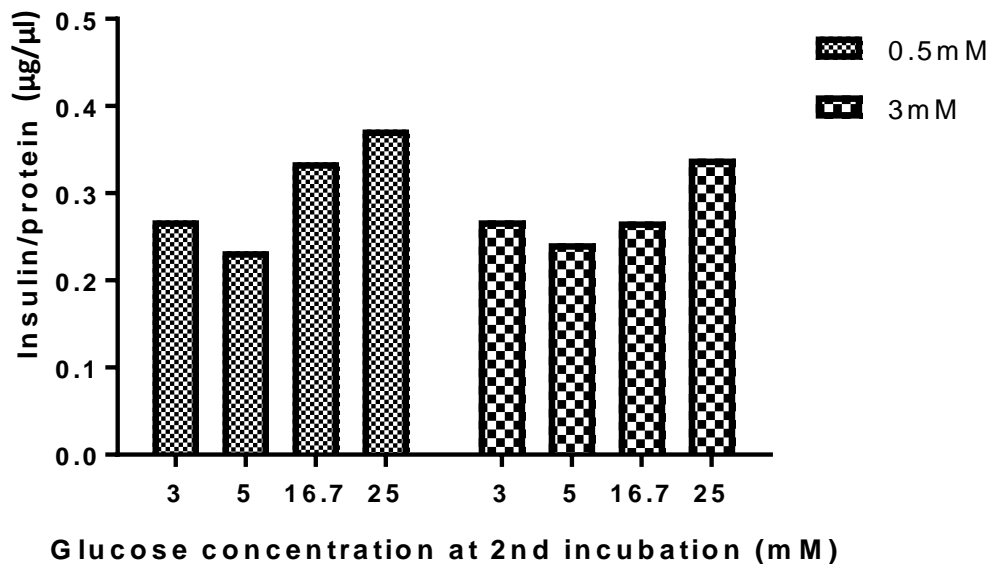


Figure 20. Optimising Glucose Concentration for GSIS.

Insulin secretion response of MIN6 (P21-P25) cultured as pseudoislets for 5 days and incubated for 30 minutes at either 0.5mM or 3mM glucose then 1 hour at either 3mM glucose or 16.7mM glucose. N=1

3.6.2. Effect of Seeding Density on Insulin Secretion

The insulin secretion response measured was still not optimal so the effect of using different seeding densities when setting up the pseudoislet cultures was investigated. The seeding densities used when plating the MIN6 for pseudoislet formation were 1.4×10^5 cells/ml, 2.8×10^5 cells/ml, or 4.2×10^5 cells/ml. Insulin secretion was measured

during incubation with 5mM glucose and 25mM glucose. There was no difference in insulin secretion response between the monolayers and pseudoislets formed from any of the three cell densities (Figure 21). The viability was highest in the pseudoislets seeded at the middle density, 2.8×10^5 cells/ml so this is the density that will be used in future experiments.

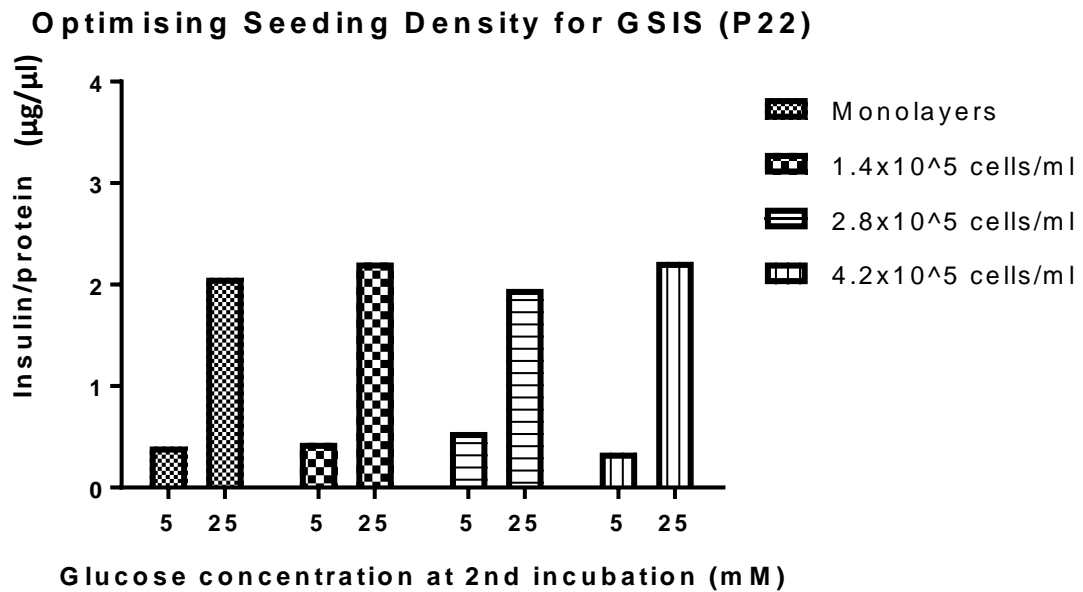


Figure 21. Optimisation of Seeding Density for GSIS

Insulin secretion response of MIN6 (P21-P25) cultured as monolayers or pseudoislets with one of 3 different initial seeding densities for 5 days and incubated for 30 mins in 0.5mM Glucose media then 1 hour at either 5mM glucose

3.6.3. Effect of cell passage on insulin secretion

MIN6 cells have been characterised as stable for 30 to 40 passages but the GSIS response tends to decrease beyond P30 [111]. This loss is associated with changes in gene expression, protein levels and metabolism [7]. The high passage MIN6 cells display decreased glucose uptake and oxidation resulting in reduced ATP levels in cells under high glucose [112]. Due to the loss of responsiveness of the older MIN6 monolayers, the influence of passage number on basal insulin secretion was determined. A comparison of insulin secretion response in MIN6 monolayers at low and high passage numbers, defined as <P26 and >P26, respectively, showed a significantly higher basal insulin secretion in the high passage cells (Figure 22). Low passage ranged from P22 to P25, whilst high passage ranged from P26 to P29. The glucose responsiveness was impaired in the higher passage cells with low passage displaying a 3.5-fold increase in insulin secretion and high passage displaying only a 1.6-fold increase. This was also shown by plotting the basal insulin secretion against passage number, here there is a clear upwards trend in basal insulin secretion with passage number (Figure 23). The basal insulin secretion response of pseudoislets was not influenced by passage number but the increase in insulin secretion at high glucose only became significant at high passage (Figure 24).

MIN6 Monolayer Insulin Secretion at High and Low Passage

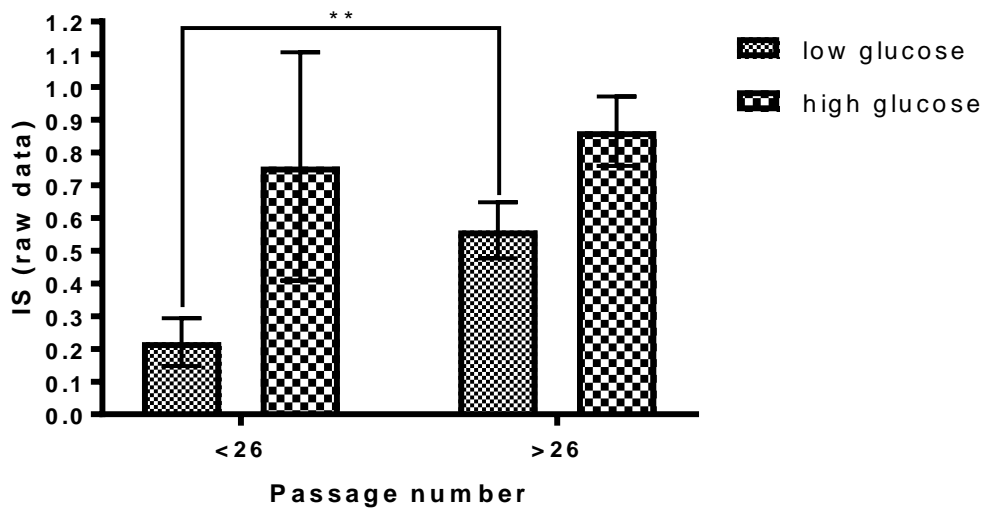


Figure 22. MIN6 Monolayer Insulin Secretion at High and Low Passage

Insulin secretion response of MIN6 cultured as monolayers for 5 days then incubated in 0.5mM glucose for 30 minutes before being exposed to low glucose $\leq 5\text{mM}$ or high glucose $\geq 16.7\text{mM}$. N=7 for low passage (P21-P25), n=6 for high passage (P26-P29) (** P<0.007).

Monolayer Basal Insulin Secretion

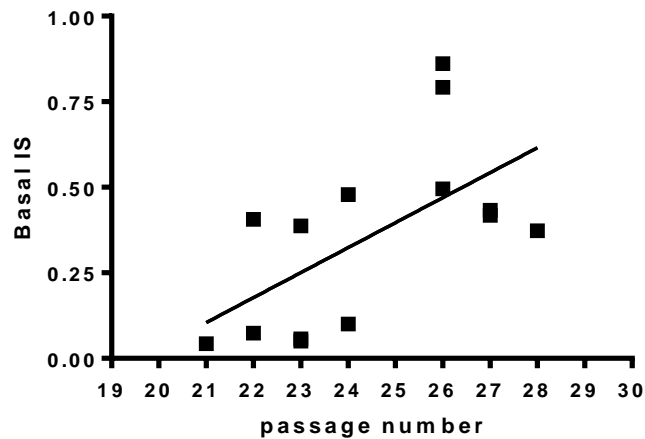


Figure 23. Monolayer Basal Insulin Increase with Passage Number

Basal insulin secretion of MIN6 (P21-P29) cultured as monolayers and incubated for 30 minutes at 0.5mM glucose then 1 hour at 3mM glucose N=13 ($R^2=0.3675$, P=0.02, linear regression)

MIN6 Pseudoislet Insulin Secretion at High and Low Passage

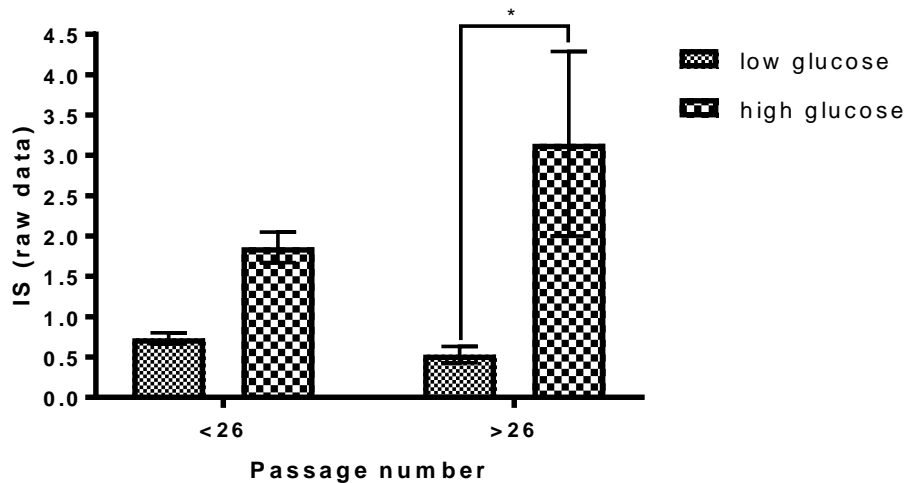


Figure 24. MIN6 Pseudoislet Insulin Secretion at High and Low Passage

Basal insulin secretion of MIN6 (P21-P29) cultured as pseudoislets for 5 days and incubated for 30 minutes at 0.5mM glucose then 1 hour at low glucose $\leq 5\text{mM}$ or high glucose $\geq 16.7\text{mM}$. N=5 * P<0.03

3.6.4. comparing glucose induced insulin secretion in 2D vs 3D Structures

Once it had been established that changes in function between 2D and 3D structures are more obvious at higher passages when the beta cells begin to function less efficiently, GSIS was assessed in monolayer and pseudoislet MIN6 using only higher passage cells, P25-P28. The monolayers showed no significant increase in insulin secretion between low glucose and high glucose but a significant increase in insulin secretion was seen between pseudoislets at low glucose and high glucose (P<0.001) (Figure 25). The pseudoislet increase in insulin secretion was 7.4-fold whilst the monolayers were much less responsive showing only a 1.5-fold increase in insulin secretion. The basal insulin secretion may be slightly higher in monolayers, but this is not statistically significant.

GSIS Response in Monolayer Vs Pseudoislet MIN6

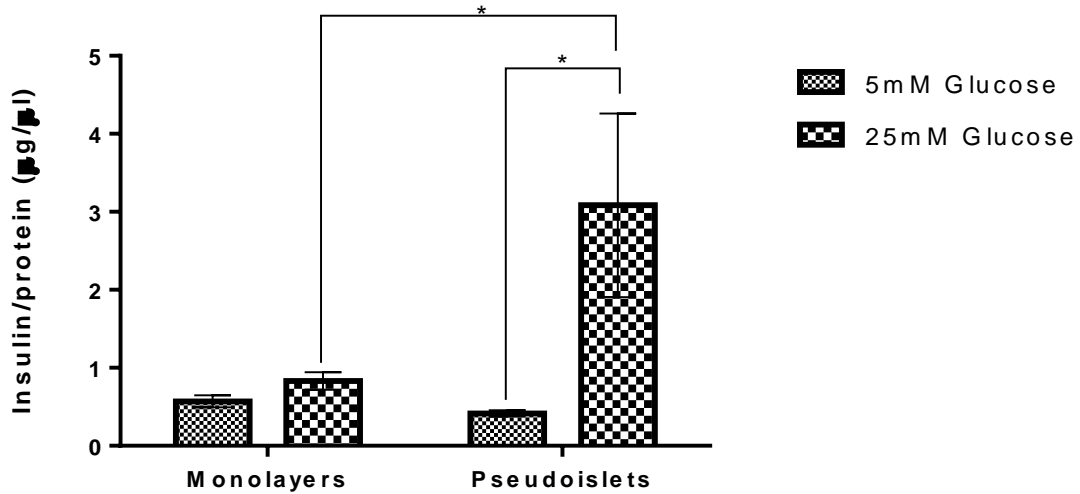


Figure 25. GSIS Response in Monolayer Vs Pseudoislet MIN6

Insulin secretion response of MIN6 (P25 to P29) cultured as either monolayers or pseudoislets for 5 days and incubated for 30 minutes in 0.5mM glucose media then 1 hour at either 5mM glucose or 25mM glucose. N=5, * = $p < 0.005$, ** = $p < 0.001$. No significant differences between basal insulin secretion in monolayers and pseudoislets.

3.7. CONCLUSION

3.7.1. Pseudoislet Formation

The first aim of this investigation was to develop a protocol to produce pseudoislets that were consistent in size, viability and function. Review of previous studies utilising pseudoislets showed that the methods currently used to produce pseudoislets vary and so different culture methods and seeding densities were compared to determine the optimal method for producing consistent pseudoislets. In most studies pseudoislets were formed over five to eight days on either a non-adhesive tissue culture plate [84] or in gelatin coated wells [77] and seeding densities ranged from 2×10^4 cells/ml [105] to 1×10^5 cells/ml [84].

In this study it was found that MIN6 cultured in gelatine coated wells and in petri dishes both aggregated to form pseudoislets but in the gelatine coated wells the pseudoislets began to attach to the bottom of the well after the first day. Therefore, petri-dishes were used for the remainder of the study. The ideal islet size to be used in this study is between 100 and 200 μ m based on the average diameter of a native islet being 150 μ m [8]. Approaches to optimise seeding density showed that many of the pseudoislets formed at the lowest density (1.4×10^5 cells/ml) were small, below 100 μ m in diameter, and often fragmented whilst pseudoislets formed at the highest seeding density displayed a much greater range in size but also showed lower viability. This may be because the larger islets, particularly those over 200 μ m in diameter, developed necrotic cores due to the restricted flow of nutrients to the cells in the centre of the islet. The middle seeding density of 2.9×10^5 cells/ml produced the pseudoislets with the highest viability and the lowest variability in size with most islets being between 50 and 200 μ m in diameter. The insulin secretion response of pseudoislets formed from MIN6 seeded at the three densities was also measured and it was found that seeding density had no influence on insulin secretion response when the cells were at a low passage number but at a higher passage number the response of pseudoislets from the highest seeding density was lower. From these findings the seeding density of 2.9×10^5 cells/ml in petri

dishes was selected as the optimal conditions for static culture, this was similar to the seeding density used by Bernard, 2012 [86].

Some studies have suggested that over prolonged culture, stirred suspension culture systems offer tighter control over cluster sizes and improved transfer in metabolites, which may maintain the viability of the cells [105]. In this study, pseudoislets were formed over 5 days either on continuous static culture or with stirred suspension for the final 2 days. There was no change in the size and viability of the pseudoislets on day 5 suggesting that over 5-day culture, stirred suspension doesn't offer any benefit. Other studies reporting improved viability with stirred suspension were cultured over longer time periods, up to two weeks [105]. It may be that there was less clustering of fully formed islets in the stirred suspension system, but this was not quantified. Propidium iodide staining showed that the stirred suspension offered slightly more consistency in viability but not enough to outweigh the benefits of the islet size distribution offered by the static culture. The static culture system showed viability of more than 80% and so provided a good model for the formation of all further pseudoislets used in this study.

3.7.2. Passage Number Influences Insulin Secretion

At low passage number, <P26, the monolayers displayed good GSIS that was similar to the GSIS seen in pseudoislets. However, at high passage number, >P26, the GSIS response in monolayers was less efficient. Basal insulin secretion was higher and the increase in insulin secretion at high glucose compared to low glucose was small, this is similar to the functional phenotype in models of T2DM [20, 113]. Using both *in situ* tissue technology and acute human pancreas specimens, Cohrs et al showed that functional deterioration occurred in beta cells during early stages of T2DM before stages where loss of beta cell mass was observed [114]. This deterioration in function included an increase in basal insulin release and a loss in first phase insulin release. Function declined further as the pathogenesis as T2DM progressed with the second phase insulin secretion beginning to also decline. In another study, dynamic parameters of beta cell function

were measured in 188 individuals (19 lean NGT, 42 obese NGT, 22 IGT, and 105 T2DM)[115]. The parameters included glucose sensitivity, rate sensitivity, and potentiation. They showed that impaired glucose sensitivity began in the early stages of IGT and beta cell function continued to decline through progression to T2DM. Longitudinal studies involving Pima Indians indicated that both insulin secretion and insulin action significantly decrease early in the development of T2DM [116], and that a high fasting plasma insulin concentration is predicative of T2DM [117]. Pseudoislets showed an improved GSIS response compared to monolayers which was only evident at a higher passage number. Hauge-Evans et al also report that differences in function between monolayers and pseudoislets become more obvious at higher passages, P43-P53 [77]. Studies reporting that pseudoislets display a superior insulin secretion response compared to monolayers do not always include the cell passage number or include a large range of passage numbers (P20-P35 [104], P25-P40 [105]). This means the effect of passage number on insulin secretion is not clear. It is possible that at low passages the function of the beta cells is already optimal and cannot be improved by arranging the cells as pseudoislets so differences in insulin secretion response between pseudoislets and monolayers only becomes clear in older cells to drop. This is only relevant to the MIN6 system as changes have been shown in dispersed versus reaggregated rodent islets [16].

3.7.3. Pseudoislet Formation Appears to Improve Insulin Secretion Response

Once the insulin secretion assay was optimised, our studies showed that pseudoislets offered an improved insulin secretion response similar to that shown in previous studies. There is a large increase in insulin secretion in the pseudoislets with glucose stimulation from 0.4 to 3 $\mu\text{g}/\mu\text{l}$ but only a slight increase is seen in the monolayers (0.6 to 0.8 $\mu\text{g}/\mu\text{l}$). It appears that the basal insulin secretion was slightly higher in monolayers than in pseudoislets, although this did not reach statistical significance. Previous studies have also shown that basal insulin secretion is higher in cells lacking connections through either dispersion, monolayer culture or Cx36 knock down [70, 118]. It is important that

basal insulin secretion is low to prevent inappropriate insulin secretion in the absence of glucose so this increase could indicate a less efficient insulin secretion pathway [53].

CHAPTER 4. ANALYSIS OF METABOLIC FUNCTION IN 2D VS 3D STRUCTURES

4.1. Introduction

It has been shown, both in previous literature [14, 76-78, 83, 88, 89, 101-103] and using the pseudoislets formed in this study, that beta cells arranged as a 3D structure display a greater insulin secretion response to glucose than beta cells cultured in monolayer. As a good insulin secretion response relies on optimal metabolism through the glycolytic and mitochondrial pathways [57] it is of interest to investigate differences in metabolic function between the two culture systems. It is known that an optimal insulin secretion response relies on the beta cells displaying a specific metabolic phenotype. This metabolic phenotype is discussed in section 1.4.2. but in summary involves tight coupling between glycolytic and mitochondrial metabolism [53] with low expression of hexokinase-1, lactate dehydrogenase, and monocarboxylate transporters [54, 55]. This phenotype exists to optimise ATP production from glucose metabolism to ensure a robust GSIS response from beta cells.

The oxygen consumption rate of islets has been measured using Clark oxygen electrodes and using Seahorse XF Bioanalysers [100, 119-121]. Oxygen consumption rate is directly linked to the flow through the electron transport chain and therefore ATP produced in the mitochondria. High oxygen consumption rates in islets have been shown to improve transplant efficacy [122]. However, proton leak across the mitochondrial membrane leads to some oxygen consumption which is not linked to ATP production. A high level of proton leak in beta cells indicates a lower bioenergetic efficiency. Wilkstrom et al compared the extent of mitochondrial proton leak in the rat insulinoma cell line, INS-1, and islets from both mouse and human donors. This study used oxygen consumption rate in the presence of oligomycin and FCCP to calculate the rate of proton leak as a percentage of basal respiration. They reported that mouse islets displayed the highest levels of proton leak, between 50 and 60% whilst INS-1 cells and human islets from both diabetic and non-diabetic donors all displayed around 38% proton leak, a significantly

lower amount than the mouse islets. This highlights possible differences in the bioenergetic profile of mouse and human islets [123]. Investigation into the stimulation of human islets by four different fatty acids showed 1.1 to 1.5 fold increases in OCR and 1.2 to 1.6 fold increases in ECAR when compared to basal rates [124]. The metabolic phenotype of insulin producing human embryonic stem cell derived beta cells (SC- β) was compared with that of human embryonic stem cells (hESCs). The highly glycolytic stem cells increased their mitochondrial mass and activity as they differentiated towards a beta cell like phenotype thereby switching to oxidative phosphorylation as the primary energy source. The ratio of glycolytic to mitochondrial respiration (ECAR/OCR) was calculated at high (20mM) and low (2mM) glucose. This ratio was shown to be higher in hESCs than in SC- β s indicating relatively higher glycolysis in hESCs. The ratio increased slightly when the glucose concentration increased which may indicate an increase in glycolytic contributions to energy production under stimulating conditions [121].

In this study, to determine whether the improved GSIS in pseudoislets could be due to improved coupling of glycolysis to mitochondrial metabolism, flux through glycolysis and mitochondrial respiration was assessed using the seahorse bioanalyser (Agilent). This system allows accurate measurement of the oxygen consumption rate oxygen consumption rate (OCR) and extracellular acidification rate (ECAR) in real time by lowering a probe containing an oxygen sensor and a pH sensor into each well and taking measurements in a transient micro-chamber above each cell sample [100]. Compounds can then be injected into the wells and the influence on the metabolism recorded. Typically, the first measurements will be taken before any injections; these initial measurements record basal metabolism. At seven-minute intervals, the oxygen consumption and proton excretion rate were measured for a period of three minutes, from this the OCR and ECAR can be calculated. After three measurements of basal cellular OCR and ECAR have been recorded, compounds or substrates to activate or inhibit respiration were added sequentially through injection ports. The first injection was either base media at 0.5mM glucose, 25mM glucose or 10mM pyruvate. The second injection contained the ATP synthase inhibitor oligomycin to block oxidative phosphorylation so that the mitochondrial respiration associated with ATP production

can be calculated from the resulting decrease in OCR. The third injection used in the Agilent seahorse protocols is the uncoupling agent FCCP which results in the uninhibited electron flow through the electron transport chain so that oxygen is maximally consumed by complex IV to establish maximal respiratory capacity. Finally, either Antimycin A is injected inhibiting complex III to assess non-mitochondrial respiration or 2-DG to block glycolysis and measure non-glycolytic acidification. Figure 26 shows common cellular responses to the compounds listed in the Agilent protocols and some of the mitochondrial and glycolytic parameters that can be calculated from the data.

Glycolytic rate is determined by measurement of extracellular acidification which is predominantly determined by lactate release from cells since lactate separates at neutral pH to form two lactate ions and two protons, leading to a decrease in pH. However, CO₂ produced during the mitochondrial metabolism of glucose through the TCA cycle also contributes to extracellular acidification. In the TCA cycle, one glucose molecule will yield six CO₂ molecules resulting in six HCO₃⁻ and six protons [125]. From this we can see that the ECAR due to mitochondrial metabolism is three times greater than that due to glycolysis. The rate of mitochondrial metabolism is already calculated from the OCR, so any contributions of mitochondrial metabolism to the ECAR can be subtracted allowing the rate of glycolysis to be calculated from the remaining ECAR. The pH and buffering potential of the media was also considered in this calculation. This method of measuring the contributions of ATP production from glycolysis has been verified by Mookerjee et al [126].

4.1.2. Aims

The aim was to compare the metabolic flux of 2D vs 3D structures to determine whether the improvement in GSIS can be explained by changes in the metabolic profile of the cells.

Objectives

- Optimise seahorse bioanalyser protocols to compare metabolism of beta cells cultured in 2D or 3D structures
- Measure ATP production from glycolysis and mitochondrial metabolism in beta cells
- Compare metabolic responses to glucose and pyruvate in the 2D and 3D structures.
- Assess metabolic profile of human islets and comparison with pseudoislets

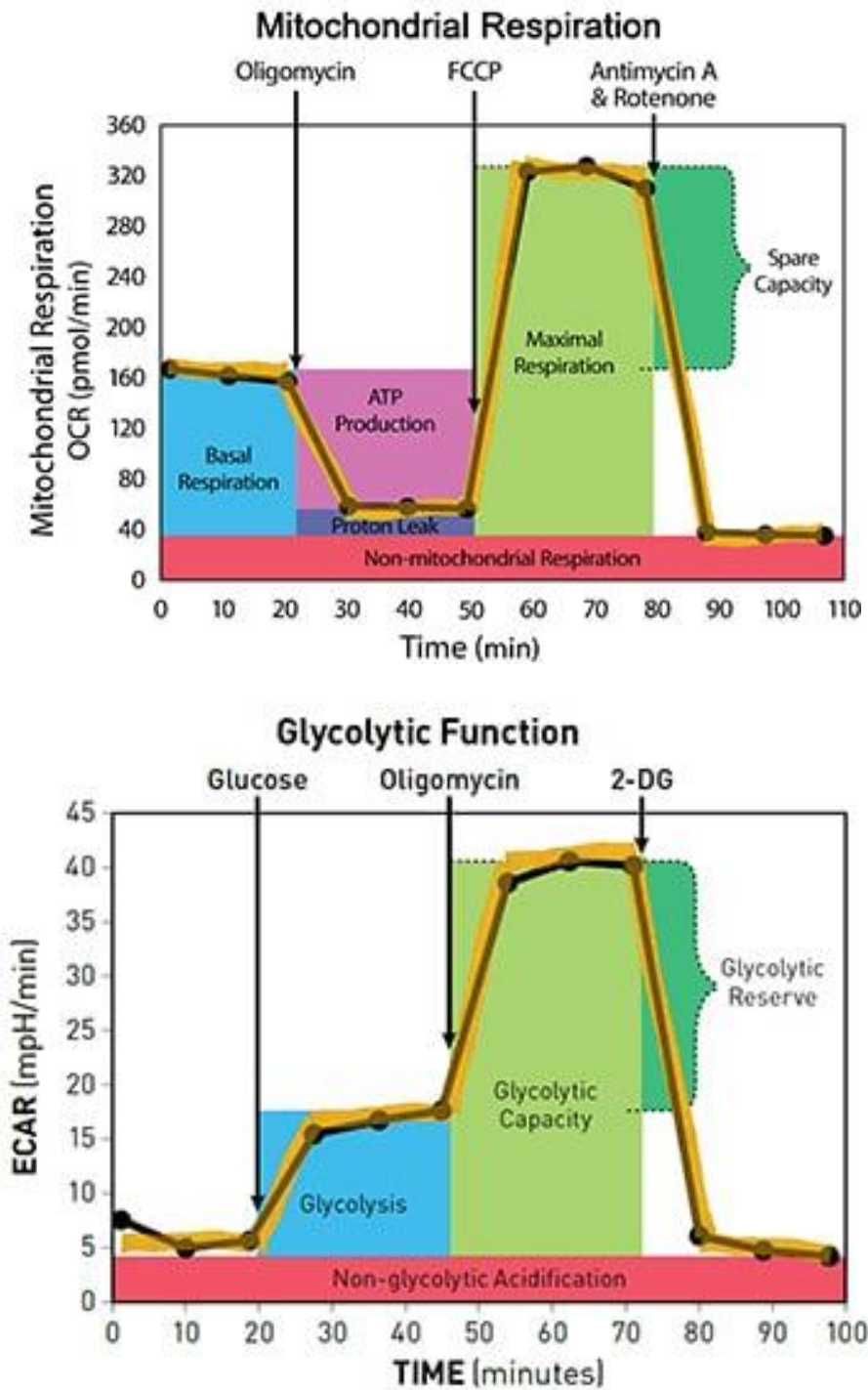


Figure 26. Seahorse Bioanalyser Parameters [100]

Examples of metabolic function parameters that can be calculated from Seahorse Bioanalyser data taken from the “Agilent Seahorse XF Cell Mito Stress Test Kit User Guide” and the “Agilent Seahorse XF Glycolysis Stress Test Kit User Guide”

4.2. XFe96 Bioanalyser Optimisation

To begin optimisation for measuring the metabolic function of beta cells in 2D and 3D structures, the Agilent Seahorse XF user guides were used. The utilisation of the XFe96 bioanalyser was explored first as this machine was in the same building as the cells and would avoid any unnecessary transport of the samples to other locations. Initially, the Agilent user guide was used to determine whether this format would be appropriate for accurate measurement of flux in both 2D and 3D structures. The plan was to determine the appropriate conditions and concentrations of oligomycin to assess ATP-linked mitochondrial respiration and FCCP to assess the maximal respiration capacity. This was done first in monolayer culture as it is a more simplistic model. The next step was to use these optimised conditions to assess the validity of the method to measure metabolic flux in 3D structures. Using a 96 well plate format, the oligomycin and FCCP concentrations required to gain maximal functional response in MIN6 cells were optimized. All other concentrations used throughout the use of the XFe96 bioanalyser were according to those listed in the user guides. The concentrations of compounds placed in the cartridge to be injected were 10 times higher than the final concentration in the well after injection. To avoid confusion, the concentrations described always refer to the final concentration in each well.

4.2.1. Selection of oligomycin and FCCP concentrations for seahorse analyser

ECAR and OCR measurements were recorded at varying concentrations of oligomycin and FCCP respectively (figures 27-30). ECAR changes were measured by subtracting the third ECAR measurement after glucose addition from the highest measurement after oligomycin addition, the resulting values showed an increase between 0.5 μ M and 2 μ M oligomycin with the greatest response seen at 2 μ M oligomycin which is the highest recommended dose in the seahorse Agilent protocols (Figure 27, Figure 28). OCR changes were measured by subtracting the third OCR measurement after oligomycin addition from the highest measurement after FCCP addition, this showed an increase

between 0.125 μ M FCCP and 0.5 μ M FCCP but no further increase was seen at higher doses so 0.5 μ M FCCP was selected to be used in future experiments (figures 29 and 30).

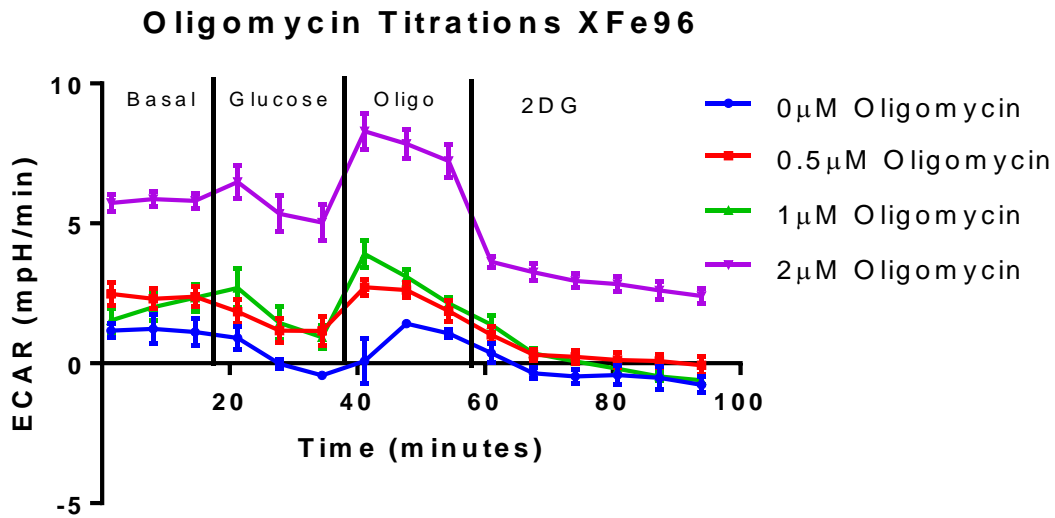


Figure 27. ECAR Response to Oligomycin Titrations

ECAR response in MIN6 (P21 - P25) monolayers after addition of 25mM glucose, either 0 μ M, 0.5 μ M, 1 μ M or 2 μ M oligomycin, then 50mM 2-DG measured on a seahorse XFe96 bioanalyzer. MIN6 were cultured for 24 hours on a 96 well microplate and starved for one hour in 0.5mM glucose prior to the experiment. 4 to 5 technical repeats per data point, n=1.

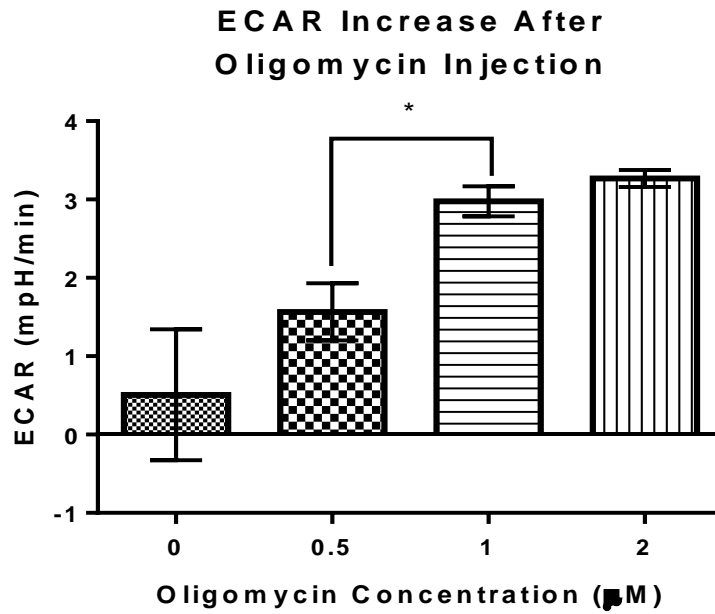


Figure 28. ECAR Increase After Oligomycin Injections

ECAR response on MIN6 (P21 – P25) monolayers after addition of oligomycin at 0.5µM, 1µM, or 2µM measured on a seahorse XFe96 bioanalyzer. MIN6 were cultured for 24 hours on a 96 well microplate and starved for one hour in 0.5mM glucose prior to the experiment. n=4. * = P<0.01

FCCP Titrations XFe96

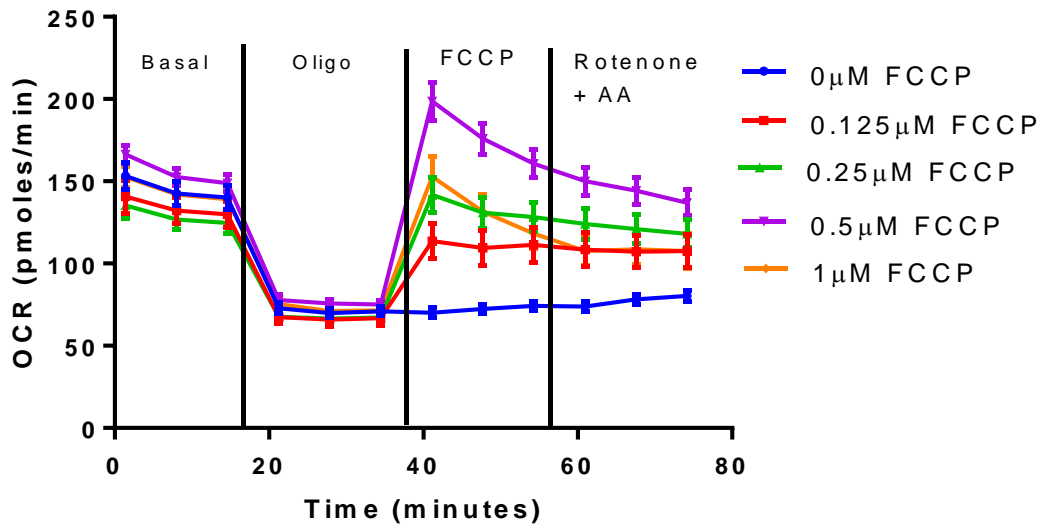


Figure 29. OCR Response to FCCP Titrations

OCR response in MIN6 (P21 – P25) monolayers after addition of 2μM oligomycin, FCCP at one of six different concentrations, then 0.5μM rotenone and antimycin A measured on a seahorse XFe96 bioanalyzer. MIN6 were cultured for 24 hours on a 96 well microplate and starved for one hour in 0.5mM glucose prior to the experiment. 14 to 16 technical repeats per data point, n=1.

OCR Increase After FCCP Injection

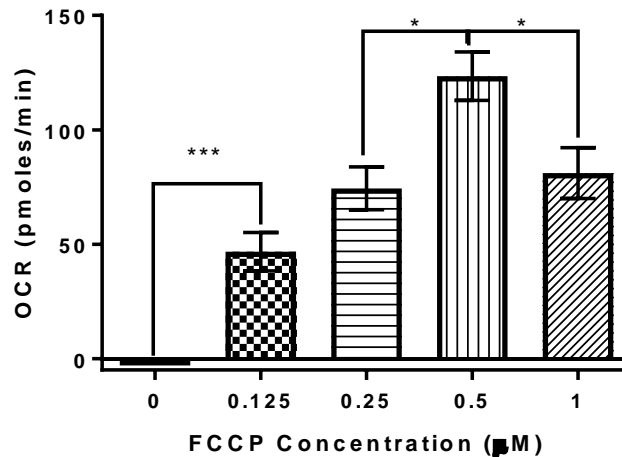


Figure 30. OCR Increase after FCCP Injections

OCR increase shown by MIN6 (P21 – P25) monolayers under 2μM oligomycin after addition of FCCP at 0μM, 0.125μM, 0.25μM, 0.5μM, or 1μM measured on the XFe96 seahorse bioanalyzer. MIN6 were cultured for 24 hours on a 96 well microplate and starved for one hour in 0.5mM glucose prior to the experiment. 14-16 technical repeats N=1, * = p<0.005, *** p<0.0001

4.2.2. OCR and ECAR Measurements of 2D vs 3D Structures

i. Monolayers

The OCR of MIN6 monolayers was measured in response to injections of oligomycin, FCCP, and a combined injection of antimycin A and rotenone added sequentially and recorded over time (figure 31). Injection of oligomycin decreased OCR enabling a clear measurement of ATP production from mitochondrial respiration. The FCCP injection caused the OCR to return to the basal level recorded in the initial measurements before any injections showing that basal respiration is similar to maximal respiration and the rotenone and antimycin A were successful in blocking mitochondrial respiration.

The measurement of ECAR to establish glycolytic function involved an initial injection of 25mM glucose, this concentration was chosen because it is known to stimulate insulin secretion in beta cells. The second and third injections contained oligomycin and 2-DG respectively (figure 32). After the first injection of 25mM glucose a clear increase in ECAR is seen, followed by a decrease in response to the oligomycin injection. There didn't seem to be any effect when 2-DG was added.

Monolayer OCR Response in XFe96 analyser

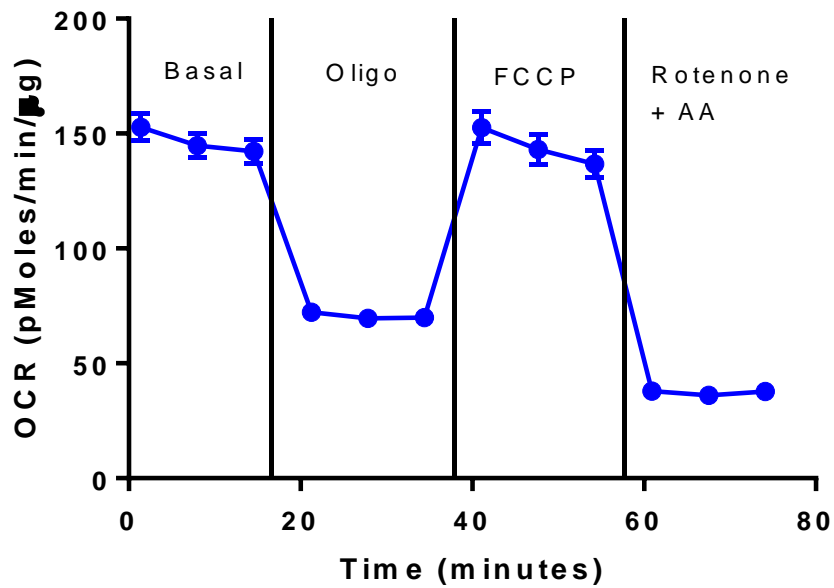


Figure 31. Monolayer OCR Response in XFe96 Analyser

OCR response on MIN6 (P21 – P25) monolayers in 10mM glucose after addition of 2µM oligomycin, 0.5µM FCCP, then 0.5µM rotenone and antimycin A. Measured on a seahorse XFe96 bioanalyser, MIN6 were cultured for 24 hours on a 96 well microplate and starved for one hour in 0.5mM glucose prior to the experiment.

Monolayer ECAR Response in XFe96 analyser

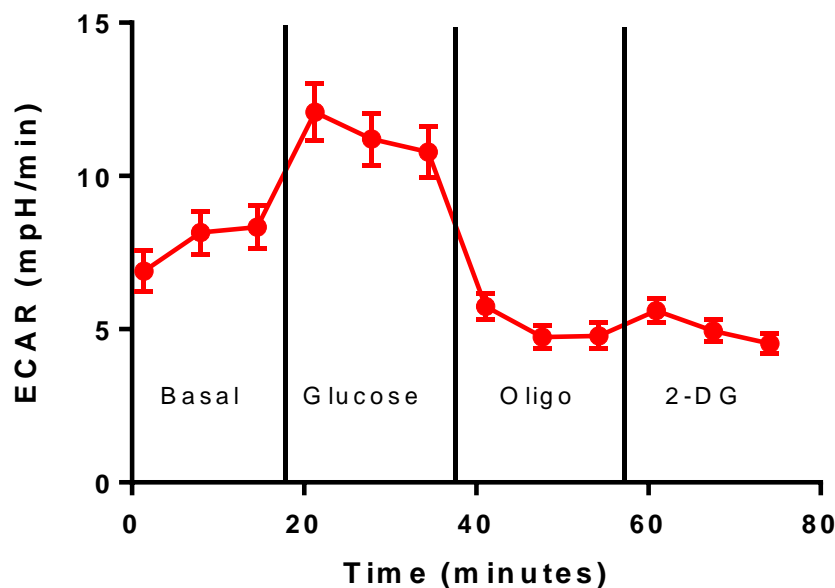


Figure 32. Monolayer ECAR Response in XFe96 Analyser

ECAR response on MIN6 (P21 – P25) monolayers after addition of 25mM glucose, 2 μ M oligomycin, and then 50mM 2-DG measured on a seahorse XFe96 bioanalyser. MIN6 were cultured for 24 hours on a 96 well microplate and starved for one hour in 0.5mM glucose prior to the experiment. Data shown is representative of 5 experiments, error bars based on technical replicates.

ii. Pseudoislets

Once concentrations were optimised for the MIN6 monolayers, the same protocols were used for pseudoislets plated onto the 96 well plates. For accurate measurement of metabolic flux it is essential that 3D structures are located in the centre of the well to allow for alignment with the sensors on the probe. Any movement would cause disruption of these measurements. Therefore, pseudoislets were attached to the wells of a XFe96 spheroid microplate through 20 minutes of pre-incubation with Cell-Tak at room temperature. The pseudoislets were then placed into each well with seahorse base media and the plate was centrifuged to help the pseudoislet to attach firmly. After the final wash before the seahorse run around one third of the pseudoislets remained

in place attached to the bottom of the well, the metabolic function of these pseudoislets was recorded.

The OCR and ECAR was measured in pseudoislets following the same protocol used for the monolayer samples. Due to difficulties in securely attaching the pseudoislets to the bottom of each well the measurements were much more variable with large error bars (figures 33-34). Often the pseudoislets were washed away before the protein content could be analysed. In other cases, pseudoislets moved out of alignment with the sensor meaning no or minimal function was recorded. The OCR response of pseudoislets showed indications of responsiveness to oligomycin and FCCP but again the data is too variable to determine any clear changes (figure 33). The final injection containing rotenone and antimycin A successfully blocked mitochondrial respiration in all wells. The pseudoislets appear to respond to the addition of glucose by showing an increased ECAR after an initial delay but the data shown in figure 34 along with other data is too variable to determine a clear pattern or to be reliably used in any further analysis.

As with the monolayers, these measurements were repeated in four other experiments all showing some very slight indication of responsiveness but with too much variability to make any accurate conclusions from the data produced.

Pseudoislet OCR Response in XFe96 analyser

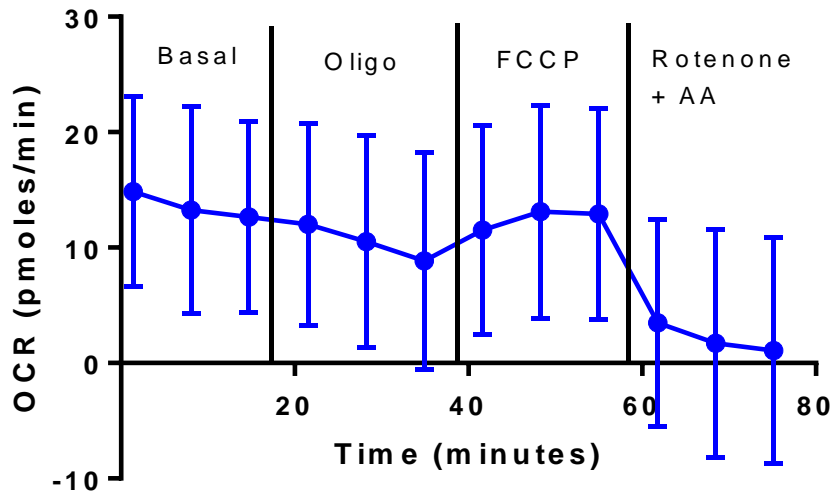


Figure 33. Pseudoislet OCR Response in XFe96 Analyser

OCR response of MIN6 (P21 – P25) pseudoislets after addition of 2 μ M oligomycin, 0.5 μ M FCCP, then 0.5 μ M rotenone and antimycin A, measured on a seahorse XFe96 bioanalyzer. MIN6 pseudoislets formed over 5 days then were cultured for 24 hours on a 96 well microplate and starved for one hour in 0.5mM glucose prior to the experiment. Representative of 5 experiments, error bars representative of technical repeats.

Pseudoislet ECAR Response in XFe96 analyser

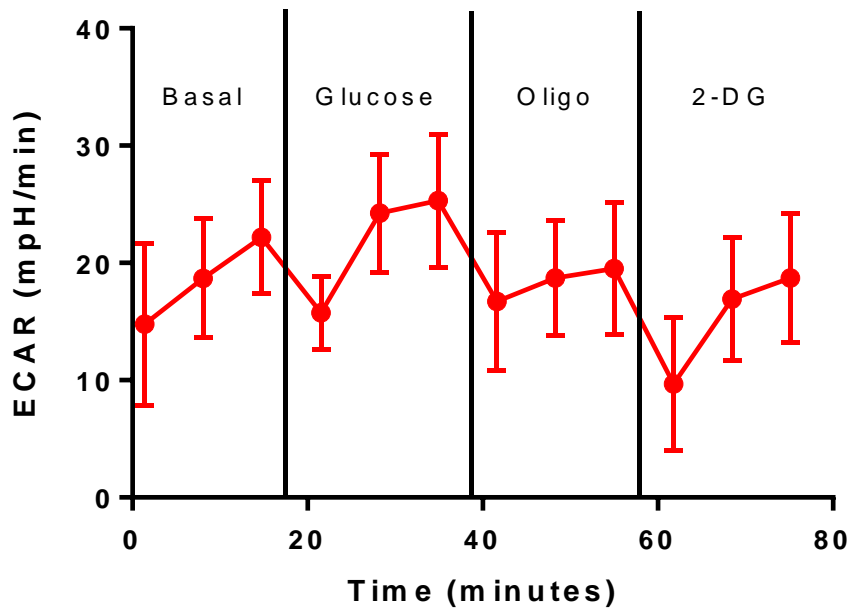


Figure 34. Pseudoislet ECAR Response in XFe96 Analyser

ECAR response on MIN6 (P21 – P25) pseudoislets after addition of 20mM glucose, 2 μ M oligomycin, and then 50mM 2-DG measured on a seahorse XFe96 bioanalyser. MIN6 pseudoislets formed over 5 days were then cultured for 24 hours on a 96 well microplate and starved for one hour in 0.5mM glucose prior to the experiment. Representative of 5 experiments.

4.3. Seahorse XFe24 analyser optimisation

Due to the large variation in function and protein measurements for the pseudoislets, an alternative method was investigated. In previous literature islet capture plates have been used during the metabolic analysis of islets and pseudoislets [127-129]. Using the islet capture plate, the islets are placed in a depression at the base of the well and held in place by a capture screen eliminating the need to secure the pseudoislets to the base of the well. This type of plate is only available in a 24 well format so requires the use of the XFe24 analyser. The 24 well plate allows a larger number of islets to be plated per well reducing the problems associated with accurate protein quantification of a single islet. The number of islets per well could be increased from 1 islet to up to 500.

Figure 35 shows light microscope images of the pseudoislets as they are placed in the well under the islet capture screen.

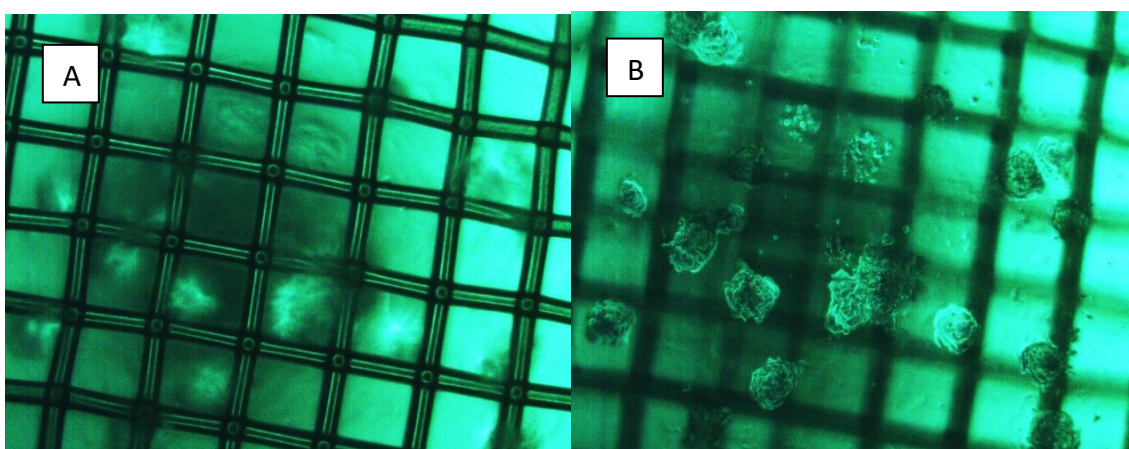


Figure 35. Light Microscope Image of Pseudoislets in Islet Capture Plate

Light microscope images of MIN6 pseudoislets in a 24 well plate under an islet capture screen with the focus on a) the mesh of the islet capture screen and b) the pseudoislets underneath the screen.

Protocols using the XFe24 analyser were optimized. First the optimal seeding density for the monolayer plates was established (Figure 36). There was an increase in recorded

function seen by a higher basal OCR at a seeding density of 80,000 cells/well than 60,000 cells/well but negligible difference seen between the two highest seeding densities of 80,000 cells/well and 100,000 cells/well, flux was corrected for protein concentration. From this, the seeding density of 80,000 cells/well was selected for future investigations. The FCCP concentration was optimised again this time following advice from protocols in the laboratory where the XFe96 bioanalyser was used. The first FCCP injection at 3 μ M FCCP was followed with a further FCCP injection of 1 μ M to establish if there was any further increase in maximal respiration. The second injection had little effect so a concentration of 3.5 μ M FCCP was chosen to be sufficient.

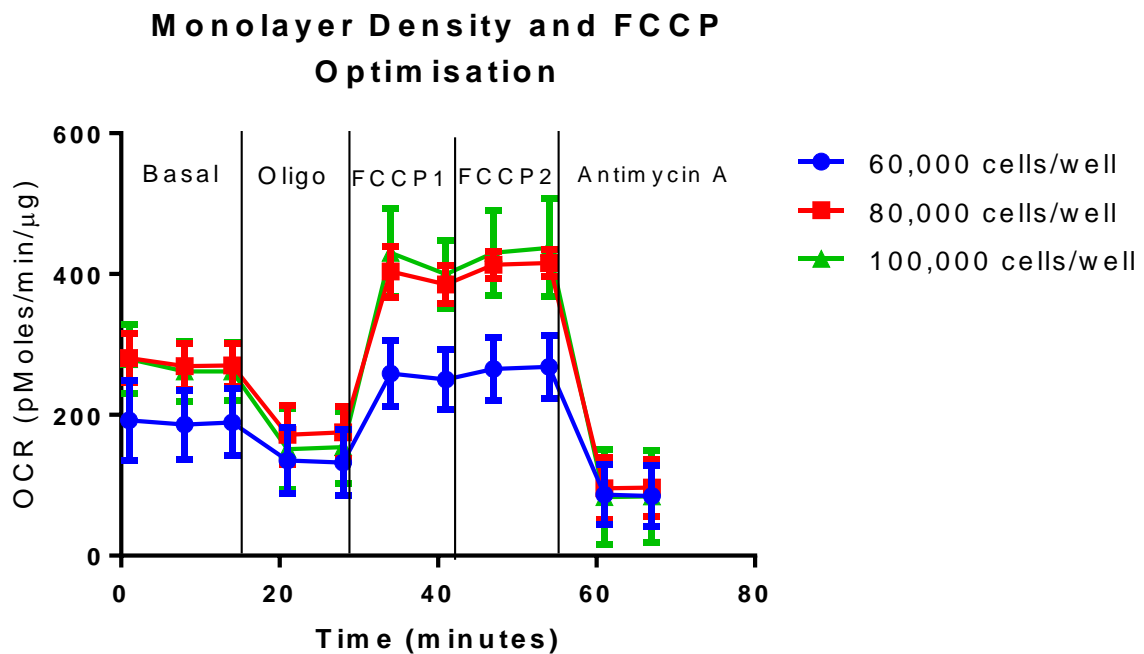


Figure 36. Monolayer Density and FCCP Optimisation

OCR response in MIN6 (P26 – P29) monolayers cultured at densities of 60,000 cells/well, 80,000 cells/well and 100,000 cells/well after addition of 1mM oligomycin, 3 μ M FCCP, a further 1 μ M FCCP then at Antimycin A. Measured on a seahorse XFe24 bioanalyser and starved for one hour in 0.5mM glucose prior to the experiment. Six technical repeats per data point, n=1.

The optimal protocol for the plating of the islets was then investigated (Figure 37). Islets were seeded at either 100 or 300 islets per well and half were plated on the morning of

the run (day six) with the other half being plated into the islet capture plate the night before the run (day five). The highest basal measurements and greatest responsiveness to stimulating compounds were seen in pseudoislets plated at the higher density (300 islets) and plated the night before the run allowing them time to recover after moving. However, it was also clear from these results that more adjustments needed to be made to the protocol. With the exception of the initial basal measurements, the OCR did not reach a plateau meaning the maximal respiration after each injection couldn't be measured. To allow the pseudoislets time to reach a plateau, the time between injections was increased. This was not necessary for the monolayers as a clear maximal response was seen after each injection. Also, there was no clear response to glucose or oligomycin in the pseudoislet measurements and this needed to be understood before collecting the final data.

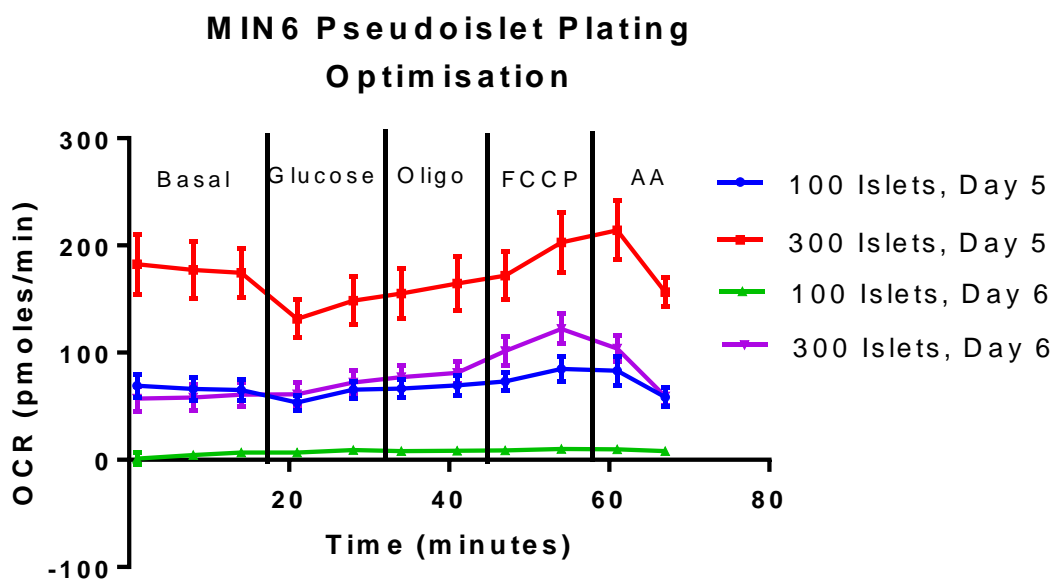


Figure 37. Pseudoislet Seahorse Plating Optimisation

Measurements taken on the XFe24 seahorse bionalyser. OCR measurements of MIN6 (P26 – P29) pseudoislets plated at low or high densities either on the morning of the seahorse experiment (Day 6) or the night before (Day 5). Initial measurements were taken in basal media at 0.5mM glucose then injections of 25mM glucose, 2µM oligomycin, then antimycin A were added sequentially. MIN6 pseudoislets were cultured for 24 hours on a 24 well microplate and starved for one hour in 0.5mM glucose prior to the experiment. Representative of 5 experiments.

The OCR measurements of monolayer and pseudoislet cultures were compared (figure 38). Whilst the monolayers reached a clear plateau after the addition of oligomycin, the pseudoislets did not respond to the oligomycin injection. It has been reported that higher concentrations of oligomycin are required to penetrate through 3D structures [130]. To explore if this was the case with pseudoislets, the oligomycin concentration was increased by 10 times in future experiments (figure 39).

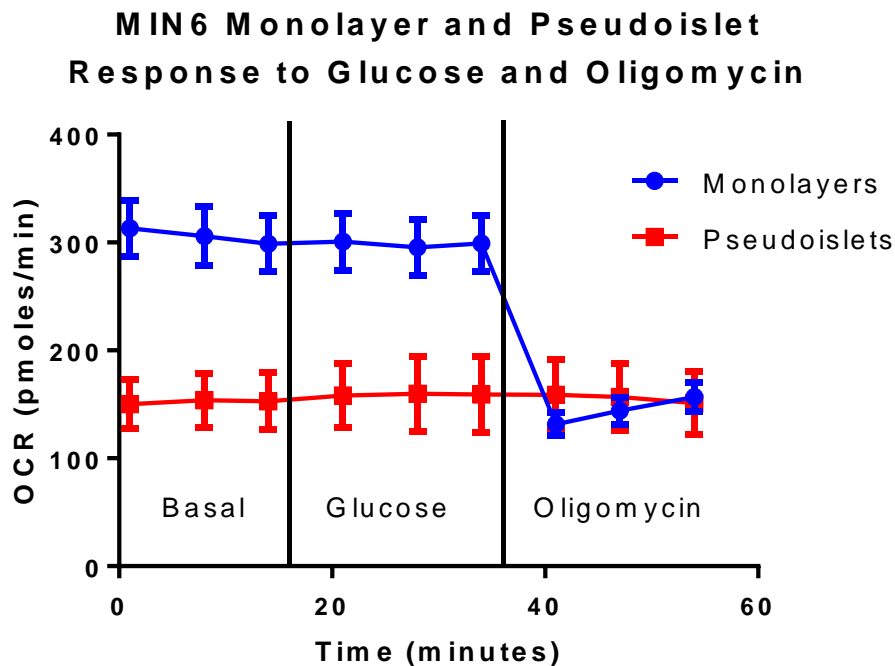


Figure 38. MIN6 Monolayer and Pseudoislet Response to Oligomycin

OCR response of monolayer and pseudoislet MIN6 (P26 – P29) after addition of 25mM Glucose then 2µM oligomycin. Measured on a seahorse XFe24 bioanalyzer. MIN6 pseudoislets formed over 5 days were then cultured for 24 hours on a 24 well islet capture plate. Monolayer samples were cultured for one hour in a 24 well microplate. Samples were starved for one hour in 0.5mM glucose prior to the experiment N=1

Neither culture type, monolayers nor pseudoislets, responded to the glucose injection (figures 38). These MIN6 are known to produce a large insulin secretion response under the levels of glucose injected as shown in chapter 3 which would rely on a high level of metabolism and therefore oxygen consumption. It is possible that the pyruvate in the base media is providing the MIN6 with fuel for the insulin secretion, which is masking the effect of the added glucose, so it was removed from the media in the next

experiment. As beta cells are not expected to be responsive to pyruvate [54], the effect of a pyruvate injection on the beta cell metabolism will also be investigated.

4.4. Comparison of Metabolic Function for monolayer and pseudoislet MIN6

4.4.1. OCR Measurements

Using the optimal seeding protocols and compound concentrations determined above the OCR and ECAR of MIN6 monolayers and pseudoislets were measured in order to calculate the ATP contributions from both glycolytic and mitochondrial metabolism. The OCR measurements required for these calculations included the OCR under the following conditions:

1. basal glucose
2. glucose stimulation
3. pyruvate
4. oligomycin
5. antimycin A.

The use of both rotenone and antimycin A was not deemed necessary as antimycin A would sufficiently block mitochondrial respiration [131]. For the calculation of the glycolytic contribution to ATP production, only the maximal ECAR under stimulation was used. The use of 2-DG to block glycolysis was not effective in beta cells due to the low expression of low Km of hexokinase [58] and as ECAR was reduced to negligible levels in the presence of antimycin A, 2-DG was omitted.

The MIN6 cultured as monolayers showed a similar increase in OCR after addition of either glucose or pyruvate (figure 39). There was a decrease in OCR after addition of oligomycin indicating successful inhibition of oxidative phosphorylation and a further decrease in OCR after addition of antimycin A indicating complete inhibition of the electron transfer chain. Rates reached a plateau before each subsequent injection. In

contrast, pseudoislets responded robustly to glucose but not to pyruvate (figure 40). As with monolayers, a clear response to oligomycin and antimycin A was recorded.

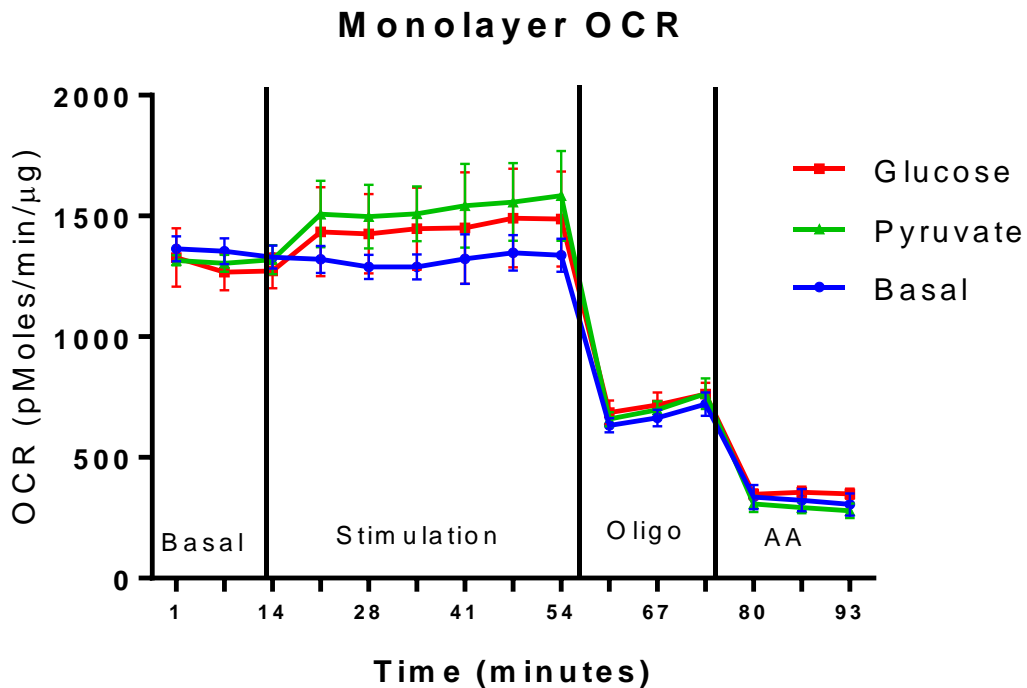


Figure 39. OCR of Monolayer MIN6

OCR response in MIN6 (P26 – P29) monolayers after addition of either i) 25mM glucose, 0.5mM glucose injection (Basal), or 1mM pyruvate; ii) 2μM oligomycin; iii) 0.5μM Antimycin A. Measured on a seahorse XFe24 bioanalyzer. Monolayer samples were cultured for 24 hours in a 24 well microplate then starved for 1 hour in 0.5mM glucose for one hour prior to the experiment. N=3.

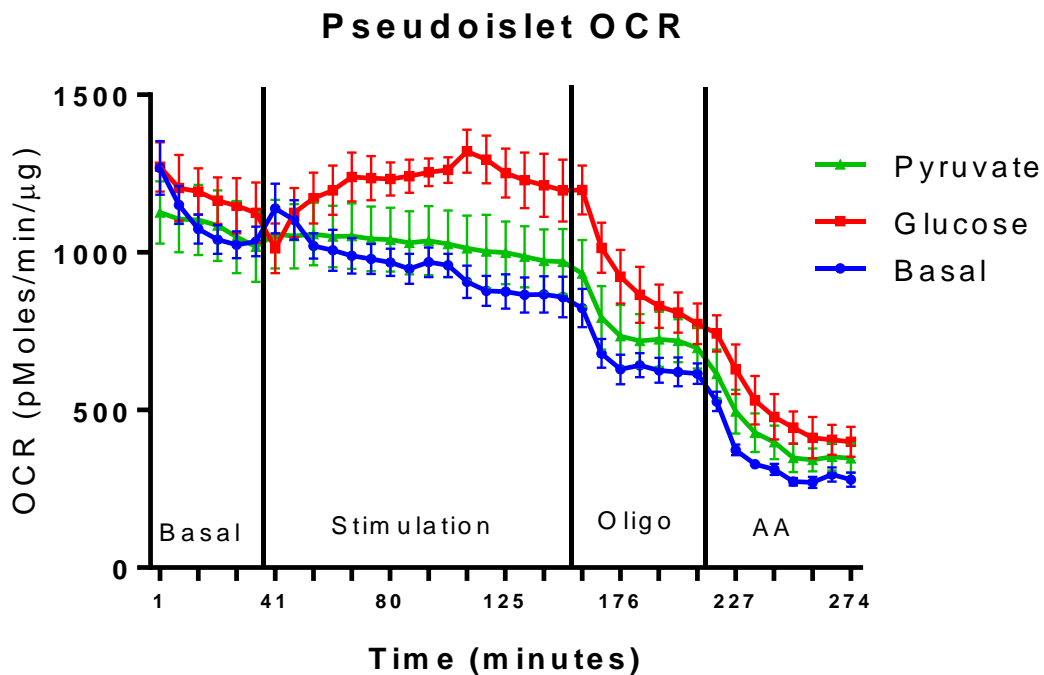


Figure 40. OCR of Pseudoislet MIN6

OCR response in MIN6 (P26 – P29) pseudoislets after addition of either i) 25mM glucose, 0.5mM glucose injection (Basal), or 1mM pyruvate; ii) 20μM oligomycin; iii) 0.5μM Antimycin A. Measured on a seahorse XFe24 bioanalyzer. MIN6 pseudoislets formed over 5 days then were cultured for 24 hours on a 24 well microplate and starved for one hour in 0.5mM glucose prior to the experiment.

4.4.2. ECAR Measurements

The ECAR measurements for the monolayer cultures showed a small but consistent response to glucose (figure 41). However, these responses were much more evident in the pseudoislet cultures suggesting a larger reliance on glycolysis for GSIS (figure 42).

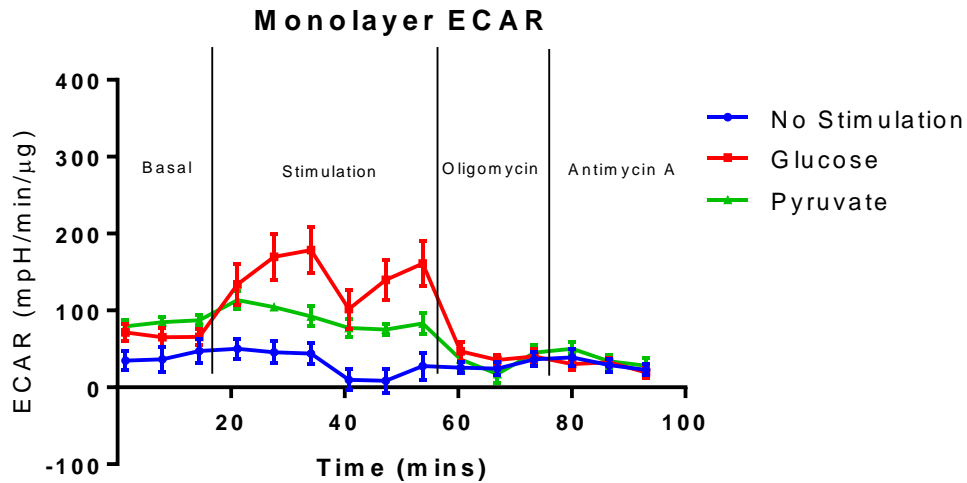


Figure 41. ECAR of Monolayer MIN6

ECAR response in MIN6 (P26 – P29) monolayers after addition of either i) 25mM glucose, 0.5mM glucose injection (No Stimulation), or 1mM pyruvate; ii) 2 μ M oligomycin; iii) 0.5 μ M Antimycin A. Monolayer samples were cultured for 24 hours in a 24 well microplate then starved for 1 hour in 0.5mM glucose for 1 hour prior to the experiment. Measured on a seahorse XFe24 bioanalyzer. N=3

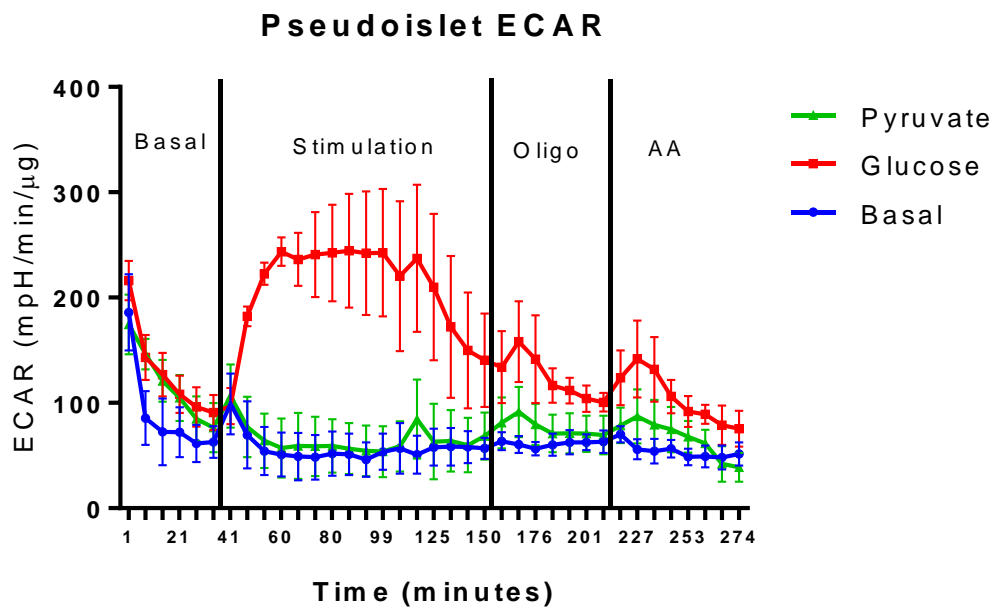


Figure 42. ECAR of Pseudoislet MIN6

ECAR response in MIN6 (P26 – P29) pseudoislets after addition of either i) 25mM glucose, 0.5mM glucose injection (Basal), or 1mM pyruvate; ii) 20 μ M oligomycin; iii) 0.5 μ M Antimycin A. Measured on a seahorse XFe24 bioanalyzer. MIN6 pseudoislets formed over 5 days then were cultured for 24 hours on a 24 well microplate and starved for one hour in 0.5mM glucose prior to the experiment.

4.4.3. Contribution of oxidative phosphorylation and glycolysis to ATP Production in MIN6 monolayers and pseudoislets

The mitochondrial oxygen consumption rate correlates to mitochondrial ATP production and can be calculated from the total cellular oxygen consumption rate minus the cellular consumption rate not associated with mitochondrial activity such as through proton leak across the mitochondrial inner membranes (see calculation in methods [131]). Increases in ECAR in response to the production of lactate through glycolysis and glycolytic ATP production can be calculated from the total cellular ECAR minus the contribution to extracellular acidification from carbonic acid generated from CO₂ produced during the complete oxidation of glucose in mitochondrial metabolism [131]. The ATP production per mg protein was calculated using the OCR and ECAR data generated to find the total ATP production from oxidative phosphorylation and glycolysis.

The overall ATP production from the monolayers was more variable than that of the pseudoislets possibly due to being more sensitive to MIN6 passage number (figure 43). There was no significant difference between the basal ATP production between monolayers and pseudoislets but there was a trend towards lower basal ATP in pseudoislets which is consistent with the trend towards lower basal insulin secretion in section 3.7.4. Pseudoislets showed a significantly ($P=0.0111$) larger insulin secretion response to glucose stimulation compared to monolayers (figure 25). There appears to be a slightly higher ATP production in monolayers stimulated by pyruvate than in pseudoislets although the response measured was quite variable and no statistical significance was found. This suggests that monolayers responded to both glucose and pyruvate whilst pseudoislets responded only to glucose and not pyruvate.

Monolayers showed a significantly higher basal ATP production from oxidative phosphorylation. Neither glucose nor pyruvate increased ATP production from oxidative phosphorylation in the monolayers but this may be due to a high variability between samples (figure 44). However, pseudoislets showed a clear increase in ATP production via OCR response to glucose stimulation but not pyruvate.

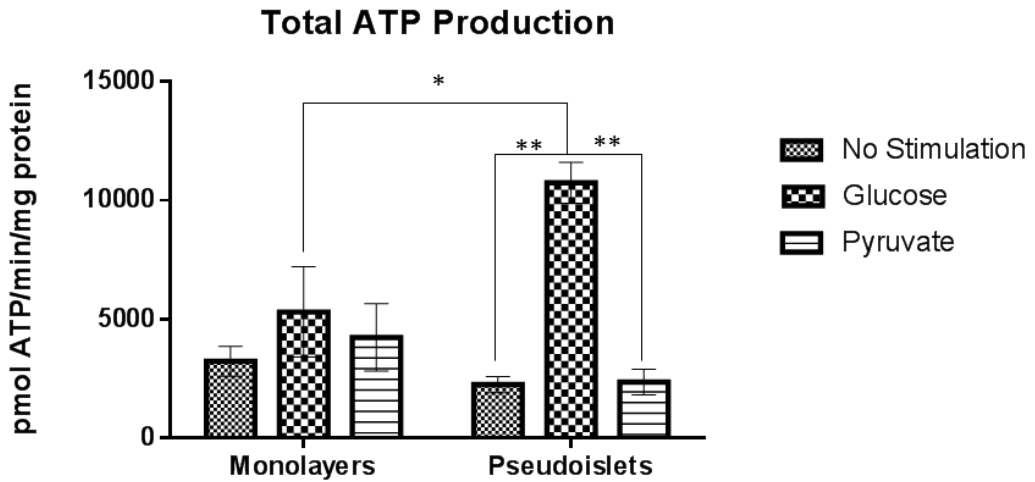


Figure 43. Total ATP Production in Monolayers and Pseudoislets

Total ATP produced per minute by monolayers and pseudoislets stimulated by either glucose or pyruvate. Measured by the seahorse XFe24 bioanalyser. MIN6 (P26 – P29) pseudoislets formed over five days were then cultured for 24 hours on a 24 well islet capture plate. Monolayer samples were cultured for 24 hours in a 24 well microplate. N=3, *=P<0.05, **=P<0.01. Statistical analysis performed but not found to be significant when not indicated.

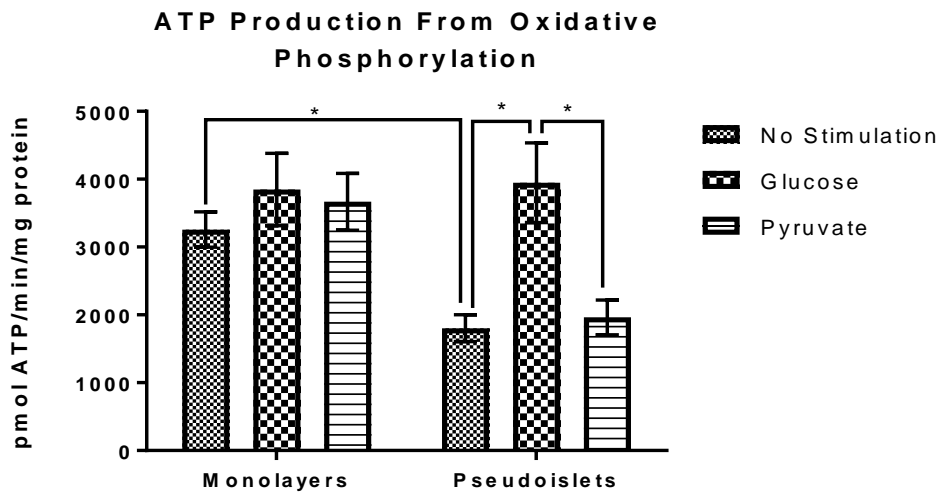


Figure 44. ATP Production from Oxidative Phosphorylation in Monolayers and Pseudoislets

Total ATP produced per minute by oxidative phosphorylation in MIN6 (P26 – P29) cultured as monolayers and pseudoislets and stimulated by either glucose or pyruvate compared with glycolytic ATP production of MIN6 monolayers and pseudoislets kept in basal media at 0.5mM glucose. Measured by the seahorse XFe24 bioanalyser N=3, *=P<0.05

Basal glycolytic rates were low in both monolayers and pseudoislets (figure 45). However, pseudoislets showed a greater (4-fold) increase in glycolysis in response to glucose compared to monolayers.

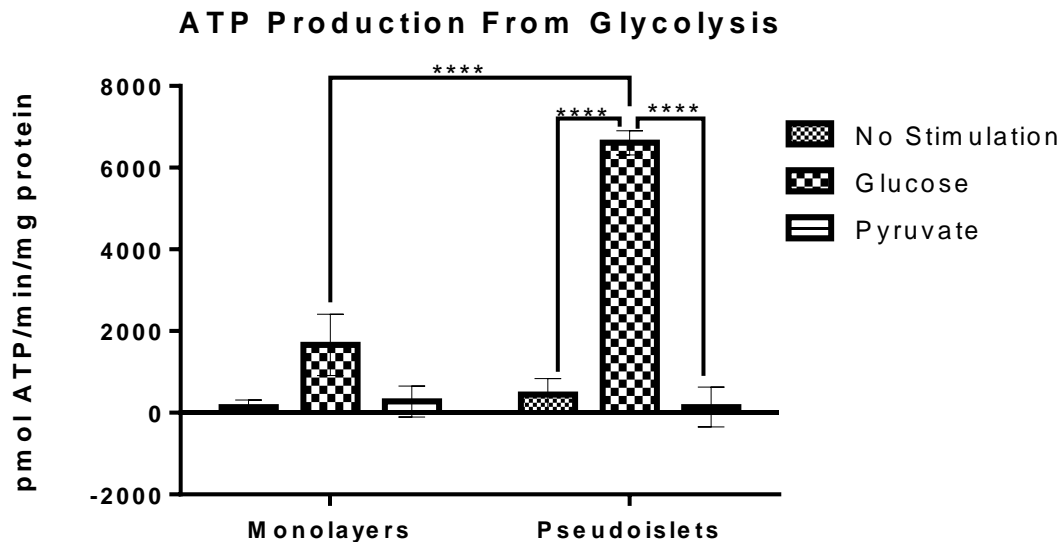


Figure 45. ATP Production from Glycolysis in Monolayers and Pseudoislets

Total ATP produced per minute by glycolysis in MIN6 (P26 – P29)

cultured as monolayers and pseudoislets and stimulated by either glucose or pyruvate compared with ATP production of MIN6 monolayers and pseudoislets kept in basal media at 0.5mM glucose. Measured by the seahorse XFe24 bioanalyser N=3, ****=P<0.0001. Statistical analysis performed but not found to be significant when not indicated.

4.5. Analysis of Metabolic Function in Human Islets Stimulated by Glucose or Pyruvate

Comparison of the MIN6 pseudoislet function with isolated human islet function will help in understanding whether aspects of the metabolic function are a feature of the MIN6 model. In previous studies, human islets have been analysed using the seahorse bioanalyser [124, 132, 133], where the OCR has been shown to increase on addition of glucose [134]. The ECAR is not mentioned in most studies but one paper reported that the enhanced insulin secretion in response to addition of fatty acids was due to both

OCR and ECAR increases indicating an increase in both glycolytic and mitochondrial ATP contributions [124]. To explore the metabolic function of human islets, OCR and ECAR were measured using the same Seahorse bioanalyser protocols used to measure metabolic function in the MIN6 monolayer and pseudoislets. Human islets were cultured for one day post isolation to allow recovery from any stresses before experiments.

The OCR measurements shown in figure 46 appear to show a slight increase in OCR following addition of glucose and no response in islets with no stimulation or pyruvate stimulation. There are many factors of different natures before, during, and after isolation which can affect the function of the human islets. This led to a large variability in the function of the islets.

Investigations into the effect of glucose and pyruvate on the ECAR of human islets (figure 47) showed a similar metabolic function to that seen in the MIN6 pseudoislet samples. The ECAR does show a very clear increase after glucose is added suggesting uncoupling of glycolysis from mitochondrial metabolism.

Human Islet OCR

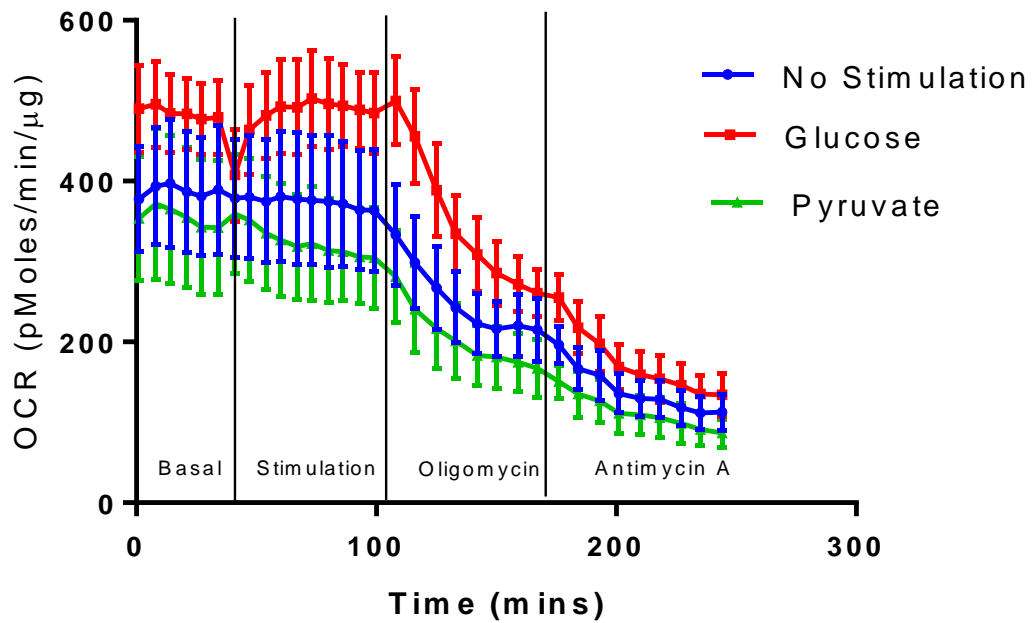


Figure 46. OCR of Human Islets

OCR response in human islets after addition of either i) 25mM glucose, 0.5μM glucose injection (No Stimulation), or 1mM pyruvate; ii) 20μM oligomycin; iii) 0.5μM Antimycin A. Measured on a seahorse XFe24 bioanalyzer. Islets were cultured for 24 hours on a 24 well microplate and starved for one hour in 0.5mM glucose prior to the experiment. N=4.

Human Islet ECAR

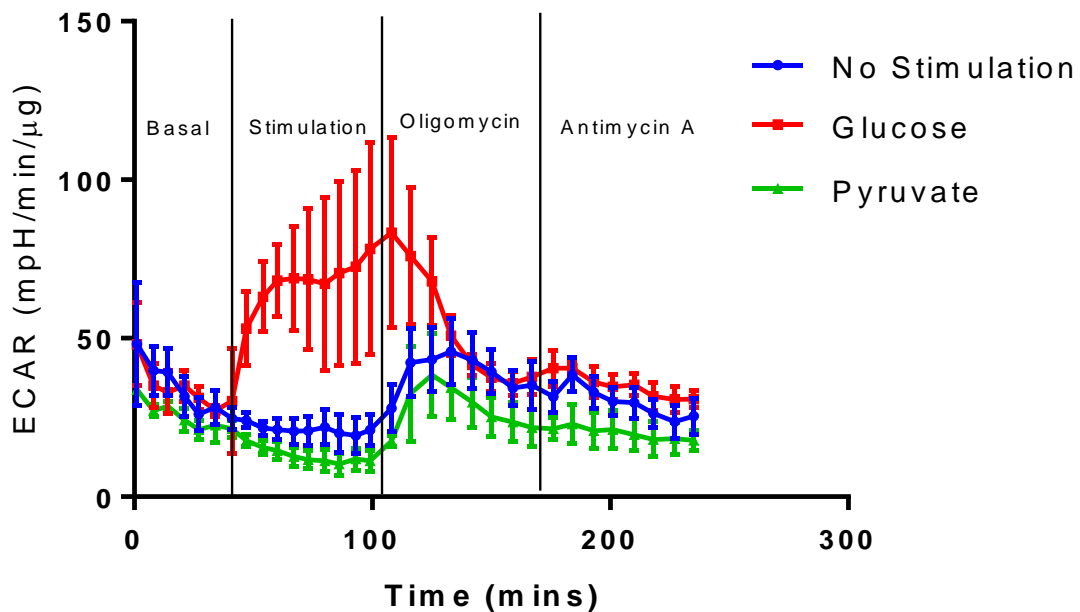


Figure 47. ECAR of Human Islets

ECAR response in human islets after addition of either i) 25mM glucose, 0.5μM glucose injection (No stimulation), or 1mM pyruvate; ii) 20μM oligomycin iii) 0.5μM Antimycin A. Measured on a seahorse XFe24 bioanalyzer. Islets were cultured for 24 hours on a 24 well microplate and starved for one hour in 0.5mM glucose prior to the experiment. N=4.

4.6. Contribution of oxidative phosphorylation and glycolysis to ATP Production in Human Islets

The total ATP production in response to glucose was significantly higher (3-fold) for human islets stimulated by glucose than for those with no stimulation (figure 48). There is no difference between the overall ATP production of islets with no stimulation and in the presence of pyruvate. This was similar to the response of the pseudoislets with a large glucose triggered ATP production and no response to the pyruvate.

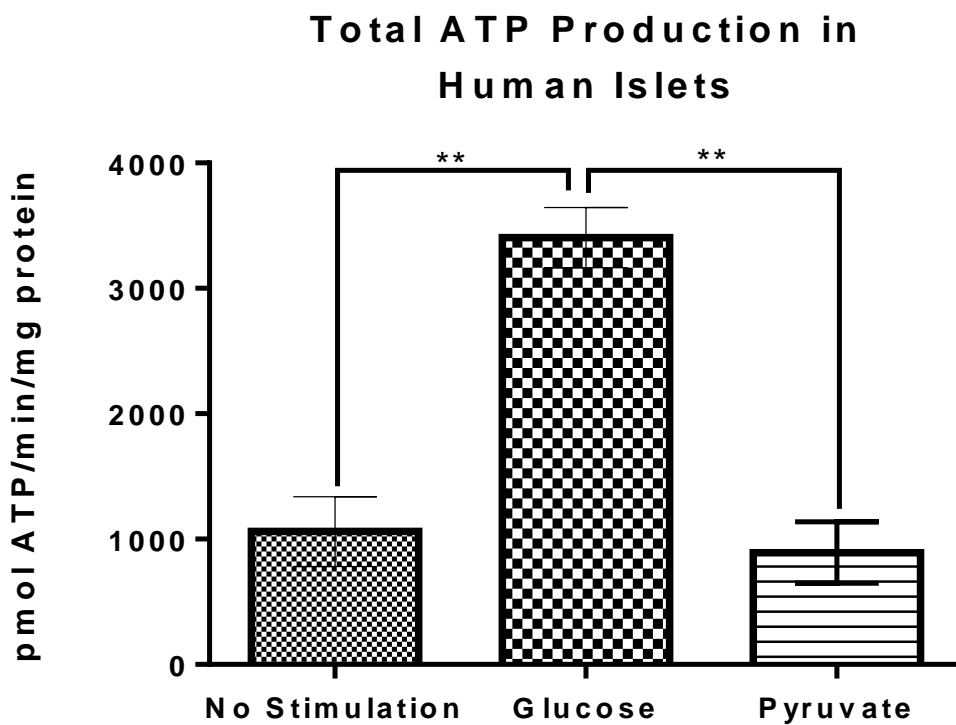


Figure 48. Total ATP Production in Human Islets

Total ATP produced per minute by human islets stimulated by either glucose or pyruvate. Measured by the seahorse XFe24 bioanalyser. Islets were plated on a 24 well islet capture microplate 24 hours before the run and kept in basal media at 0.5mM glucose. N=3, **=P<0.005

The individual contributions of oxidative phosphorylation and glycolysis to ATP production in human islets mirrored the pattern seen in the overall contribution. Calculations showing ATP production from both oxidative phosphorylation and glycolysis showed that there was no response after the addition of pyruvate.

ATP production due to oxidative phosphorylation increased on addition of glucose (figure 49). A large portion, around 75%, of ATP production at basal glucose levels was contributed to by oxidative phosphorylation.

A larger contribution to the increased ATP in response to glucose was made by glycolysis (figure 50). There was no statistically significant increase in ATP Production between islets with no stimulation and glucose stimulation but a large statistically significant increase in glycolytic ATP production between these two conditions.

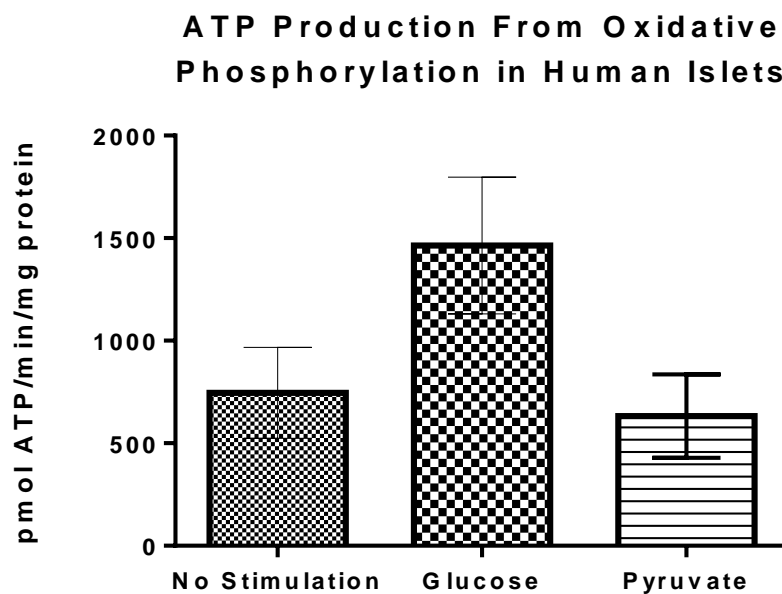


Figure 49. ATP Production from Oxidative Phosphorylation in Human Islets

Total ATP produced per minute by oxidative phosphorylation in human islets stimulated by either glucose or pyruvate. Measured by the seahorse XFe24 bioanalyser. Islets were plated on a 24 well islet capture microplate 24 hours before the run and kept in basal media at 0.5mM glucose. N=3. Statistical analysis performed but not found to be significant.

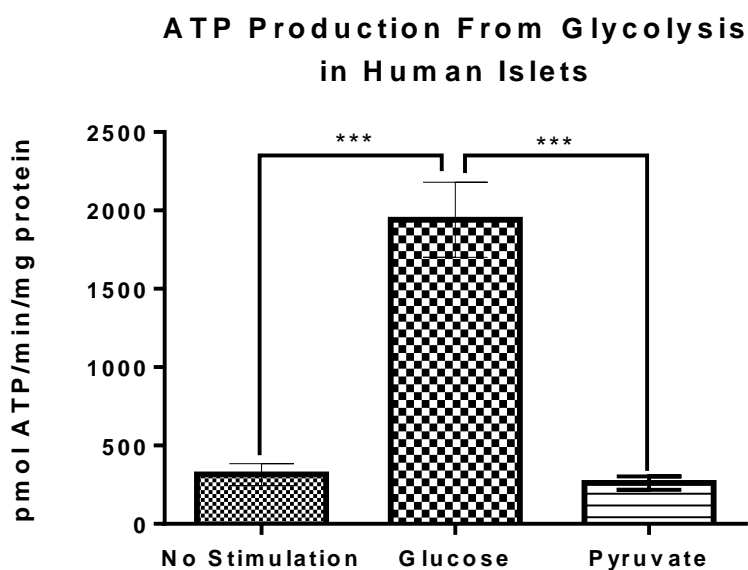


Figure 50. ATP Production from Glycolysis in Human Islets

Total ATP produced per minute by glycolysis in human islets stimulated by either glucose or pyruvate. Measured by the seahorse XFe24 bioanalyser. Islets were plated on a 24 well islet capture microplate 24 hours before the run and kept in basal media at 0.5mM glucose. N=3, *=P<0.001**

4.7. Conclusion

4.7.1. Seahorse Bioanalyser Optimisation

Attempts to optimize protocols for bioenergetic measurements using the XFe96 analyser were successful for monolayer cultures. Measurements recorded using the 96 well spheroid plates for pseudoislets showed some responsiveness to the compounds injected but the variation between wells was too great to obtain accurate data. This was mainly caused by difficulties in securing islets in the base of the well causing pseudoislets to move out of alignment with the sensors during measurements or to be lost during washes meaning protein could not be quantified. Other studies have successfully used both coated 96 well spheroid plates [133, 134] to analyse islets and 24 well islet capture plates [132, 135].

The protocols developed on the XFe96 analyser were further developed on the XFe24 analyser. This larger well volume allowed more islets to be plated per well and incorporated an islet capture screen which held the islets in place throughout measurements. After further optimization, the variation in the data generated for the pseudoislet OCR and ECAR was reduced so that responses to the compounds injected could be measured accurately. Additionally, some changes were made to the media and compounds used in the injections in a movement away from the Agilent seahorse protocols to focus only on data relevant to this study. Initially, in data produced during optimisation of the oligomycin concentration, the OCR was not affected by injection of high glucose for either culture types which may be explained by base media containing pyruvate. To assess the influence of glucose stimulation on OCR the pyruvate was removed from the base media. Previous studies have shown that cells are unable to reach their maximum respiration capacity in the presence of FCCP when pyruvate is not present in the media and as the use of FCCP was not required in the calculation for the ATP production of the MIN6 cells this injection was removed. Finally, 2-DG was judged to be ineffective in the inhibition of glycolysis due to the low expression of low Km hexokinases in beta cells, so the final injection contained only antimycin A [58].

In early experiments pseudoislets appeared slower to respond to compounds and to reach a plateau or seemed to not respond at all. This may be due to the time taken for the diffusion of compounds, particularly oligomycin, through the 3D structure of the pseudoislets. The number of measurements between each injection was therefore increased during pseudoislet experiments and a higher concentration of oligomycin was used to fully inhibit ATP linked respiration. This optimisation approach allowed development of the technique to allow for accurate comparison of monolayer and pseudoislet samples. Although there are limitations due to some differences in the experimental setup for 2D and 3D structures, the Seahorse XF bionalyser has been successfully used to compare metabolic characteristics of 2D and 3D structures [130, 136, 137]. Russell et al also showed that in comparison to 2D structures, 3D structures showed delayed effects after addition of oligomycin but not after addition of FCCP, rotenone, or antimycin A. Oligomycin has a relatively larger molecular weight which

could slow penetration through the 3D structure but it was shown that this feature was not solely responsible for the delayed response [130]. Using this system to compare monolayer and pseudoislet samples provides useful information but limitations in direct comparisons caused by the different cultures requiring different experimental set ups should be considered at all stages.

4.7.2. Total ATP Production in Response to Glucose is Greater in 3D Structures

The total cellular ATP production rate was calculated using the data generated by the seahorse bioanalyser. An increase in ATP production under high glucose by pseudoislets would indicate improved cell functionality as insulin secretion is tightly linked to ATP production [54, 59, 67]. The MIN6 consistently responded to glucose stimulation with pseudoislets showing a significantly larger ATP production rate than monolayers under high glucose conditions. The improved ATP production response mirrors glucose stimulated insulin secretion data in chapter 3. Pseudoislets stimulated by high glucose levels showed a 4.8-fold increase in overall ATP production (figure 43) and a 7.4-fold increase in insulin secretion levels (figure 25). The MIN6 monolayers were much less responsive showing only a 1.6-fold increase in ATP production (figure 43) and a 1.5-fold increase in insulin secretion (figure 25). This data shows that changes in metabolic flux directly correlate with insulin secretion.

There was no significant effect of glucose on monolayer ATP production, this may be complicated by the high levels of variation evident in these data sets, possibly due to varying passage numbers. Previous data presented in section 3.5.3 and discussed in section 3.8.2 showed that the insulin secretion response of monolayers decreased with passage number whilst the MIN6 arranged as pseudoislets retained their function regardless of passage number. It may also be due to differences in functionality of the MIN6 between batches [138]. The more consistent levels of response displayed by the pseudoislets may be due to improved connections and therefore communications between beta cells resulting in a more co-ordinated response. Previous studies have

shown that cell-cell communication between beta cells is necessary for efficient GSIS, the secretion response of dispersed islets was reported to be lower than that of intact islets and return to near previous levels when the beta cells were allowed to re-aggregate [72]. The data in this study suggests that the effect of pseudoislet formation on GSIS is perhaps not only due to Ca^{2+} synchronisation as previously suggested [98] but supports a role for a change in metabolic phenotype. We hypothesised that pseudoislets would show improved coupling of glycolysis to mitochondrial metabolism. We did see an increase in glucose-induced oxidative phosphorylation in pseudoislets compared to monolayers, but the largest effect was in uncoupled ATP production which is not consistent with the original hypothesis. Very few studies have investigated the relationship between glycolysis and GSIS. However, Chowdhury et al reported higher protein expression levels of both glycolytic and mitochondrial enzymes in pseudoislets compared to monolayers [78] and a significant increase in glycolysis in response to fatty acid stimulation has been reported in human islets [124].

4.7.3. Increased Basal ATP Production in 2D Beta Cells is caused by an Increase in Oxidative Phosphorylation

The ATP contributions from both oxidative phosphorylation and glycolysis were then examined separately. The most obvious difference within the production of ATP from oxidative phosphorylation was the increased level of basal ATP production in the monolayer samples. The lack of significant effect of glucose on total ATP production in monolayers may be explained by the higher level of basal ATP production. The overall ATP production and the insulin secretion data both showed slightly raised basal levels in monolayer samples, but this is much more pronounced in OCR data suggesting it is a feature of increased oxidative phosphorylation. High ATP production in beta cells at low glucose levels can trigger inappropriate insulin release and is indicative of a less efficient pathway [14, 87, 112, 139].

It has also been shown that inhibition of Cx36 in beta cells results in a higher basal insulin secretion [140]. This is because hyperpolarising Ca^{2+} waves can spontaneously occur in

beta cells, these waves can be dispersed throughout the islet when there is communication between beta cells but isolated beta cells are not able to do this and so prone to increased basal insulin secretion rates [73, 74, 98, 140]. Dispersed beta cells such as those cultured as monolayers have much fewer intercellular connections such as Cx36 than beta cells within islets and pseudoislets and so the lack of this gap junction serves as another potential cause of the increased basal ATP production [94, 103]. This is a more likely cause for the increased basal OCR in monolayers and investigation into the effect of Cx36 expression on basal OCR would be of interest in understanding the mechanisms behind this.

All samples showed an increase in OCR with high glucose which correlates to increased ATP production from oxidative phosphorylation. There was no difference in ATP production under high glucose between monolayer and pseudoislet samples suggesting ATP was being produced through a different pathway, so this was further explored in the next section through the analysis of glycolytic ATP contributions.

4.7.4. Pancreatic Beta Cells Display Improved ATP Production Responsiveness When Cultured as 3D Structures due to Increased Glycolysis

The increased ATP production seen in the pseudoislets was mainly due to the increased glycolytic contribution and human islets used in this study also displayed a similar increase in glycolysis in response to high glucose. Both human islets and MIN6 pseudoislets produced more than half of the overall ATP under high glucose from glycolytic contributions. Existing literature investigating pseudoislet metabolism using the seahorse bioanalyser focuses only on the OCR portion of metabolism. Some articles that do include ECAR data consistently show an increase in ECAR in response to glucose stimulation [141-143]. However, none of this data is analysed further or discussed and ATP contributions are not calculated so it is not comparable with the OCR data.

A large glycolytic response could be a sign of hypoxia. Isolation of islets requires disrupting the vascular network supplying the islets with oxygen and leaves diffusion as the only option to supply the nutrients and oxygen required by the islets. This means that all islets suffer some effects of hypoxia following isolation, particularly in the core of the islet. The effects of hypoxia are present to some degree until transplantation and revascularisation is complete [144]. The increase in glycolysis seen in the islets and pseudoislets may indicate a limitation in the study of islets outside their natural environment.

To maintain blood glucose at sufficient levels to meet the body's demands it is important that insulin is not released at low glucose levels. GLUT2 is a major glucose transporter in rodent beta cells that allows rapid equilibrium between intracellular and extracellular glucose concentrations [145]. This transporter is vital in enabling the cells to respond almost immediately to any changes in glucose concentration. Once glucose has been transported into the beta cell, glucokinase acts as a glucose sensor; metabolising glucose only once it exceeds physiological levels [58]. It is important that the low K_m hexokinase-1 is not expressed in beta cells. High expression of hexokinase-1 would lead to inappropriate insulin secretion during fasting [53]. There is evidence that hypoxia decreases basal OCR but it also decreases maximal respiratory capacity [146]. The maximal capacity wasn't recorded in this study as the use of FCCP was deemed unsuitable, however, the pseudoislets indicated an increase in glucose mediated OCR suggesting the data is not consistent with a loss of aerobic respiration that would be expected in hypoxia. Hypoxia increases basal insulin secretion through increased basal glycolysis so investigation into the expression of GLUT2 and hexokinase in the pseudoislets compared to monolayers could help clarify any changes in the glucose sensing pathways and hence, basal glycolysis.

4.7.5. Beta Cells in 2D Structures Show Some Response to Pyruvate Stimulation

The metabolic response of MIN6 and human islets to pyruvate stimulation was also measured. To achieve good blood glucose control it is important that beta-cells do not respond to extracellular pyruvate [54]. The levels of pyruvate and lactate in the blood increase following exercise. If these molecules were to be transported into the beta cells to be metabolised, they would stimulate insulin secretion causing a potentially dangerous drop in blood glucose levels. To prevent this inappropriate insulin secretion response the expression of monocarboxylate transporter 1 (MCT 1) is repressed in beta cells so that the lactate and pyruvate cannot enter the cell [53].

The MIN6 pseudoislets and human islets in this study did not respond to pyruvate stimulation. ATP production in the presence of pyruvate was similar to the ATP production with no stimulation. However, the monolayers showed an increase in ATP production through oxidative phosphorylation in response to pyruvate stimulation. This suggests that configuration of beta cells as monolayers changes the metabolic properties of the beta cell to allow them to respond to pyruvate which is not physiological. Further analysis is required to further explore this mechanism. Insulin secretion in response to pyruvate has also been seen in cases of exercise induced hyperinsulinemic hypoglycaemia (EIH), which is characterised by inappropriate insulin secretion following anaerobic exercise [147]. It has been shown that this form of hyperinsulinemic hypoglycaemia is caused at least in part by overexpression of the MCT1 transporter. Investigating the expression of this transporter in the MIN6 could help to explain the pyruvate response seen in this study.

CHAPTER 5. COMPARISON OF BETA CELL METABOLIC ACTIVITY IN 2D VS 3D STRUCTURES

5.1. Introduction

Data in previous chapters showed that MIN6 cells cultured as pseudoislets display an improved glucose stimulated insulin secretion response compared to monolayer MIN6. This insulin secretion data mirrors metabolic data which was then produced using the seahorse bionalyser showing that there is a strong link between ATP production and insulin secretion. The data from the seahorse bioanalyser provided some insight into the effects of cell culture technique on the metabolic function of beta cells under stimulating and non-stimulating conditions. This chapter aims to further investigate how metabolic pathways are influenced by the improved connectivity seen in beta cells cultured as 3D structures and will seek to explain the mechanisms behind the changes in function described in the previous chapters. MIN6 pseudoislets showed a similar metabolic phenotype to human islets. This includes a low basal ATP production, high ATP production in high glucose conditions, and a large proportion (over 50%) of the high ATP production being due to an increase in glycolysis. MIN6 monolayers also showed an insulin secretion response to extracellular pyruvate. Insulin secretion in response to pyruvate can lead to inappropriate insulin secretion causing hypoglycaemia so this indicates another potential area of beta cell dysfunction found in 2D culture.

Optimal insulin secretion is thought to rely on tight coupling between glycolytic and mitochondrial metabolism so a beta cell functioning in optimal conditions would be expected to produce most of its ATP through oxidative phosphorylation [57, 148]. The high glycolytic contribution suggests aerobic respiration is being prevented from performing at full capacity and so the beta cells are relying on glycolysis to meet the energy demands of the cell [149]. It is possible that this is due to hypoxia. Hypoxia can be defined as either an oxygen level at which mitochondrial metabolism is compromised or as an oxygen concentration lower than that normally experienced by the cell [144, 149-152]. Hypoxia is known to be a common issue in the core of the pseudoislets and

human islets due to the distance required for the oxygen to diffuse to reach the inner cells, because of this, larger islets are inherently more prone to the effects of hypoxia [13, 85, 105]. Beta cells have a carefully regulated molecular response to hypoxic conditions which begins with the hypoxic inducible factor (HIF) complex which is known to influence the expression of at least 70 genes [149]. The genes of interest in this chapter are those that allow the cell to adapt to anaerobic metabolism. Metabolic markers known to be upregulated in response to hypoxia include GLUT1, PFK, Aldolase, GAPDH, and PGK1 along with the down regulation of glucokinase and GLUT2 [145, 153]. MCT4 is also upregulated as it is required to transport lactate produced from the pyruvate out of the cell [154]. Studies have shown that HIF expression in beta cells leads to increased glycolysis, higher basal insulin secretion and impaired glucose tolerance demonstrated by a reduced GSIS response [144, 151, 152].

The metabolic profile of pseudoislets showed some properties consistent with a hypoxic response but also other features that are not. One feature consistent with hypoxia was a high glycolytic component of ATP production in response to glucose stimulation. However, the overall increase in ATP production and insulin secretion in pseudoislets compared to monolayers suggests the high glycolytic contribution recorded was not a result of hypoxia. Previous studies report a blunted GSIS response when hypoxia was present [144, 149, 151, 152, 154]. Features of the pseudoislet and human islet metabolic phenotype inconsistent with hypoxia included a lower basal insulin secretion and basal rate of oxidative phosphorylation and a high glucose stimulated rate of oxidative phosphorylation. Although the oxidative phosphorylation contributions to overall ATP production weren't as high as the glycolytic contributions, 3D structures displayed an increased glucose stimulated OCR compared to monolayers. This suggests that the 3D arrangement of beta cells allowed for some enhancement of the pathways in mitochondrial metabolism.

As described previously, efficient glucose sensing should prevent insulin secretion at low glucose as this can lead to hyperinsulinemic hypoglycaemia. It would be expected that

inappropriate glucose sensing would result in an increase in glycolysis, which was not seen. To investigate the mechanisms causing the increased basal insulin secretion in monolayers, the expression of GLUT2 and hexokinase 1 were investigated as these proteins act together in sensing and responding to extracellular glucose levels. It is clear that there are complex mechanisms involved in the metabolic and functional changes between the 2D and 3D structures and these may be elucidated by further exploring the changes in activity and expression levels of enzymes within glycolysis and oxidative phosphorylation.

5.2. Aims

To identify the underlying mechanism driving the changes in metabolic profile of pseudoislets.

Objectives

- Determine the impact of pseudoislet formation on the expression and activity of enzymes involved in glycolysis and the TCA cycle
- Assess whether pseudoislet formation alters the basal flux of glucose in the beta cell.
- Explore expression of hypoxic markers in pseudoislets compared to monolayers.

5.3. Comparison of Glycolytic Enzyme Activities in 3D vs 2D Structures

An increase in glycolytic enzyme activity may indicate an increase in glycolysis. The activity of the glycolytic enzymes, phosphoglucose isomerase (PGI), phosphofruktokinase 1 (PFK1), Aldolase, GAPDH, and pyruvate kinase (PK) were measured for both monolayer and pseudoislet cultures to determine whether formation of pseudoislets influenced glycolytic activity (figures 51-55). PFK1 activity was significantly higher in pseudoislets compared to monolayers (figure 52). GAPDH activity was measured in high passage MIN6 and found to be consistently higher in pseudoislets than monolayers $P=0.00014$ based on $n=4$ (figure 54). The culture system had no effect on the remaining three enzymes (figures 51, 53, and 55).

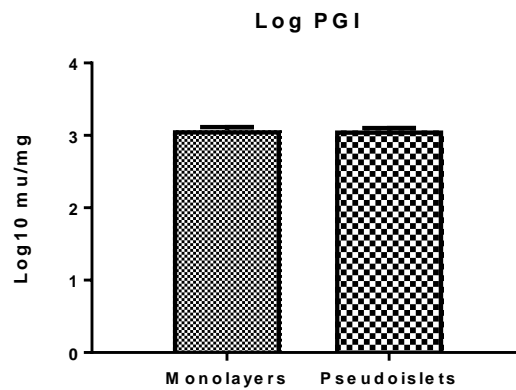


Figure 51. Phosphoglucose Isomerase Activity in Monolayers and Pseudoislets

Mean \pm SEM of phosphoglucose isomerase (PGI) activity in cell homogenate of low passage MIN6 cells cultured as monolayers vs pseudoislets. N=8. Statistical analysis performed but not found to be significant when not indicated.

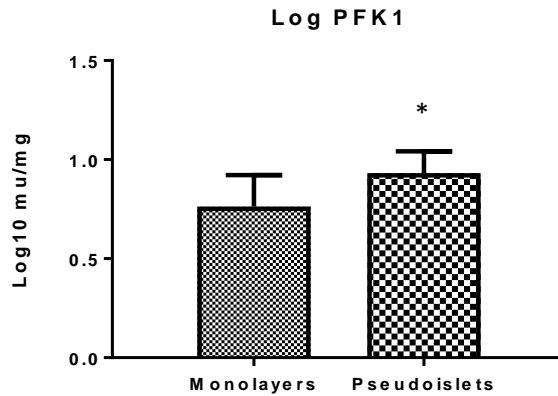


Figure 52. Phosphofructokinase 1 Activity in Monolayers and Pseudoislets

Mean \pm SEM of phosphofructokinase 1 (PFK1) activity in cell homogenate of low passage MIN6 cells cultured as monolayers (ML) vs pseudoislets (PI). N=8, P<0.05

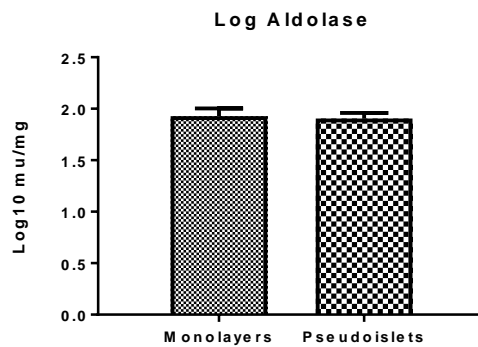


Figure 53. Aldolase Activity in Monolayer and Pseudoislets

Mean \pm SEM of aldolase activity in cell homogenate of low passage MIN6 cells cultured as monolayers (ML) vs pseudoislets (PI). N=8. Statistical analysis performed but not found to be significant when not indicated.

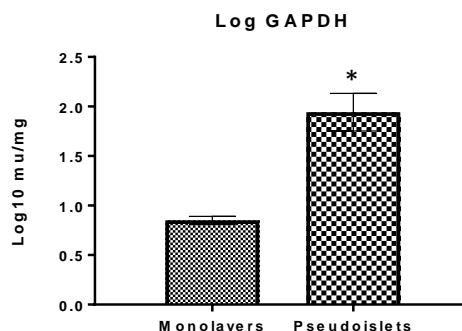


Figure 54. GAPDH Activity in Monolayers and Pseudoislets

Mean \pm SEM of GAPDH activity in total cell homogenate of high passage MIN6 cells cultured as monolayers (ML) vs pseudoislets (PI). N=4, P<0.0001

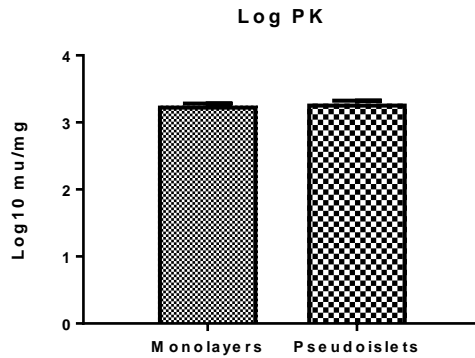


Figure 55. Pyruvate Kinase Activity in Monolayers and Pseudoislets

Mean ± SEM of pyruvate kinase (PK) activity in cell homogenate of low passage MIN6 cells cultured as monolayers (ML) vs pseudoislets (PI). N=8. Statistical analysis performed but not found to be significant when not indicated.

It is necessary for LDH activity to be low in beta cells in order to maintain the tight coupling between glycolytic and mitochondrial metabolism [69]. LDH activity was measured in the same culture systems as the previous glycolytic enzymes (figure 56). The activity was consistently higher in the MIN6 cultured as pseudoislets however this difference was too small to be statistically significant with a P value of 0.0613.

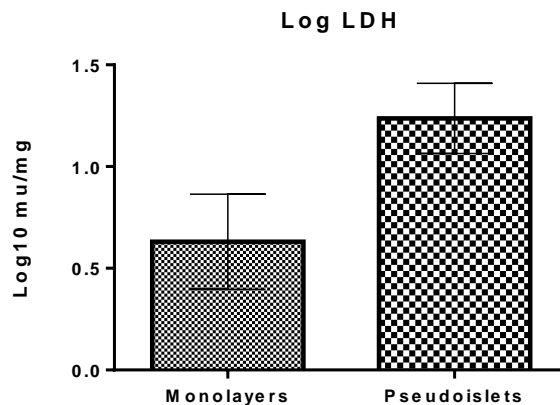


Figure 56. Lactate Dehydrogenase Activity in Monolayers and Pseudoislets

Mean ± SEM of lactate dehydrogenase (LDH) activity in total cell homogenate of high passage MIN6 cells cultured as monolayers (ML) vs pseudoislets (PI). N=8. Statistical analysis performed but not found to be significant when not indicated.

The higher enzyme activity of several glycolytic enzymes is consistent with the increased glycolytic flux measured using the seahorse XFe24 bioanalyser in section 4.4.

5.4. Comparison of Mitochondrial Enzyme Activities in 2D vs 3D Structures

Mitochondrial enzyme activity of TCA cycle enzymes was investigated in monolayer and pseudoislet cultures. An increase in mitochondrial enzyme activity could indicate increased mitochondrial metabolism which would contribute to enhanced insulin secretion. The activities of a few key enzymes for which methods could be optimised were measured. The activities of pyruvate carboxylase, citrate synthase, α -ketoglutarate dehydrogenase, and malate dehydrogenase (MDH) were higher in pseudoislets than in monolayers as shown in figures 57, 58, 60, and 61 respectively.

ICD is an enzyme involved in the TCA cycle that is carefully regulated to avoid over accumulation of α -ketoglutarate. This was the only mitochondrial enzyme that was not consistently higher in all pseudoislet sample fractions.

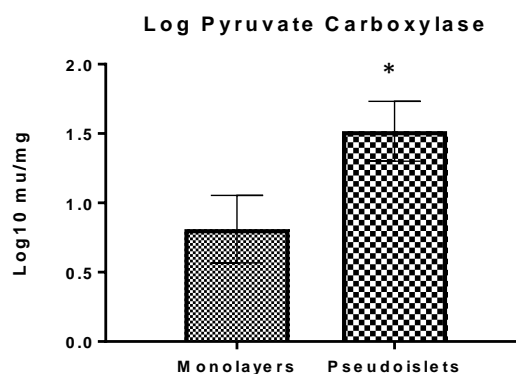


Figure 57. Pyruvate Carboxylase Activity in Monolayers and Pseudoislets

Mean \pm SEM of Pyruvate carboxylase activity in cell homogenate of high passage MIN6 cells cultured as monolayers (ML) vs pseudoislets (PI). N=5 P<0.05

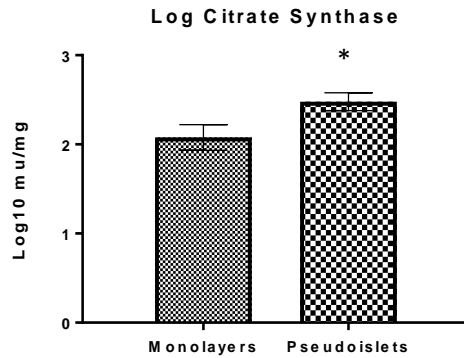


Figure 58. Citrate Synthase Activity in Monolayers and Pseudoislets

Mean \pm SEM of Citrate Synthase activity in cell homogenate of high passage MIN6 cells cultured as monolayers (ML) vs pseudoislets (PI). N=5 P<0.03

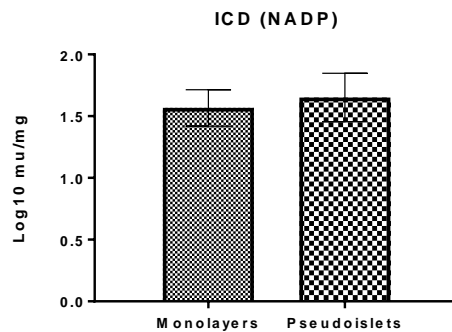


Figure 59. Isocitrate Dehydrogenase Activity in Monolayers and Pseudoislets

Mean \pm SEM of isocitrate dehydrogenase (ICD) activity in low passage MIN6 cultured as monolayers vs pseudoislets for five days. N=4. Statistical analysis performed but not found to be significant when * indicated.

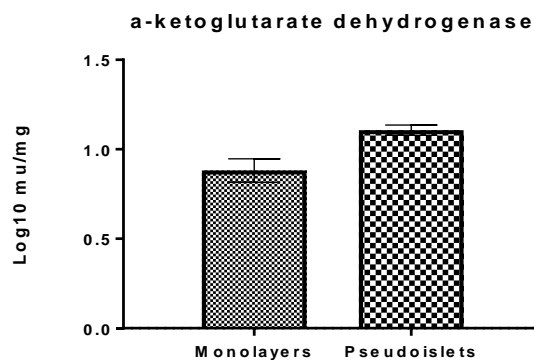


Figure 60. α -Ketoglutarate Dehydrogenase Activity in Monolayers and Pseudoislets

Mean \pm SEM of α -ketoglutarate dehydrogenase activity in low passage MIN6 cultured as monolayers vs pseudoislets for five days. N=4 P<0.03

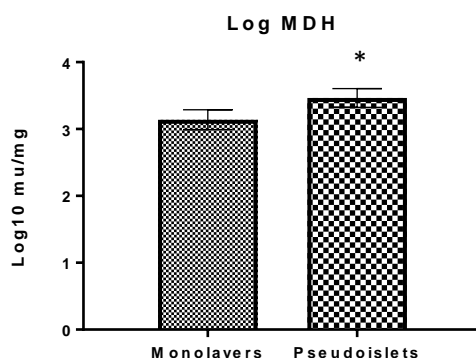


Figure 61. Malate Dehydrogenase Activity in Monolayers and Pseudoislets

Mean ± SEM of MDH activity in cell homogenate of high passage MIN6 cells cultured as monolayers (ML) vs pseudoislets (PI). N=3 P<0.05

The higher activity of the enzymes from the TCA cycle investigated is consistent with the increased rates of oxidative phosphorylation measured using the seahorse XFe24 bioanalyser in section 4.4.

5.5. Assessment of Hypoxia in Monolayer Vs Pseudoislets

The pseudoislets and human islets used in this study showed a high glycolytic contribution to ATP which may be explained by hypoxia. In hypoxic conditions HIFs promote a change from aerobic to anaerobic respiration. This involves increasing the activity of some glycolytic enzymes along with GLUT1, PDK1, and LDH. The overall effect of this is a decrease in mitochondrial oxygen consumption and an increase in glycolytic ATP production.

The expression of these genes, GLUT1, PDK1, and LDH, in pseudoislet and monolayer MIN6 was quantified using PCR. The results in figure 62 show that the expression of hypoxic genes does seem to be higher in pseudoislets but that it is also very variable. This is probably due to the variability in sizes of the pseudoislets and the fact that beta

cells in the centre of the pseudoislets were much more susceptible to hypoxia than the outer beta cells.

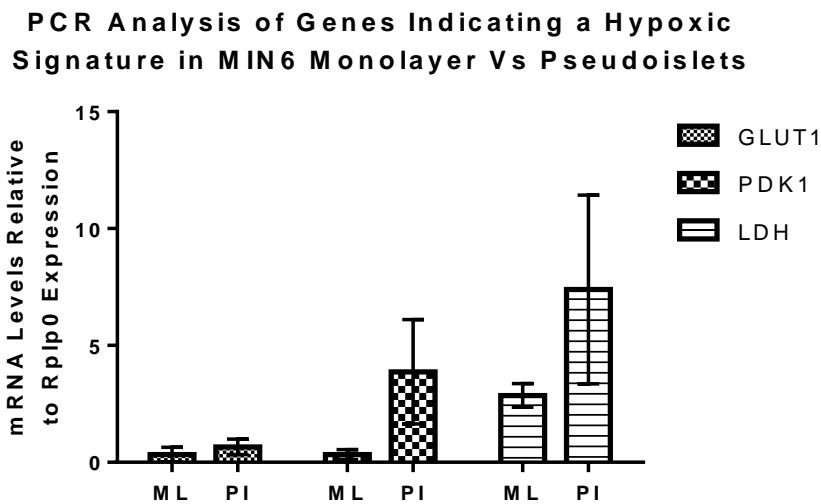


Figure 62. PCR Analysis of Hypoxic Markers in Monolayers and Pseudoislets

Mean ± SEM mRNA expression of genes indicative of hypoxia, Glut1, PDK1, and LDH. Expression was measured in monolayer (ML) and pseudoislet (PI) MIN6 (P26 – P29) after five days of culture. N=4,3,3 respectively. Statistical analysis performed but not found to be significant when not indicated.

5.6. Investigation into increased Basal ATP Production in 2D structures

The next aim of this chapter is to understand the underlying mechanisms for the increase in basal ATP production and insulin secretion that has been shown in monolayer MIN6. GLUT2 and glucokinase work together in a glucose sensing mechanism that allows the cell to respond almost immediately to changes in extracellular glucose concentrations. A decrease in GLUT2 expression is associated with diabetes onset in rodents and a reduced ability for the beta cells to respond to changes in glucose concentration [153, 155]. GLUT2 is also positively related to the state of differentiation of beta cells [156].

Western blotting (figure 63) showed that GLUT2 expression was significantly higher, $P=0.0343$, in pseudoislet MIN6 than in monolayer MIN6 suggesting that the monolayer cultures have a reduced capability in responding quickly to changes in glucose concentration.

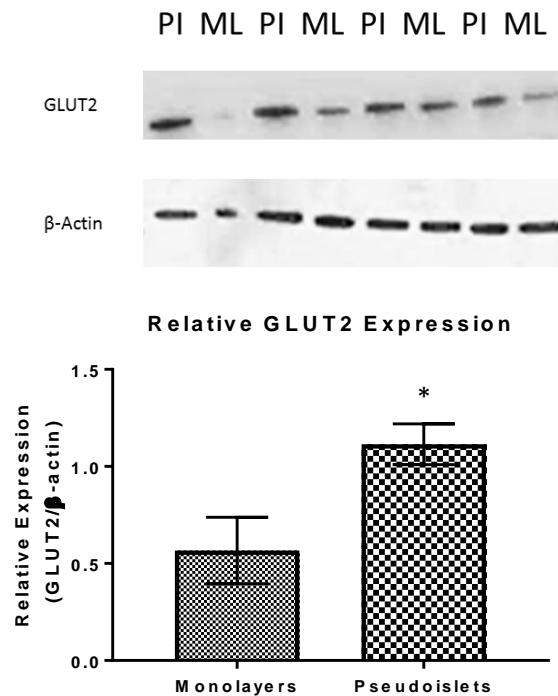


Figure 63. Western Blot Analysis of GLUT2 Expression

Western blot showing GLUT2 expression in MIN6 monolayers and pseudoislets after 5 days of culture. Beta actin was the housekeeping protein used to normalise. 20 μ g protein loaded, MIN6 P26-P28. Graph shows mean \pm SEM of normalised GLUT2 expression. N=4 $P<0.05$

The second part of the glucose sensing mechanism requires low expression of low K_m HK and high expression of glucokinase [78]. First, the activities of these enzymes were measured in monolayer and pseudoislet cultures to determine whether pseudoislet formation altered expression. There was a slight increase in low K_m hexokinase activity in the monolayer cultures that was approaching significance with a P value of 0.0595 (figure 64). No differences were found between activities glucokinase in the two different culture systems (figure 65).

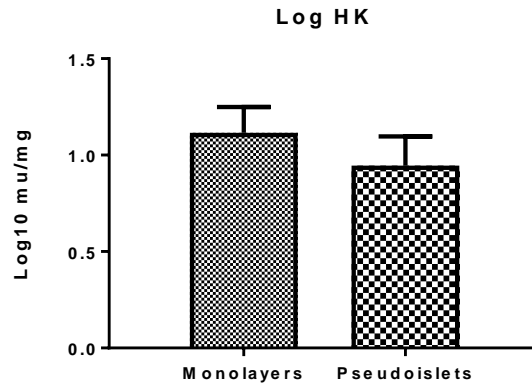


Figure 64. Hexokinase Expression in Monolayers and Pseudoislets

Mean ± SEM of hexokinase activity in the supernatant of low passage MIN6 cells cultured as monolayers vs pseudoislets. N=6. Statistical analysis performed but not found to be significant when not indicated.

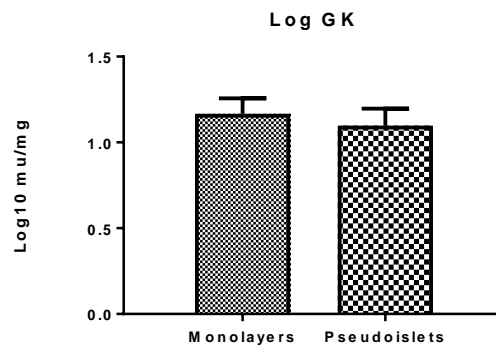


Figure 65. Glucokinase Expression in Monolayers and Pseudoislets

Mean ± SEM of glucokinase activity in the supernatant of low passage MIN6 cells cultured as monolayers vs pseudoislets. N=6. Statistical analysis performed but not found to be significant when not indicated.

The expression of hexokinase I was then also measured using western blotting, the expression of hexokinase II and hexokinase III were not investigated due to lack of specific antibodies in house. This also showed a higher expression of hexokinase I in monolayers than in pseudoislets (figure 66). The increased hexokinase expression and decreased GLUT2 expression in the monolayer MIN6 both suggest a decreased glucose sensing capacity when the beta cells aren't cultured in 3D pseudoislet structures consistent with the trend towards higher basal insulin secretion in the 2D structures.

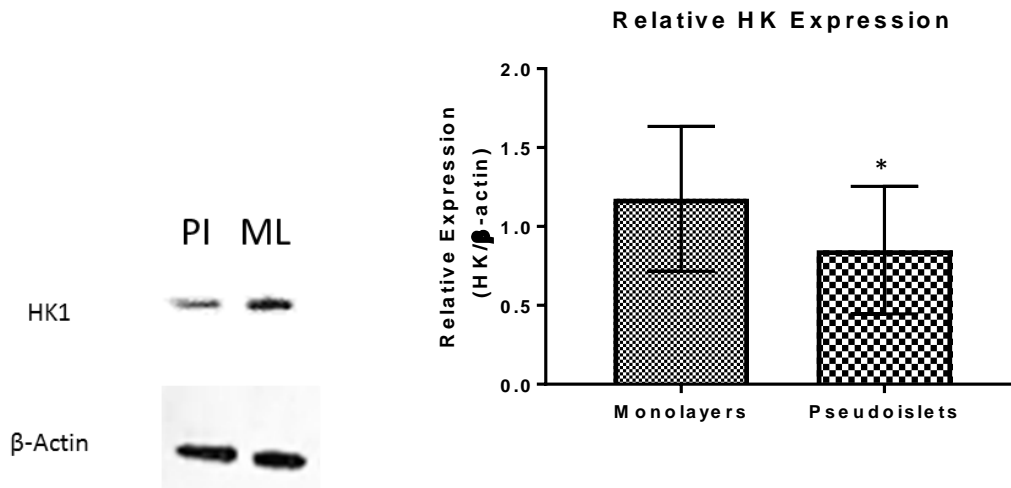


Figure 66. Western Blot Analysis of Hexokinase I Expression in Monolayers and Pseudoislets

Western blot showing Hexokinase expression in MIN6 monolayers and pseudoislets after 5 days of culture. Beta actin was the housekeeping protein used to normalise. Graph shows mean \pm SEM of normalised Hexokinase expression. N=3, P<0.05

5.7. UK5099 Inhibition

Pyruvate produced through glycolysis is shuttled into the mitochondria via mitochondrial pyruvate carriers (MPCs) where it is either used as a substrate in oxidative phosphorylation, or to replenish intermediates in the TCA cycle [54, 56, 58, 65]. MPC plays a role in the beta cell insulin secretion response to glucose and amino acids [157]. It has been shown that the addition of the MPC inhibitor, α -cyano- β -(1-phenylindol-3-yl)-acrylate (UK5099), impairs respiration under both basal and high glucose conditions meaning that continuous transport of pyruvate into the mitochondria is required to maintain respiratory rates [158].

UK5099 was used to inhibit transport of endogenous pyruvate through the MPC transporters in monolayer and pseudoislet MIN6 and the change in OCR was measured using the seahorse bioanalyser. The MIN6 media contained basal levels of glucose and L-glutamine and 1mM pyruvate. Figures 67 and 68 show OCR data for monolayers and pseudoislets respectively from one experiment and is representative of three

experiments. Calculations from this data found that pseudoislets showed a significantly higher percentage reduction in OCR than monolayers (figure 69). This suggests that more pyruvate is being shuttled into the mitochondria under basal conditions meaning that the oxidative phosphorylation pathway is more active in pseudoislets than monolayers in basal conditions.

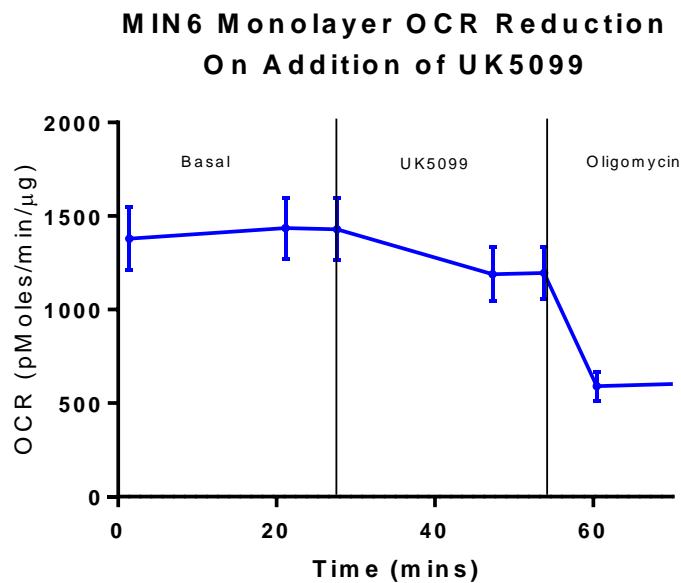


Figure 67. Monolayer OCR Reduction with UK5099

OCR response in MIN6 (P26 – P29) monolayers in media containing 0.5mM glucose and 1mM pyruvate after addition of 100μM UK5099 then 2μM oligomycin. Measured on a seahorse XFe24 bioanalyzer. Monolayer samples were cultured for 24 hours in a 24 well microplate then starved for 1 hour in 0.5mM glucose for 1 hour prior to the experiment. N= 4 technical repeats, data representative of 3 experiments.

MIN6 Pseudoislet OCR Reduction On Addition of UK5099

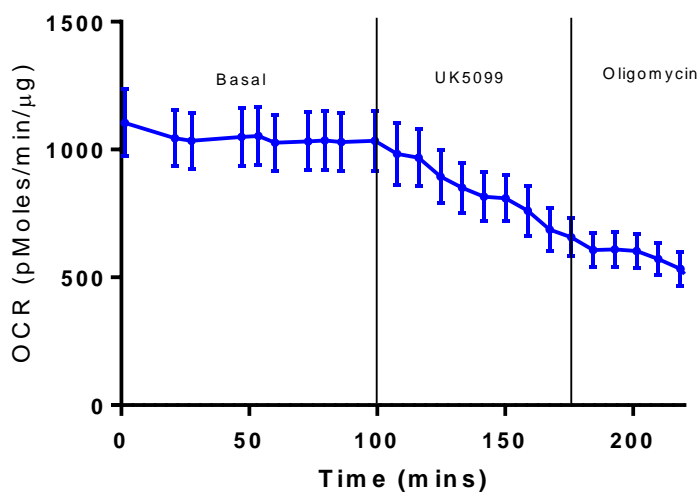


Figure 68. Pseudoislet OCR Reduction with UK5099

OCR response in MIN6 (P26 – P29) pseudoislets in media containing 0.5mM glucose and 1mM pyruvate after addition of 100μM of the MPC transporter UK5099 then 2μM oligomycin. Measured on a seahorse XFe24 bioanalyzer. Monolayer samples were cultured for 24 hours in a 24 well microplate then starved for 1 hour in 0.5mM glucose for 1 hour prior to the experiment. N= 4 technical repeats, data representative of three experiments.

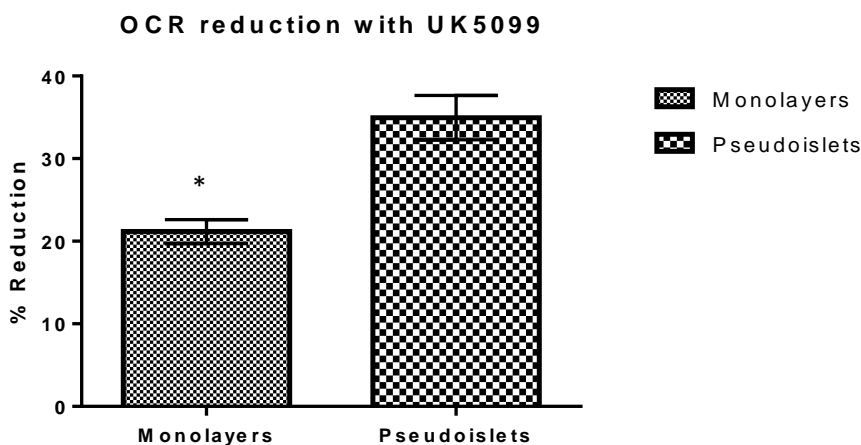


Figure 69.OCR Reduction with UK5099

Mean ± SEM of the percentage reduction in OCR of monolayer and pseudoislet MIN6 (P26 – P29) after addition of 100μM of the MPC inhibitor, UK5099. Data was recorded using a Seahorse Bioanalyser XFe24 N=3, P<0.05

5.8. MCT1 Inhibition

Antibodies were optimised for the detection of MCT1 expression through western blotting. Figure 70 shows detection of MCT1 in mouse brain and heart tissue. However, no MCT1 was detected in either monolayer or pseudoislets samples of MIN6, results not shown.



Figure 70. Western Blot Analysis of MCT1 Expression

Western blot analysis of monocarboxylate transporter 1 (MCT1) in murine brain and heart tissue. Protein loaded at 20µg, 10µg, and 5µg for both brain and heart tissue.

5.9. Conclusion

Understanding how metabolic pathways are influenced by differences in intercellular connections between beta cells in 2D and 3D architectures could help in understanding why beta cell function is lost during the isolation process. Using this knowledge to improve isolation techniques could lead to improved outcomes in islet transplant therapies.

5.9.1. Increased Glycolytic Contribution in Pseudoislets

i. Glycolytic Enzyme Activity

Seahorse data showed higher glycolytic ATP production in pseudoislet and human islets compared to monolayer MIN6. An increase in glycolytic enzyme activity may indicate an increase in glycolysis so the activities of PGI, PFK1, aldolase, glucokinase, GAPDH, and PK were compared in the monolayer and pseudoislet samples. The enzymes that were significantly influenced by culture system were PFK1 and GAPDH. These were increased in the pseudoislet samples when compared to monolayers. PFK1 is associated with the regulation of the glycolytic pathway and the generation of insulin oscillations that are present in pseudoislets but not monolayers [79].

LDH activity can interfere with glucose sensing as anaerobic metabolism of pyruvate produces less ATP than would be produced through mitochondrial metabolism [54]. It would therefore be expected that pseudoislets which are reported to have a high insulin secretion response would express lower levels of LDH than monolayers which are reported to be less responsive to glucose. However, the results in figure 56 show that there was a slight trend towards higher LDH activity in pseudoislets than in monolayers. Although this trend is inconsistent with the insulin secretion responses reported it does support the findings in Chowdhury et al where a 1.4 fold increase in LDH expression was reported in pseudoislets when compared to monolayers [80]. It also supports the seahorse data which showed that although the pseudoislets were producing more ATP

and therefore secreting more insulin than monolayers, a large percentage of this ATP was produced through uncoupled glycolysis.

To investigate whether the increase in uncoupled glycolysis was due to the presence of hypoxia within the pseudoislet structures, the expression of some key markers of hypoxia were measured in pseudoislets and monolayers using RT-PCR. The genes included LDH, GLUT1, and PDK1. PDK1 and LDH displayed a trend towards increased expression in pseudoislets but with high variability. Hypoxia is known to be a common issue in islets as oxygen cannot freely diffuse to the centre of larger islets and this can lead to a reduction in function and necrosis [144, 149, 151, 152, 154]. The high variability in hypoxic gene markers suggests that at least some beta cells within the islets are displaying signs of hypoxia but the effect this will have on the overall function of the islet is not certain. However, the decrease in basal ATP production and basal insulin secretion is not consistent with a classical hypoxic response. In hypoxia there is an upregulation of hexokinase II which increases flux at low glucose concentrations [150]. Pseudoislets would be expected to respond to hypoxia through an increase in basal ATP production and insulin secretion but in this case the converse is true. Hypoxia may be driving the increase in uncoupled glycolysis, but it cannot explain the pseudoislet decrease in basal insulin secretion nor the increased glucose responsiveness.

ii. Mitochondrial Enzyme Activity

The activities of the mitochondrial enzymes, PC, citrate synthase, ICD, α -Ketoglutarate dehydrogenase, and MDH were recorded in monolayers and pseudoislets. Pseudoislets showed an increase in the activities of all these enzymes with the exception of ICD. These results suggest an increase in TCA cycle activity in MIN6 cultured as pseudoislets compared to in those cultured as monolayers. The reason for this increase in activity is unclear. An increase in mitochondrial activity could offer a greater capacity for coupling and improved flux through the TCA cycle, this is consistent with increased OCR in pseudoislets compared to monolayers and is consistent with data from Chowdhury et al

[80]. It could also be a result of increased mitochondrial biogenesis which can be investigated through mitochondrial staining or PCR analysis of mitochondrial mRNA.

5.9.2. Increased Basal Insulin Secretion

Monolayer MIN6 showed an increased level of basal insulin secretion compared to pseudoislets and human islets. Glucokinase has a low affinity for glucose and so plays an important role in maintaining the low basal rate of insulin secretion. Overexpression of low K_m hexokinase which has a high affinity for glucose is associated with an increase in insulin secretion response at low glucose levels [57]. The results of this study show that there was no change in Glucokinase activity but that there was a trend towards increased hexokinase activity in MIN6 cultured as monolayers and a significant increase in hexokinase I expression when compared to those cultured as pseudoislets. High GLUT2 expression is required for rapid glucose sensing as extracellular levels fluctuate [145, 153]. A higher GLUT2 expression was found in pseudoislets than in monolayers. This suggests that pseudoislets are more efficient in sensing changes in extracellular glucose concentration. Monolayers showed no change in basal ATP production from glycolysis, but a higher basal oxidative phosphorylation rate (figures 44 and 45). This increased basal insulin secretion is a feature seen in T2DM. Proposed mechanisms for this increase include hypertrophy of the beta cells, an increase in intercellular glycogen stores, and an increase in a constitutive secretory pathway working independent of metabolic signals [139].

5.9.3. MPC inhibition

Transport of exogenous pyruvate into the beta cell is restricted through a lack of the plasma membrane transporter MCT1 [147]. On the other hand, transport into the mitochondria of endogenous transport produced through glycolysis within the beta cell is necessary for optimal ATP production and therefore insulin secretion [58]. In this study endogenous pyruvate transport into the mitochondria was blocked through the MPC inhibitor UK5099. This resulted in a greater percentage reduction in the OCR of

pseudoislets than monolayers. Possibly because the high insulin secretion response seen in pseudoislets is reliant on the shuttling of pyruvate into the mitochondria to produce maximal ATP through oxidative phosphorylation. When Islets are cultured under starvation conditions, leucine promotes anaplerotic flux of glutamine through glutaminase and GDH [159]. As the glucose concentration of the media was low (0.5mM) it is possible that L-glutamate was a key fuel source. Future experiments involving UK5099 would assess changes in OCR in media containing stimulating levels of glucose.

CHAPTER 6. INFLUENCE OF CX36 KNOCKDOWN ON BETA CELL FUNCTION

6.1. Introduction

3D structures showed an improved functional response to 2D cultures as described in chapters 3-5. This improved function is also well documented in other studies [80, 85, 86, 97, 101, 104, 105]. Further analysis into the pathways involved in the metabolic function of beta cells in 2D and 3D structures showed two key features. One is that 3D structures display a superior glucose sensing function at both basal and high glucose levels when compared to 2D culture. The second is that there are still some limitations in the pseudoislet and human islet models most likely caused by the difficulties associated with maintaining the high oxygen demand to all parts of the islet. Nonetheless pseudoislets functioned in a very similar manner to human islets and remain the most accessible and relevant model in studying pathways associated with diabetes.

Changes in blood glucose concentrations result in oscillations in Ca^{2+} concentrations within the beta cell which trigger insulin secretion [73, 160]. Dispersed beta cells display a high variability in Ca^{2+} responses to glucose stimulation. Once beta cells have formed 3D structures cytoplasmic Ca^{2+} concentrations become synchronised leading to synchronised insulin secretion oscillations. It is currently believed that the increased GSIS response seen in 3D structures in comparison to dispersed beta cells is due to synchronisation of calcium signals [98, 140]. This synchronisation results in a greater insulin secretion response under stimulation and a more predictable threshold for insulin secretion stimulation [107]. The integrated insulin secretion response of the islet is greater than the sum of the individual responses of the beta cell within the islet [98]. It has been shown that direct contact between the cells is necessary for the improvements in the secretory response to be seen so this is not thought to be an effect of paracrine activity [98].

The formation of the 3D structures has been shown to rely on and result in the formation of intercellular connections discussed in section 1.5. These connections include cell adhesion molecules, gap junctions and communication via paracrine signalling. E-cadherins are a common cell adhesion molecule that have been shown to play an important role in maintaining the structural integrity of the islet and to act as mechanoreceptors. Although required for the formation of the islets or pseudoislets, e-cadherins have not been found to influence the synchronised responses of beta cells [9, 107]. Paracrine signalling from both beta cells and non-beta cells has not been shown to play an important role in regulating the insulin secretion response. Gap junctions provide metabolic and electrical coupling between beta cells and have been directly correlated with insulin content in the beta cells [9]. It is thought that these gap junctional couplings are also responsible for the synchronised insulin secretion response seen in 3D structures.

One gap junction which has been shown to be important in the co-ordination of beta cell responses within islets is Connexin 36 (Cx36) also known as gap junction delta 2 protein (GJD2). Six protein subunits of Cx36 together form a pore in the beta cell which will form a channel when aligned with Cx36 subunits of a neighbouring cell. Molecules are then able to pass freely between the beta cells. Cx36 expression has been associated with expression of the insulin gene [161]. Pharmacological modulation of connexins has so far been non-specific, there are no current pharmacological agents that act exclusively on Cx36 and compounds that are used for Cx36 inhibition such as mefloquine and heptanol have a limited half-lives so this method of investigation has not reported any successful investigations into the effects of Cx36 on beta cell function [95]. Knockdown of Cx36 in mice has shown that deleting the Cx36 gene resulted in a lack of Cx36 gap junctions forming and this had various effects on the islets. Lucifer yellow is a fluorescent tracer compound used to visualise intracellular communication. The lack of Cx36 channels prevented the exchange of the lucifer yellow between cells suggesting that the gap junction is required to functionally couple the cells. Secondly, the knockdown in Cx36 islets resulted in a lack of Ca^{2+} synchronicity and therefore loss of pulsatile insulin secretion which was accompanied by a significant increase in basal

insulin secretion [140]. Another study investigating partial and complete knockdown of Cx36 reported that islets with partial Cx36 knockdown showed no changes in basal insulin secretion but a decrease in the stimulated insulin secretion response. Total knockdown of Cx36 in this study resulted in a raised basal insulin secretion as well as the lack of insulin secretion response to glucose [94]. The expression of Cx36 has also been shown to increase in beta cells arranged in 3D structures compared to those cultured as monolayers [82].

6.2. AIMS

This chapter aims to investigate the involvement of Cx36 in regulating beta cell metabolic function and consequent insulin secretion response.

Objectives:

- To develop a mouse beta cell model with inducible Cx36 knockdown.
- To use this model to determine the influence of Cx36 on insulin secretion and metabolic function.

6.3. MIN6 CELL CONNEXIN 36 KNOCKDOWN MODEL DEVELOPMENT

With the main aim of this chapter being to determine if Cx36 mediates the improved functionality of pseudoislets versus monolayers, the first step was to develop MIN6 with stable knockdown of Cx36 using shRNA. The pseudoislets form over five days so a stable inducible transfection system was chosen over a transient system. This allowed the MIN6 cells time to form the pseudoislets before the Cx36 knockdown was induced to ensure that experiments focused only on the effects of Cx36 knockdown on function and not on the formation of the pseudoislets. A SMARTvector inducible lentiviral shRNA system was used. Figure 71 shows the elements that make up the vector and the purpose of each one is explained in table 6. This system enabled selection of the transduced cells through antibiotic selection, visual identification of transduced cells, and an inducible knockdown response in the presence of doxycycline.

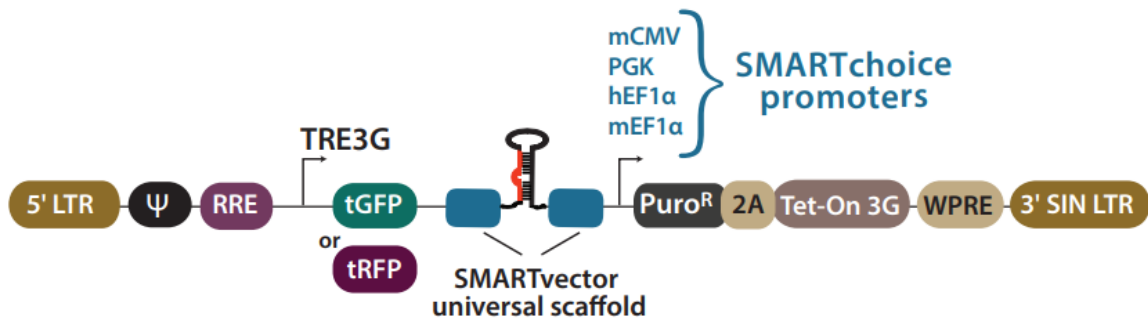


Figure 71. SMARTvector Inducible Lentiviral shRNA Vector

Elements of SMARTvector inducible lentiviral shRNA vector. Image taken from SMARTvector Inducible Lentiviral shRNA technical manual.

VECTOR ELEMENT	PURPOSE
5' LONG TERMINAL REPEAT (5' LTR)	Necessary for lentiviral production and integration into the host cell.
PSI PACKAGING SEQUENCE (Ψ)	Allows lentiviral genome packaging.
REV RESPONSE ELEMENT (RRE)	Increases packaging efficiency to enhance titre.
TETRACYCLINE RESPONSE ELEMENTS (TRE3G)	Allows induction of promoter in the presence of doxycycline.
TGFP OR TRFP	Reporter for visual tracking of transduction. In this case tGFP was used.
SMARTVECTOR UNIVERSAL SCAFFOLD	Scaffold based on native primary microRNA in which gene targeting sequence is embedded.
PUROMYCIN RESISTANCE GENE (PURO ^R)	Allows antibiotic selection of transduced cells
2A	Self-cleaving peptide enabling Puro ^R and Tet-On 3G transactivator expression from a single promoter.
TET-ON 3G	Encodes doxycycline-regulated transactivator protein.
WOODCHUCK HEPATITIS POST-TRANSCRIPTIONAL REGULATORY ELEMENT (WPRE)	Enhances transgene expression in target cells.
3' SELF-INACTIVATING LONG TERMINAL REPEAT (3' SIN LTR)	For generation of replication incompetent lentiviral particles.

Table 6. shRNA Construct Elements

Explanation of utilities of lentiviral shRNA construct elements. Table adapted from information in the SMARTvector Inducible Lentiviral shRNA technical manual.

6.3.1. Optimisation of Transduction Conditions

Before selecting the construct to be used in this investigation, the optimal conditions for transduction of MIN6 cells with the shRNA lentiviral constructs were determined. This included cell seeding density, polybrene concentration and FBS presence. Two plates were set up following the plate layout shown in figure 72. On the second day the confluency of the wells was visually inspected, the seeding density of 30,000 cells/well provided the optimal confluency for transduction. Transduction media both with and without FBS and at varying concentrations of polybrene was then prepared and added to the wells of each plate as shown in figure 43. After six hours, culture medium was added to each well of one plate while the other plate was left overnight before culture medium was added. The following day, the cell confluency and morphologies were examined using a microscope. The MIN6 cells were seen to be detaching and less confluent on the plate which had been left overnight but growing well on the six-hour transduction plate. The cells also appeared to tolerate the lack of FBS during the six-hour transduction and the highest concentration of polybrene tolerated without effecting cell growth was 8µg/mL. These were the conditions selected to use in further transductions and the selected wells have been marked by a red box in figure 72.

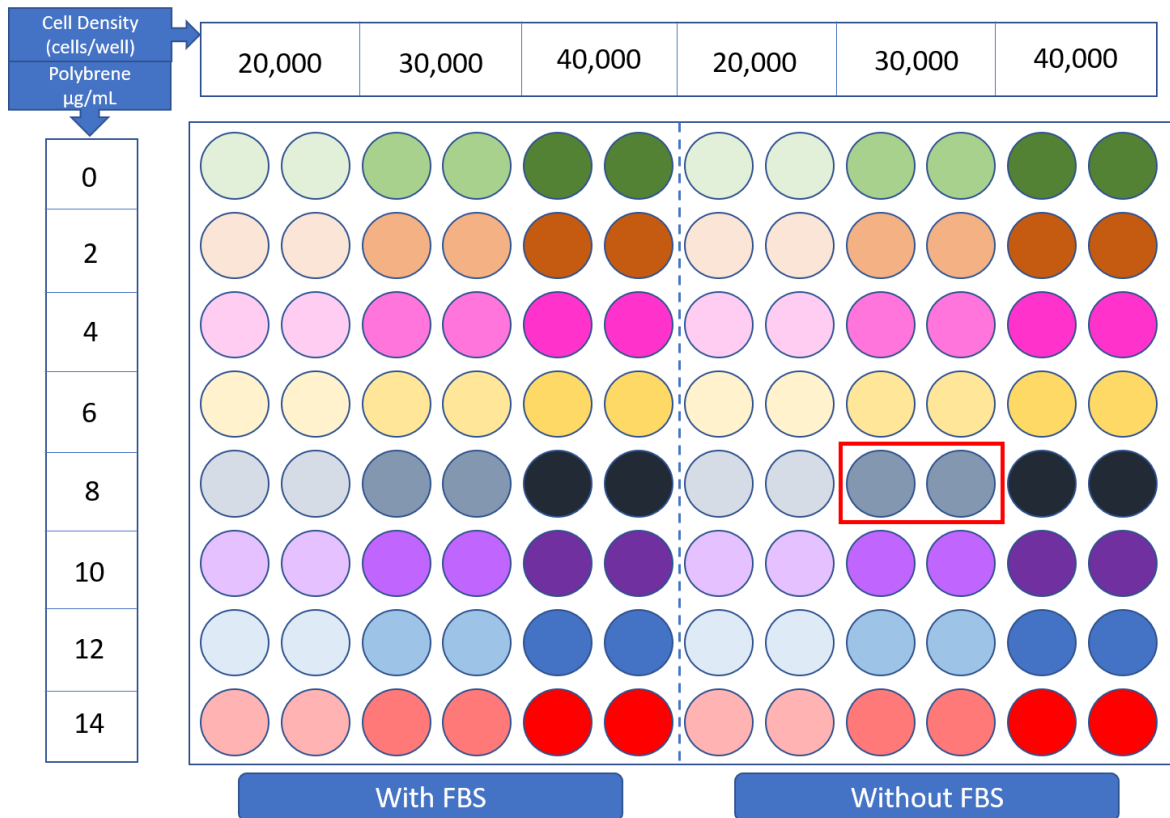


Figure 72. Plate Format for Transduction Optimisation

Template for 96 well plate layout used to select optimal transduction conditions in MIN6 cells. The optimal conditions chosen to use in further transductions has been marked by a red rectangle.

6.3.2. Selection of optimal Promotor for MIN6 Transduction

To determine the promotor that is most active in MIN6 cells, a SMARTchoice shRNA promotor selection plate was used. Using the transduction conditions determined previously, MIN6 cells were transduced with seven different SMARTvector non targeting controls, each containing a different promotor. The cells were transduced at a range of multiplicity of infections (MOIs). The activities of seven different promotors in MIN6 cells were imaged and the images displaying the highest expression of GFP for each promotor is displayed in figure 73. The mCMV promotor produced the highest fluorescence intensity indicating it would be the optimal promotor for use in MIN6.

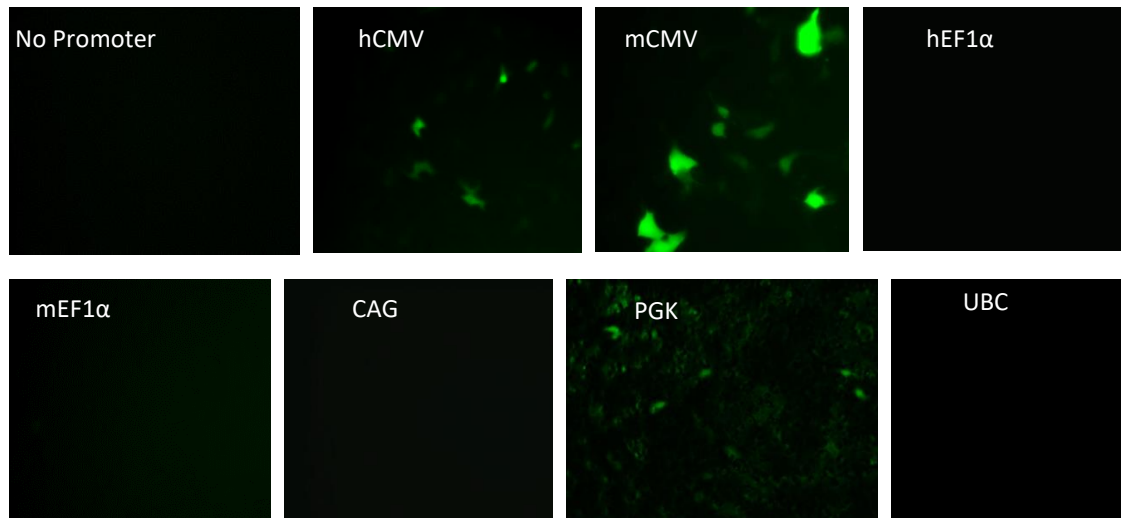


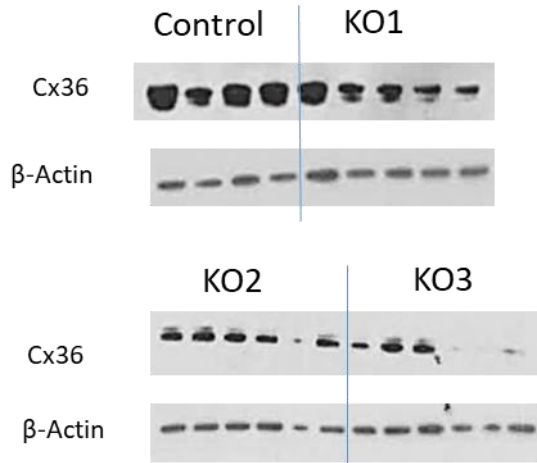
Figure 73. Fluorescence Microscopy Images of SMARTchoice Promoters

Fluorescence microscopy of MIN6 transduced with SMARTvector 8.0 Non-targetting control particles from the Dharmacon SMARTchoice Promoter Selection Plate.

6.3.3. Analysis of Doxycycline induced Connexin 36 knockdown in transduced MIN6

Three different shRNAs expressing the mCMV promotor and an inducible shRNA against Cx36 were used. These were designated KD1, KD2, and KD3. MIN6 were transduced with each shRNA and a scrambled control using conditions described in section 6.3.1. Growth media was then supplemented with 1µg/mL of freshly dissolved doxycycline to activate the knockdown at various time points over 48 hours. To select the shRNA producing the cell line with optimal inducible Cx36 knockdown, western blots were used to measure Cx36 expression.

The results from these western blots (figure 74) show that each of the three shRNA constructs tested resulted in a lower Cx36 expression than in the MIN6 transduced with the scrambled control. There was a gradual reduction in Cx36 expression proportional to increased exposure time to the doxycycline with all constructs KD3 showed the greatest effect on the Cx36 levels and thus was used for further experiments.



Western Blot Analysis of Cx36 KD

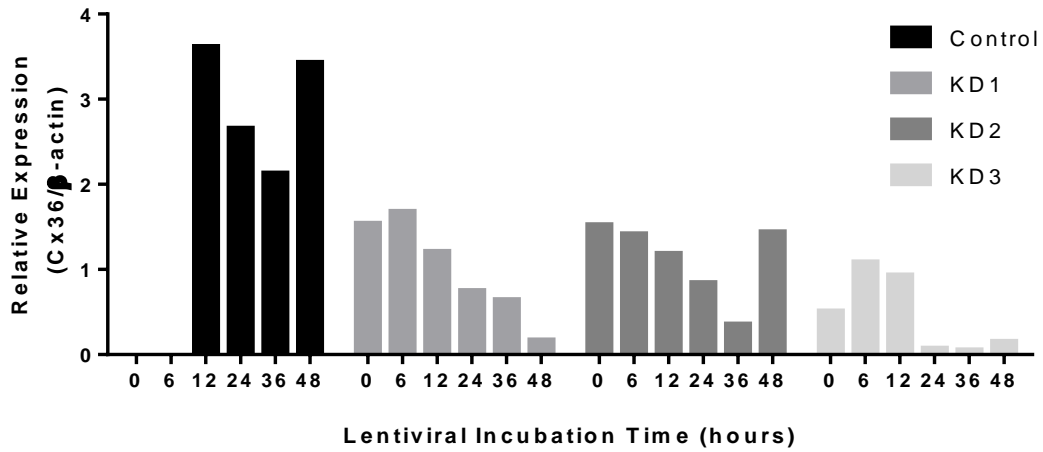


Figure 74. Western Blot Analysis of Cx36 KD

Western blot showing connexin 36 expression in high passage MIN6 pseudoislets after five days of culture with doxycycline added for the final 0, 6, 12, 24, 36, and 48 hours. Samples include MIN6 transduced with three different shRNAs containing a Cx36 knockdown gene (KD1, KD2, and KD3) and a scrambled control. Beta actin was the housekeeping protein used to normalise. Graph shows mean of normalised connexin 36 expression. N=1

6.4. INFLUENCE OF CONNEXIN 36 KNOCKDOWN ON THE INSULIN SECRETION RESPONSE OF MIN6 PSEUDOISLETS

The insulin secretion response of the MIN6 pseudoislets with Cx36 knockdown was measured in comparison to the response of MIN6 transduced with the scrambled control (figure 75). Pseudoislets used in this study were formed in standard MIN6 culture media for three days then in media with doxycycline present for a further two days, there was no obvious effect of Cx36 KD on pseudoislet formation (results not shown). The MIN6 with Cx36 KD showed much higher variability in insulin secretion response at both basal and high glucose. The basal insulin secretion was almost 4-fold higher in the Cx36 KD compared to scrambled control. The insulin secretion at high glucose also appeared higher with the induced knockdown but due to the high basal insulin secretion the fold increase in insulin secretion was lower, 2.5 for the Cx36 KD and a 3.7-fold increase in the control.

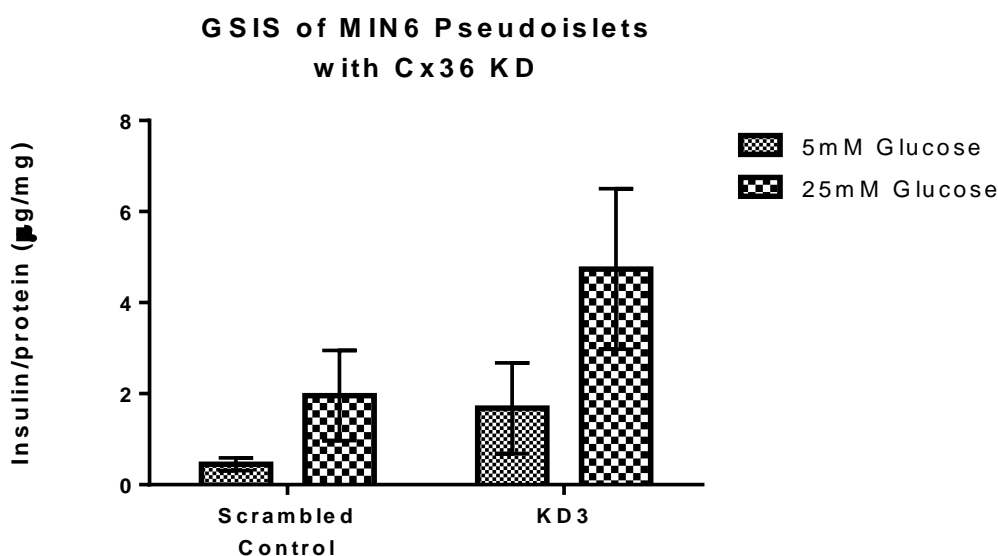


Figure 75. GSIS of MIN6 Pseudoislets with Cx36 KD

Insulin secretion response of high passage MIN6 cultured as pseudoislets for five days with connexin 36 knockdown induced on day two. Pseudoislets were incubated for 30 minutes in 0.5mM glucose media then one hour at either 5mM glucose or 25mM glucose. N=3. Statistical analysis performed but not found to be significant when not indicated.

6.5. INFLUENCE OF CONNEXIN 36 KNOCKDOWN ON ATP PRODUCTION

Using the Seahorse bioanalyser protocols developed in chapter 4 and the pseudoislet protocol as described for GSIS in 6.4, the impact of the Cx36 KD on metabolic function was analysed. MIN6 transduced with scrambled control or shRNA encoding inducible Cx36 knockdown formed pseudoislets over five days. Doxycycline was present in the final two days of pseudoislet culture to induce the knockdown. The pseudoislets were then treated for one hour in 0.5mM glucose media before analysing the metabolic activity. Figures 76 and 77 show an example experiment displaying the OCR and ECAR measurements respectively. There was no consistent effect of Cx36 KD on both basal and glucose-stimulated glycolysis as assessed by ECAR. However, there was a clear increase in basal rates of OCR following Cx36 KD. The data from three of these experiments were then analysed to calculate the ATP production from oxidative phosphorylation and glycolysis both with and without Cx36 KD, figures 78-80.

Scrambled Control Vs Cx36 KD OCR

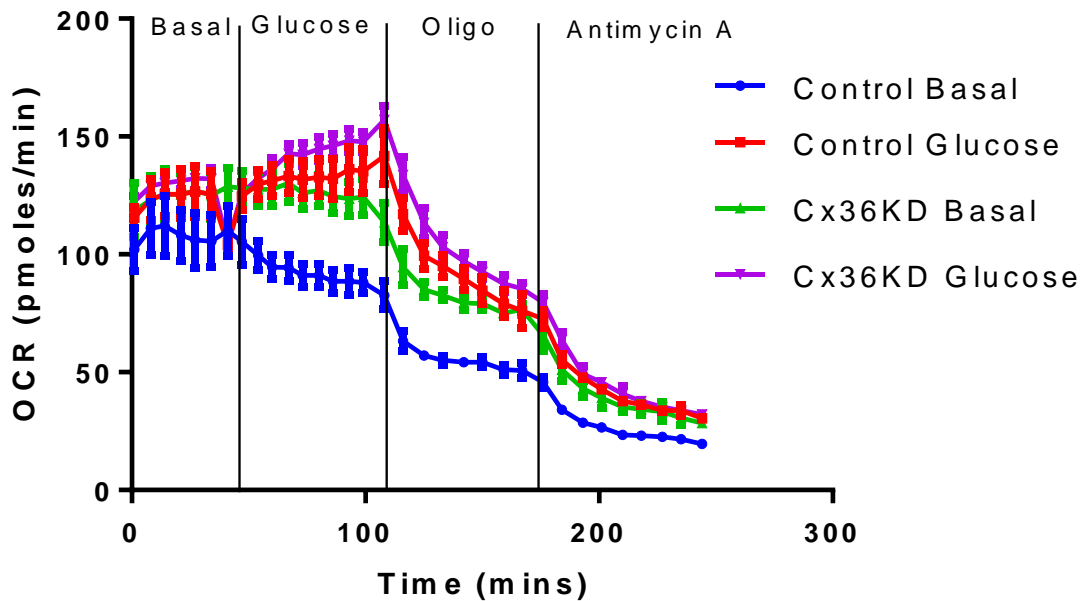


Figure 76. OCR of Pseudoislets with Cx36 KD

OCR response in high passage MIN6 Cx36 stable KD model cultured as pseudoislets for five days and with doxycycline induction on day two or no induction in the controls. The first injection contained either 25mM glucose or 0.5 μ M glucose injection and subsequent injections contained 20 μ M oligomycin, then 0.5 μ M Antimycin A. Measured on a seahorse XFe24 bioanalyzer. Islets were cultured for 24 hours on a 24 well microplate and starved for one hour in 0.5mM glucose prior to the experiment. N=3.

Scrambled Control Vs Cx36 KD ECAR

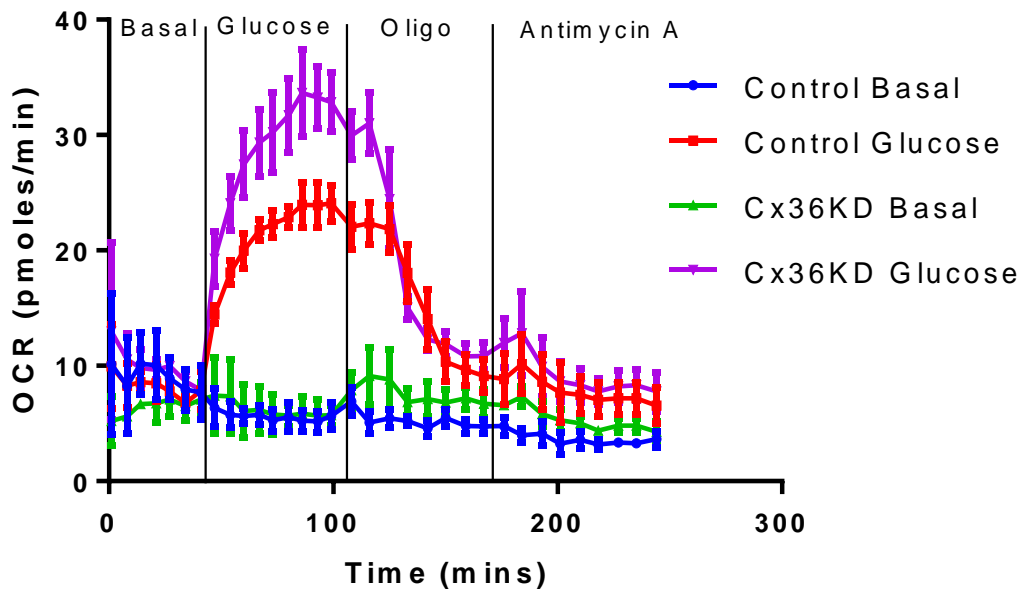


Figure 77. ECAR of Pseudoislets with Cx36 KD

ECAR response in high passage MIN6 Cx36 stable KD model cultured as pseudoislets for five days and with doxycycline induction on day 2 or no induction in the controls. The first injection contained either 25mM glucose or 0.5 μ M glucose injection and subsequent injections contained 20 μ M oligomycin, then 0.5 μ M Antimycin A. Measured on a seahorse XFe24 bioanalyzer. Islets were cultured for 24 hours on a 24 well microplate and starved for one hour in 0.5mM glucose prior to the experiment. N=3.

The total ATP production from all metabolic pathways in Cx36 KD and control cell were then calculated and are shown in figure 78. This data suggests that the knockdown of Cx36 results in a slightly higher basal ATP production and higher ATP production at high glucose. However, the fold change in overall ATP Production was 3.03-fold for MIN6 pseudoislets with the scrambled control and 2.9-fold for the pseudoislets with Cx36 KD. These differences between these fold changes is smaller between the differences seen between the fold changes in insulin secretion response but do support trends in insulin secretion shown in figure 75. The total ATP production is expected to be tightly linked to insulin secretion but analysing the separate contributions of glycolysis and oxidative phosphorylation to the ATP production can provide more insight into the pathways.

The ATP contributions from oxidative phosphorylation are shown in figure 79. These results show that the increased basal ATP production in Cx36 KD MIN6 is at least in part caused by an increase in basal oxidative phosphorylation. The MIN6 with Cx36 Knockdown also showed a slight increase in ATP production at high glucose. The fold increase between oxidative phosphorylation contributions to ATP production at basal and stimulating glucose levels was 1.4 for MIN6 with Cx36 knockdown and 2-fold for the control however these increases did not reach statistical significance.

Figure 80 shows the ATP contribution from glycolytic metabolism. This data shows that Cx36 expression does not influence glycolytic activity at basal glucose levels but that ATP production through glycolysis is higher at stimulating levels of glucose in MIN6 with the Cx36 knockdown.

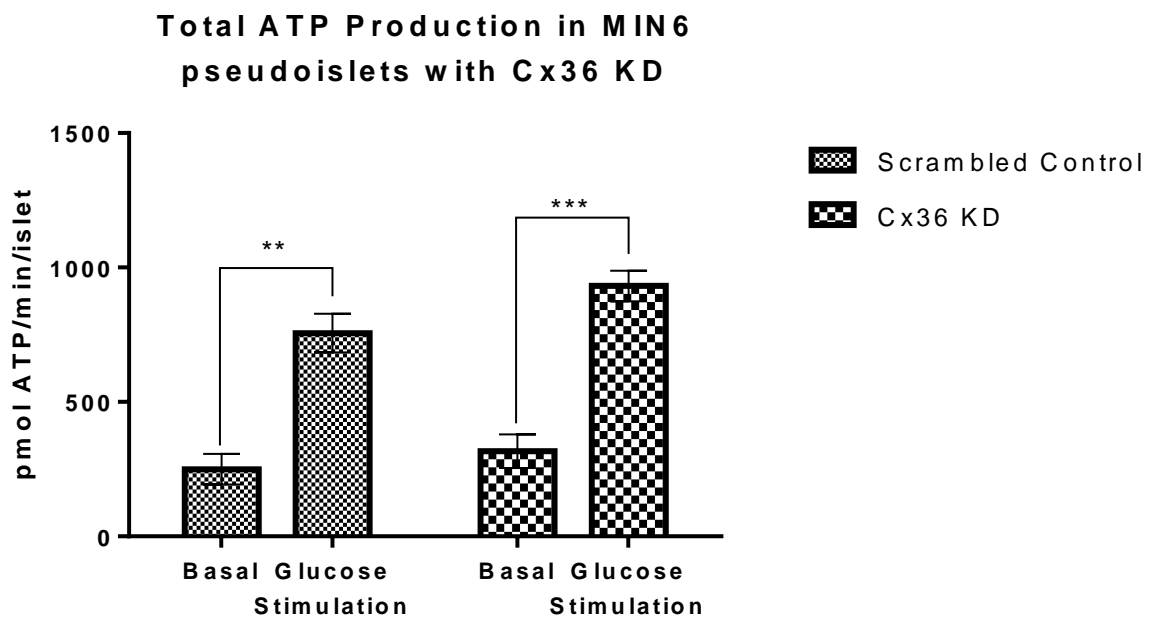


Figure 78. ATP Production in Pseudoislets with Cx36 KD

Total ATP produced per minute by pseudoislets stimulated by glucose. Measured by the seahorse XFe24 bioanalyser. MIN6 pseudoislets formed over five days were then cultured for 24 hours on a 24 well islet capture plate. N=3, **=P<0.01, *=P<0.005**

ATP Production From Oxidative Phosphorylation in MIN6 pseudoislets with Cx36 KD

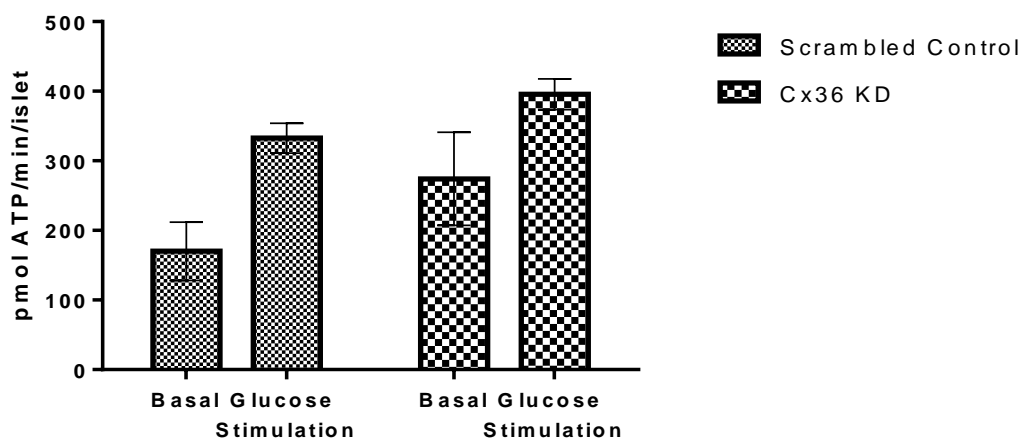


Figure 79. ATP Production from Oxidative Phosphorylation in Pseudoislets with Cx36KD

Total ATP produced per minute through oxidative phosphorylation by pseudoislets stimulated by glucose. Measured by the seahorse XFe24 bioanalyser. MIN6 pseudoislets formed over five days were then cultured for 24 hours on a 24 well islet capture plate. N=3. Statistical analysis performed but not found to be significant when not indicated.

ATP Production From Glycolysis in MIN6 pseudoislets with Cx36 KD

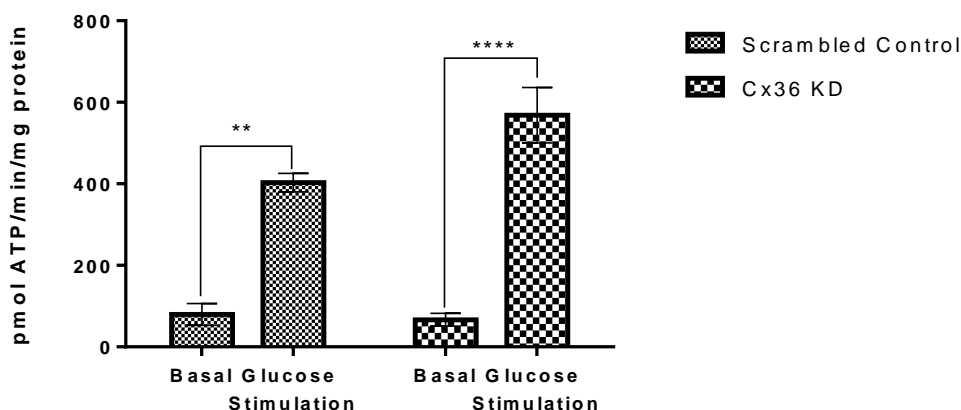


Figure 80. ATP Production from Glycolysis in Pseudoislets with Cx36 KD

Total ATP produced per minute through glycolysis by pseudoislets stimulated by glucose. Measured by the seahorse XFe24 bioanalyser. MIN6 pseudoislets formed over five days were then cultured for 24 hours on a 24 well islet capture plate. N=3, **=P<0.01, **=P<0.001**

6.6. CONCLUSION

6.6.1. Development of Cx36 Knockdown Model

This chapter aimed to investigate the role of Cx36 in regulating the function of pancreatic beta cells. The influence of Cx36 on beta cell function has been investigated through a variety of approaches. Firstly, beta cells cultured as dispersed 2D monolayers have limited intercellular communication. This dispersal of islets is well known to have an immediate negative impact on beta cell secretory function [16, 101]. Pharmacological agents are able to create chronic or acute inhibition of transport through gap junctions without preventing the formation of the islets. However, the mechanism of action and specificity of these drugs are not well understood, and nonspecific interactions may influence results [95, 162]. Rodent models with partial or complete Cx36 KO have reported beta cell dysfunction [89, 94, 140, 163]. Due to the time and cost restraints in this study generating a mutant mouse model was not an option and as the specificity and half-lives of the pharmacological agents are uncertain,

the influence of Cx36 was investigated through a cell line with inducible Cx36 KD in this study.

First the inducible Cx36 knockdown cell line was generated in MIN6 cells. The ideal transduction conditions, promotor, and shRNA constructs were identified. The transduction conditions and promotor conditions found to be optimal in this chapter are similar to the ideal MIN6 transduction conditions reported in previous studies [164]. This chapter only focused on MIN6 cultured as 3D structures either with Cx36 KD or transduced with a scrambled control. The pseudoislets formed over five days with doxycycline added over the final two days to induce the knockdown. The addition of doxycycline did not inhibit the continued formation of the islets which were inspected regularly under a light microscope. Western blots reporting Cx36 expression along with fluorescence microscopy to check for GFP expression confirmed successful transduction and Cx36 knockdown in the MIN6.

6.6.2. Increased functional activity at Basal Glucose in Cx36 Knockdown

The functional activity of MIN6 pseudoislets with Cx36 knockdown was measured at basal glucose conditions. This included measuring insulin secretion through an insulin enzyme linked immunosorbent assay (ELISA) and ATP production using a seahorse XFe96 bioanalyser. The pseudoislets carrying the Cx36 knockdown displayed a higher basal insulin secretion and ATP production than the pseudoislets expressing Cx36. This increased activity at basal levels was also shown in monolayers in sections 3.7.4, and 4.4 when compared to 3D structures. It is well known that basal insulin secretion is increased when beta cells are dispersed and there is evidence to show that Cx36 is required to maintain function at basal levels, so this is consistent with previous studies [94, 96, 140, 163, 165]. The Cx36 channels are thought to maintain a low basal insulin secretion response by coordinating the basal response between beta cells within the 3D structure. Spontaneous bursts of $[Ca^{2+}]$ can sometimes occur in isolated beta cells stimulating insulin secretion at basal glucose levels, the Cx36 channels distribute these $[Ca^{2+}]$ waves throughout the islet allowing the less active cells to diminish the effects of

these bursts from more active cells [95]. It is also for this reason that beta cell function measurements are less variable in 3D structures than in 2D structures. The error bars on the insulin secretion measurements in figure 75 are much larger for the samples with Cx36 knockdown suggesting that the hyperpolarizing waves from individual islets could be less well-regulated within these islets.

The data generated using the seahorse bioanalyser suggests that the increased basal activity is due to an increase in metabolism through oxidative phosphorylation. The levels of glycolytic activity did not alter between pseudoislets with or without Cx36 knockdown whilst the levels of oxidative phosphorylation increased 1.6-fold with the knockdown. This was also the case for monolayers which showed a 1.3-fold increase in basal insulin secretion and a 1.7-fold in ATP produced from oxidative phosphorylation when compared to pseudoislets. Possible reasons for the increased basal ATP production in pseudoislets compared to monolayers was discussed in section 5.9.2 and similar mechanisms could be contributing to the increase seen in the pseudoislets with Cx36 knockdown.

6.6.3. Reduced Insulin Secretion Response in Cx36 Knockdown

The pseudoislets with Cx36 knockdown demonstrated a lower fold increase in insulin secretion and in total ATP production than the scrambled control. However, the ATP production from glycolysis was slightly higher in Cx36 deficient pseudoislets. The higher rates of glycolytic metabolism may be a sign that the metabolism in the Cx36 deficient pseudoislets is not operating at optimal efficiency. Cx36 deficient mice have shown a loss of glucose stimulated insulin secretion [140, 163] and so pseudoislets with Cx36 knockdown would be expected to be glucose insensitive and not produce more ATP or secrete more insulin in response to glucose. The responses of the Cx36 KD pseudoislets was also much more variable with larger error bars which may be due to reduced synchronicity of Ca^{2+} between beta cells.

The increase in glycolysis seen in pseudoislets does not seem to be mediated by increased Cx36 channels since this was not reversed by Cx36 knockdown. The GSIS was not dramatically inhibited by the Cx36 KD in the pseudoislets and certainly not back to the levels seen in monolayer samples suggesting that the effects of pseudoislet formation on GSIS was not mediated by Cx36. Overall, it appears that basal insulin secretion in the pseudoislets was regulated by Cx36 but GSIS was not.

Insulin release is biphasic starting with an initial burst of insulin from granules that are already docked to the beta cell membrane and followed by a pulsatile release but the mechanisms behind this are poorly understood [95, 166]. A lack of Cx36 is thought to lower the response of the first insulin secretion phase and reduce the frequency but not amplitude of the second phase [163]. Further investigation into how the two phases of insulin secretion are affected by Cx36 knockdown *in vitro* could help to improve understanding of these mechanisms. It would also be of interest to explore whether the improved glucose sensing of pseudoislets displayed through the increased GLUT2 and decreased hexokinase I expression are altered during knockdown of Cx36.

CHAPTER 7. FINAL DISCUSSIONS

7.1. Effects of 3D structure on beta cell function

7.1.1. Improved Function of Beta Cells in 3D Structures

MIN6 beta cells showed improved function when configured as 3D structures known as pseudoislets including an enhanced GSIS response (figure 25) mirrored by increased ATP production at high glucose (figure 43) and decreased basal insulin secretion. This is consistent with previous reports [14, 76-78, 83, 88, 89, 101-103]. Further investigation into the changes in metabolic pathways found that the increased basal insulin secretion in monolayers was a result of increased oxidative phosphorylation (figure 44) and in pseudoislets an increase in glycolysis was largely responsible for the increased insulin secretion at high glucose (figure 45). The metabolic enzyme activity of MIN6 maintained in 25mM growth media was measured. The activities of most mitochondrial enzymes investigated including pyruvate carboxylase, citrate synthase, alpha-ketoglutarate dehydrogenase, and malate dehydrogenase, were increased in pseudoislets compared to monolayers. The rate of ATP production in response to glucose was the same in monolayers and pseudoislets but the glucose responsiveness of pseudoislets was greater due to the lower basal OCR.

The activities of glycolytic enzymes were also measured including phosphoglucokinase isomerase (PGI), glucokinase, phosphofructokinase 1 (PFK1), aldolase, GAPDH, and pyruvate kinase. Most glycolytic enzymes did not show any changes in activity between monolayer and pseudoislet samples except PFK1 and GAPDH activities, which were higher in pseudoislets. PFK1 activity is an important regulatory enzyme in the glycolytic pathway which stimulates the glycolytic pathway [80]. These results show that although the 3D configuration improved beta cell function as was expected [14, 76-78, 83, 88, 89, 101-103], the mechanisms behind the improved function are not simple and more investigation was needed to understand them.

Pyruvate carboxylase expression was higher in pseudoislets than in monolayers, this enzyme plays an important anaplerotic role in catalysing the conversion of pyruvate to replenish intermediates in the TCA cycle. It is known that changes in beta cell PC activity correlate with glucose induced insulin secretion as inhibition of pyruvate carboxylase inhibits insulin secretion and the islets of diabetic rodents show decreased Pyruvate carboxylase expression [156, 159]. It is also thought that pyruvate carboxylase plays a role in beta cell proliferation [11].

7.1.2. Beta Cell Response to Pyruvate

It is important that beta cells do not respond to pyruvate stimulation to maintain good blood glucose control as this would result in inappropriate insulin secretion [54, 55]. It is not ideal for beta cells to express MCT1 as these would allow transport of pyruvate or lactate into the cell and stimulate unwanted insulin secretion causing blood glucose levels to drop [147]. MCT1 is a monocarboxylate transporter known to be expressed in beta cells of patients with exercise induced hyperinsulinemia. These patients suffer a drop in blood glucose levels following exercise as the pyruvate produced enters the beta cell [147]. The MIN6 monolayer rate of ATP production through oxidative phosphorylation increased in response to pyruvate stimulation, the pyruvate response was only seen in monolayers and not pseudoislets or human islets. One explanation for this may be an increase in monolayer MCT1 expression. Antibodies were optimised for MCT1 detection in control tissue and expression was not detected in the MIN6 beta cells from monolayers or pseudoislets. However, this may be because the levels expressed were below detection levels but still present. Further investigation through PCR analysis would help to rule out inappropriate MCT1 expression as a cause for the pyruvate response.

7.1.3. Possible Amino Acid Stimulated ATP Production

The transport of endogenous pyruvate into the mitochondria was also investigated using the mitochondrial pyruvate carrier (MPC) inhibitor, UK5099 to further understand how pyruvate is metabolised once inside the cell. Both monolayers and pseudoislets showed a reduction in OCR after addition of UK5099 indicating that the ATP production is reliant on pyruvate uptake into the mitochondria.

The fuel source providing the pyruvate being transported into the mitochondria is unclear. Although there is some pyruvate present in the media, 1mM, it has been shown that the pseudoislets do not respond to extracellular pyruvate, we assume that this is because it cannot be transported into the beta cell. Glucose levels in the media are low too low to be considered a plausible fuel source, 0.5mM. It is possible that the L-glutamine in the media is providing a fuel source allowing for the reduction in OCR seen after the addition of UK5099. It is also possible that L-glutamine is acting through other pathways to influence the beta cell metabolism. L-glutamine is one of the most abundant amino acids found in extracellular fluid in vivo and is thought to have both acute and chronic effects on insulin secretion [167]. It has been shown to chronically alter insulin secretion rates by up regulating 148 genes and downregulating 18 genes leading to changes in the beta cells capability to respond to changes in the external environment [168]. The acute effects of L-glutamine involve generation of coupling factors such as glutathione and glutamate which lead to enhanced insulin secretion by indirectly stimulating ATP production [167]. The L-glutamate generated can also act to prime insulin secretory granules accelerating the second phase of insulin secretion [169]. The investigation of the effects of amino acids on beta cell metabolism goes beyond the scope of this study so it was not investigated beyond noting that an effect may be present.

7.1.4. Role of Cx36 in the Metabolic Phenotype of the 3D Structure

A MIN6 cell line with inducible Cx36 knockdown was generated and another transfected with a scrambled control. Functional analysis of pseudoislets formed from these cell lines found that inhibition of Cx36 expression increased basal insulin secretion. The increase in basal insulin secretion appeared to be due to contributions from oxidative phosphorylation. Increased basal insulin secretion in the absence of Cx36 is well known and is thought to be due to random hyperstimulating Ca^{2+} waves generated in isolated beta cells that would be dampened if the cell were able to transfer ions between cells in a 3D structure [94, 98, 140]. Increases in basal insulin secretion in MIN6 monolayers also correlated with an increase in oxidative phosphorylation suggesting that Cx36 plays an important role in maintaining oxidative phosphorylation rates at basal glucose. This suggests that Cx36 may be playing a more upstream role in regulating energy production rather than exclusively regulating calcium. The overall rates of insulin secretion and ATP production at high glucose were higher with the Cx36 knockdown but when the basal insulin secretion was considered the fold increase was lower. The previous studies using Cx36 deficient rodents have shown a decrease in glucose stimulated insulin secretion [94]. There was however, an increase in glycolytic ATP production in the Cx36 deficient pseudoislets as was seen in the pseudoislets expressing Cx36 and in the human islets.

This data collected using Cx36 deficient pseudoislets demonstrated that a lack of Cx36 resulted in a similar phenotype at basal glucose to MIN6 cultured as monolayers. Cx36 seems to be pivotal in regulating basal insulin secretion and this seems to be at least in part due to changes in basal ATP production through oxidative phosphorylation. There is a trend towards a lower GSIS response, but further studies are required to further explore this effect. Cx36 deficient pseudoislets provide a suitable model to further investigate the influence of gap junctional proteins on beta cell function involved in the improved function of beta cells cultured as 3D structures.

7.1.5. Comparison of Function with Human Islets

To demonstrate the relevance of the MIN6 beta cell line model studies to human studies, the metabolic function of human islets was also measured using the XFe24 Seahorse bioanalyser. The data collected from the human islets was more variable than data from the MIN6 cell line due to the large number of factors human islets are exposed to which can influence function. However, even with this variability it was clear that the metabolic phenotype of the human islets was similar to the MIN6 pseudoislets. Both exhibited low ATP production without glucose stimulation and had no response to pyruvate stimulation as would be expected of islets but had been a feature in monolayer samples.

There were comparable fold increases in ATP production under high glucose, 3-fold for human islets and 4-fold for pseudoislets. There was an increase in oxidative phosphorylation, but this was only 2-fold for both MIN6 pseudoislets and human islets so was not sufficient in explaining the overall increase in ATP production rate seen in either islet type or the subsequent increased insulin secretion response seen in the pseudoislets and reported previously in human islets [3, 5, 85]. Both pseudoislets and human islets gained most of the stimulated ATP production through glycolysis. This was not an expected result as it is largely accepted that tight coupling between oxidative phosphorylation and glycolysis is required for optimal insulin secretion [57, 170]. There has been very little investigation into the glycolytic contributions to insulin secretion in islets so these findings could not be compared to those described in previous literature. It is probable that the glycolytic increases were at least in part due to beta cells in the centre of the 3D structure being exposed to hypoxic conditions as is explored further in the following section, section 7.2.1. but may also indicate that there are other factors yet to be elucidated involved in meeting the ATP demands of stimulated insulin secretion.

7.2. In vitro Limitations

7.2.1. Possible Hypoxia in 3D structures

It is known that isolated islets and pseudoislets will normally express levels of hypoxic cores to some degree. This is because once removed from the highly vascularised pancreas the cells in the centre of the islets are not able to receive enough oxygen as it is not able to freely diffuse to the islet core [106, 152]. The levels of hypoxia in the pseudoislets used in this study was investigated. An increase in lactate dehydrogenase activity would indicate anaerobic metabolism occurring in the beta cells, possibly due hypoxia. There was a trend towards increased LDH activity in pseudoislets although this did not reach statistical significance. The presence of down-stream targets of hypoxic inducible factors (HIFs) was also measured in pseudoislets, these included GLUT1, PDK1, and LDH. PCR results indicated a trend towards upregulation of HIFs in pseudoislets compared to monolayers but the pseudoislet data was very variable so this could not be reliably concluded. It is likely that the variability in the data is due to beta cells towards the centre of the pseudoislets being exposed to a much higher risk and potential level of hypoxia than those on the outside. The trend towards increased expression of hypoxic markers and LDH activity along with the large glycolytic contribution to ATP production and lower basal OCR indicate that the pseudoislets and human islets are suffering some effects of hypoxia. This supports reports that the presence of hypoxia in *in vitro* studies involving islets and pseudoislets is a factor which must be managed carefully and taken into account when analysing results [13, 144, 151, 152, 171, 172]. However, the increase in pseudoislet glucose stimulated insulin secretion which is fuelled in part by an increase in oxidative phosphorylation compared to monolayers, the lack of increase in basal glycolysis and the lower basal insulin secretion compared to monolayers do not support a hypoxic phenotype. This implies the changes in the metabolic phenotype are more complicated and cannot be fully explained hypoxia.

7.2.2. Influence of Passage number on Results

Pseudoislet formation only increased the GSIS response at high passage, above passage 26. It was only at the higher passage numbers that differences between the pseudoislet and monolayers became obvious as the formation of the 3D structures returned the loss of the aging cells. To achieve clear data with minimal variability, only the higher passage cells were used in this study. Other studies have also chosen to select only older passage MIN6 [7, 77, 111, 112].

7.3. Long Term Significance of findings

This research holds potential for improving treatment of both type 1 and type 2 diabetes. Pseudoislets showed improved functionality mostly due to increased glycolysis which may be a feature of islets *in vitro*. The high glycolytic contribution to ATP production in both pseudoislets and native islets used in research should be noted as a possible limitation when using these 3D structures as a research model. Oxygen consumption rates of donated islets have already been shown to give an indication of transplant outcome [122, 123]. Measuring the individual contributions of glycolytic and mitochondrial metabolism could give further information on islet efficiency when selecting optimal islets for transplant.

Cx36 has been found to be more abundant in 3D structures than in beta cells cultured as monolayers [92, 94, 96, 103, 140, 163]. In this thesis, a potential role for Cx36 expression in maintaining the ideal metabolic phenotype and insulin secretory function at basal levels of glucose has been explored. The preservation of these connections through 3D culture describes another area in which improvements in islet culturing protocols could reduce loss of function in isolated islets resulting in a higher success rate in islet transplants for the treatment of type 1 diabetes.

The functional and metabolic features of the MIN6 monolayers and Cx36 knockdown pseudoislets were similar to that of beta cells from patients with type 2 diabetes [173]. Cx36 has also been shown to have decreased levels in the islets of some T2DM patients [174]. Cx36 provides a possible target in the treatment of T2DM, furthering understanding behind these mechanisms leading to the loss of function could improve preventative and therapeutic drug development.

7.4. Future Directions

7.4.1. Short term

- To produce a conclusive assessment on the extent of hypoxia in the pseudoislets and human islets used through pimonidazole staining, western blot analysis of LDH expression, and PCR analysis of MCT4 expression.
- To investigate whether the increased mitochondrial enzyme activities were due to tighter coupling between glycolytic and mitochondrial metabolism or increased mitochondrial biogenesis through mitochondrial staining and PCR analysis of mitochondrial mRNA.
- To extend Cx36 knockdown studies through enzyme activity analysis, PCR to measure chronic effects on metabolism, and imaging of calcium signalling.
- To extend human islet studies by dispersing and reaggregating islets and assessing the resulting effect on metabolic function.

7.4.2. Long term

Long term goals would be to investigate the effect of transplant-associated stresses on cell connectivity. This can be achieved by exposing islets to transplant-associated stresses such as hypoxia, glucotoxicity, and pro-inflammatory cytokines and assessing changes in Cx36 expression. The importance of cell contacts in preserving function in the transplant setting could be explored by manipulating cell contacts through monolayer and pseudoislet culture as well as Cx36 expression to establish whether any function lost through transplant associated stresses and Cx36 inhibition can be restored.

Pseudoislets could also be maintained in a more normoxic environment through stirred suspension cultures to investigate whether this would prevent changes seen in this study, this would show if the impact on glycolysis could be prevented and the consequent impact on GSIS.

8. References

1. Jain, R. and E. Lammert, *Cell-cell Interactions in the Endocrine Pancreas*. Diabetes, Obesity and Metabolism, 2009. **11**: p. 159-167.
2. Holt, R., et al., *Textbook of Diabetes*. 2010, Chichester, West Sussex: Hoboken, NJ: Wiley-Blackwell.
3. Kaddis, J.S., et al., *Human Pancreatic Islets and Diabetes Research*. JAMA, 2009. **301**(15): p. 1580-7.
4. Arrojo e Drigo R, A.Y., Diez J, Srinivasan D,, *New insights into the architecture of the islet of Langerhans: a focused cross-species assessment | SpringerLink*. Diabetologia, 2015. **58**: p. 2218.
5. Da Silva Xavier, G., *The Cells of the Islets of Langerhans*. J Clin Med, 2018. **7**(3): p. 54.
6. Jain, R., et al., *Pharmacological Inhibition of Eph Receptors Enhances Glucose-Stimulated Insulin Secretion From Mouse and Human Pancreatic Islets*. Diabetologia, 2013. **56**: p. 1350-1355.
7. Yamato E, T.F., Miyazaki J, *Microarray Analysis of Novel Candidate Genes Responsible for Glucose-Stimulated Insulin Secretion in Mouse Pancreatic β Cell Line MIN6*. PLoS ONE, 2013. **8**(4): p. e61211.
8. Lavine, R.L., et al., *Functional abnormalities of islets of Langerhans of obese hyperglycemic mouse*. <https://doi.org/10.1152/ajpendo.1977.233.2.E86>, 1977.
9. Gilon P, J.J., Henquin J, *Culture duration and conditions affect the oscillations of cytoplasmic calcium concentration induced by glucose in mouse pancreatic islets | SpringerLink*. Diabetologia, 1994. **37**(10): p. 1007-1014.

10. Wollheim, C., et al., *Somatostatin and Epinephrine Induced Modifications of 45 Ca Fluxes and Insulin Release in Rat Pancreatic Islets Maintained in Tissue Culture*. Journal of Clinical Investigation, 1977. **60**: p. 1165-1173.
11. Xu, J., et al., *The role of pyruvate carboxylase in insulin secretion and proliferation in rat pancreatic beta cells*. Diabetologia, 2008. **51**(11): p. 2022-30.
12. Brandhorst, H., et al., *The Ratio Between Collagenase Class I and Class II Influences the Efficient Islet Release from the Rat Pancreas*. Transplantation, 2008. **35**: p. 456-461.
13. Cavallari, G., et al., *Rat Pancreatic Islet Size Standardization by the "Hanging Drop" Technique*. Transplantation Proceedings, 2007. **39**(6): p. 2018-2020.
14. Halban, P.A., et al., *The possible importance of contact between pancreatic islet cells for the control of insulin release*. Endocrinology, 1982. **111**(1): p. 86-94.
15. Lacy, P. and M. Kostianovsky, *Method for the Isolation of Intact Islets of Langerhans from the Rat Pancreas*. Diabetes, 1967. **16**(1): p. 35-39.
16. Chertow B, B.N., Sivitz W, Meda P, Webb M, Shih J, *Cellular Mechanisms of Insulin Release: Effects of Retinoids on Rat Islet Cell-to-Cell Adhesion, Reaggregation, and Insulin Release*. Diabetes, 1983. **32**(6): p. 568-574.
17. Bluestone, J., K. Herold, and G. Eisenbarth, *Genetics, Pathogenesis and Clinical Interentions in Type 1 Diabetes*. Nature, 2010. **464**: p. 1293-1300.

18. Todd, J., *Etiology of Type 1 Diabetes*. Immunity, 2010. **32**: p. 457-467.
19. Harjutsalo, V., I. Sjoberg, and J. Tuomilehto, *Time Trends on the Incidence of Type 1 Diabetes in Finnish Children: A Cohort Study*. Lancet, 2008. **371**: p. 1777-1782.
20. Kahn, S., M. Cooper, and S. Prato, *Pathophysiology and Treatment of Type 2 Diabetes: Perspectives on the Past Present and Future*. Lancet, 2014. **383**: p. 1068-1083.
21. Weir, G.C. and S. Bonner-Weir, *Five Stages of Evolving Beta-Cell Dysfunction During Progression to Diabetes*. Diabetes, 2004. **53**: p. S16 - S21.
22. Wild, S., et al., *Global Prevalence of Diabetes: Estimates for the Year 2000 and Projections for 2030*. Diabetes Care, 2004. **27**(5): p. 1047-1053.
23. *Diagnosis and Classification of Diabetes*. Diabetes Care, 2009. **31**: p. S62-S67.
24. Melendez-Ramirez, L., R. Richards, and W. Cefalu, *Complications of Type 1 Diabetes*. Endocrinol Metab Clin North Am, 2010. **39**: p. 625-640.
25. Atkinson, M., G. Eisenbarth, and A. Michels, *Type 1 Diabetes*. Lancet, 2014. **383**: p. 69-82.
26. Schernthaner, G., *Cardiovascular Mortality and Morbidity in Type-2 Diabetes Mellitus*. Diabetes Research and Clinical Practise, 1996. **31**: p. Suppl:S3-13.
27. *Economic costs of diabetes in the U.S. in 2012*. Diabetes Care, 2013. **36**: p. 1033-1046.
28. Beran D, Y.J., Courten M, *Access to Care for Patients With Insulin-Requiring Diabetes in Developing Countries*. Diabetes Care, 2005. **28**(9): p. 2136 - 2140.

29. Naftanel MA, H.D., *Pancreatic Islet Transplantation*. PLoS, 2004. **1**(3): p. e58.
30. R, C.P.a.H., *Lippincott's illustrated reviews: Biochemistry*. 1994: J B Lippincott Co, Philadelphia.
31. Shapiro J, P.M., Ricordi C, *Clinical pancreatic islet transplantation*. Nature Reviews Endocrinology, 2017. **13**(5): p. 268-277.
32. Welsch C, R.W., Csete M, *Concise Review: Lessons Learned from Islet Transplant Clinical Trials in Developing Stem Cell Therapies for Type 1 Diabetes - Welsch - 2019 - STEM CELLS Translational Medicine - Wiley Online Library*. Stem Cells Translational Medicine, 2019. **8**: p. 209-214.
33. Moskalewski, S., *Isolation and Culture of the Islets of Langerhans of the Guinea Pig*. General and Comparative Endocrinology, 1965. **44**: p. 342-53.
34. Ballinger, W. and P. Lacy, *Transplantation of Intact Pancreatic Islets in Rats*. Surgery, 1972. **72**(2): p. 175-186.
35. Brendel, M., et al., *International Islet Transplant Registry*. 2013: Giessen, Germany.
36. P, A.I.o.o.p.C., et al., *Chapter 40 - Current Status of Islet Transplantation*. Academic Press, 2014: p. 583 - 598.
37. Shapiro, A., et al., *Islet Transplantation in 7 Patients with Type 1 Diabetes Mellitus Using a Glucocorticoid-free Immunosuppressive Regimen*. New England Journal of Medicine, 2000. **343**(4): p. 230-238.
38. Barton, F., et al., *Improvement in outcomes of clinical islet transplantation*. Diabetes Care, 2012. **35**(7): p. 1436-1445.

39. Pepper, A., B. Gala-Lopez, and T. Kin, *Advances in Clinical Islet Isolation*, in *Islets of Langerhans*. 2015, Springer Science: Edmonton. p. 1165-1186.
40. Bucher, P., et al., *Optimisation of Neutral Protease to Collagenase Activity Ratio for Islet of Langerhans Isolation*. *Transplant Proceedings*, 2004. **36**: p. 1145-1146.
41. Layden BT, D.V., and Lowe Jr WL, *G-Protein-Coupled Receptors, Pancreatic Islets and Diabetes*. Nature Education, 2010. **3**(9): p. 13.
42. border-box, l.d.-j.-t.t.t.s.b.-s., et al., *Genetic Control of Differential Acetylation in Diabetic Rats*. *PLOS ONE*, 2014. **9**(4).
43. Henquin, J., *Pathways in Beta-Cell Stimulus-Secretion Coupling as Targets for Therapeutic Insulin Secretagogues*. *Diabetes*, 2004. **55**(Suppl 3): p. S48-S58.
44. Rutter, G., et al., *Pancreatic Beta Cell Identity, Glucose Sensing and the Control of Insulin Secretion*. *Biochemical Journal*, 2015. **466**(2): p. 203-218.
45. Hodson, D., et al., *Incretin-Modulated Beta Cell Energetics in Intact Islets of Langerhans*. *Molecular Endocrinology*, 2014. **28**: p. 860-871.
46. Phillips, L. and J. Prins, *Update on incretin hormones*. *Annals of the New York Academy of Sciences*, 2011. **1234**: p. E55-E74.
47. Henquin, J., *Regulation of Insulin Secretion: A Matter of Phase Control and Amplitude Modulation*. *Diabetologia*, 2009. **52**: p. 739-751.
48. Komatsu, M., et al., *Glucose Stimulation of Insulin Release in the Absence of extracellular Ca²⁺ and in the*

- Absence of any Increase in Intracellular Ca²⁺ in Rat Pancreatic Islets.* Proceedings of the National Academy of Sciences, 1995. **92**: p. 10728-10732.
49. Ohara-Imaizumi, M., et al., *Imaging Exocytosis of Single Insulin Secretory Granules with Evanescent Wave Microscopy: Distinct Behaviour of Granule Motion in Biphasic Insulin Release.* The Journal of Biological Chemistry, 2001. **277**: p. 3805-3808.
 50. Bratanova-Tochkova, T., et al., *Triggering and Augmentation Mechanisms, Granule Pools, and Biphasic Insulin Secretion.* Diabetes, 2002. **51**: p. S83-S90.
 51. Chan, C.B., et al., *Increased Uncoupling Protein-2 Levels in β -cells Are Associated With Impaired Glucose-Stimulated Insulin Secretion.* Diabetes, 2001: p. 1302-1310.
 52. E, C., *Microbial Nutrition and Basic Metabolism*, in *Handbook of Water and Waste Water Microbiology*. 2003, Academic Press. p. 3-33.
 53. Schuit, F., et al., *Beta Cell Specific Gene Repression: A Mechanism to Protect Against Inappropriate or Maladjusted Insulin Secretion.* Diabetes, 2012. **61**: p. 969-975.
 54. Ishihara, H., et al., *Overexpression of Monocarboxylate Transporter and Lactate Dehydrogenase Alters Insulin Secretory Responses to Pyruvate and Lactate in Beta Cells.* Journal of Clinical Investigation, 1999. **104**: p. 1621-1629.
 55. Pullen, T., et al., *Identification of Genes Selectively Disallowed in the Pancreatic Islet.* Islets, 2010. **2**: p. 89-95.

56. Farfari, S., et al., *Glucose-regulated anaplerosis and cataplerosis in pancreatic beta-cells: possible implication of a pyruvate/citrate shuttle in insulin secretion*. *Diabetes*, 2000. **49**: p. 718-726.
57. Prentki, M., F. Matschinsky, and S. Madiraju, *Metabolic Signalling in Fuel Induced Insulin Secretion*. *Cell Metabolism*, 2013. **18**(2): p. 162-185.
58. German, M.S., *Glucose sensing in pancreatic islet beta cells: the key role of glucokinase and the glycolytic intermediates*. *Proc Natl Acad Sci U S A*, 1993. **90**(5): p. 1781-5.
59. Schuit, F., et al., *Metabolic fate of glucose in purified islet cells. Glucose-regulated anaplerosis in β cells*. *Journal of Biological Chemistry*, 1997. **272**: p. 18572-18579.
60. Jitrapakdee, S., et al., *Regulation of Insulin Secretion: Role of Mitochondrial Signalling*. *Diabetologia*, 2010. **53**: p. 1019-1032.
61. J, F., *ATP Production II: The TCA Cycle and Oxidative Phosphorylation*, in *Quantitative Human Physiology*. 2017, Academic Press. p. 227-240.
62. Korla K, V.L., Mitra C, *Kinetic Stimulation of Malate-Aspartate and Citrate-Pyruvate Shuttles in Association with Krebs Cycle*. *Journal of Biomolecular Structure and Dynamics*, 2015. **33**(11): p. 1-31.
63. Eto, K., Y. Tsubamoto, and Y. Terauchi, *Role of NADH Shuttle System in Glucose Induced Activation of Mitochondrial Metabolism and Insulin Secretion*. *Science*, 1999. **283**: p. 981-085.
64. Fernandez-Alvarez, J., et al., *Enzymatic, Metabolic, and Secretory Patterns in Human Islets of Type 2 (Non-*

- insulin-dependent) Diabetic Patients*. *Diabetologia*, 1994. **37**: p. 177-181.
65. Hasan, N.M., et al., *Impaired anaplerosis and insulin secretion in insulinoma cells caused by small interfering RNA-mediated suppression of pyruvate carboxylase*. *Journal of Biological Chemistry*, 2008. **283**: p. 28048-28059.
 66. MJ, M., *Estimates of Glycolysis, Pyruvate, (De)Carboxylation, Pentose Phosphate Pathways, and Methyl Succinate Metabolism in Incapacitated Pancreatic Islets*. *Archives of Biochemistry and Biophysics*, 1993. **305**(2): p. 205-214.
 67. Ainscow, E.K., C. Zhao, and G.A. Rutter, *Acute overexpression of lactate dehydrogenase-A perturbs beta-cell mitochondrial metabolism and insulin secretion*. 2000.
 68. Thorrez, L., et al., *Tissue-specific disallowance of housekeeping genes*. *Genome Research*, 2011. **21**: p. 95-105.
 69. Sekine, N., et al., *Low Lactate Dehydrogenase and High Mitochondrial Glycerol*. *Journal of Biological Chemistry*, 1994. **269**(7): p. 4895-4902.
 70. Halban PA, W.C., Blondel B, Meda P, Niesor EN, Mintz DH., *The possible importance of contact between pancreatic islet cells for the control of insulin release*. *Endocrinology*, 1982. **111**(1): p. 86-94.
 71. Luther, M., et al., *MIN6 β -cell- β -cell interactions influence insulin secretory responses to nutrients and non-nutrients*. *Biochemical and Biophysical Research Communications*, 2006. **343**(1): p. 99-104.

72. Pipeleers, D., et al., *Glucose-Induced Insulin Release Depends on Functional Cooperation Between Islet Cells*. PNAS, 1982. **79**: p. 7322-7325.
73. Gylfe, E., E. Grapengiesser, and B. Hellman, *Propagation of Cytoplasmic Ca²⁺ Oscillations in Clusters of Pancreatic Beta Cells Exposed to Glucose*. Cell Calcium, 1991. **12**: p. 229-240.
74. Gilon, P., J. Jonas, and J. Henquin, *Culture Duration and Conditions Affect the Oscillations of Cytoplasmic Calcium Concentration Induced by Glucose in Mouse Pancreatic Islets*. Diabetologia, 1994. **37**: p. 1007-1014.
75. Taylor, C., S. Howell, and K. Pedley, *Synchronous Changes in Ca²⁺ in Cell Clusters From Pancreatic Islets Measured by Confocal Microscopy*. Journal of Physiology, 1993. **475**: p. 105.
76. Bergsten, P., et al., *Synchronous Oscillations of Cytoplasmic Ca²⁺ and Insulin Release in Glucose-Stimulated Pancreatic Islets*. Journal of Biological Chemistry, 1994. **269**(12): p. 8749-8753.
77. Hauge-Evans, A., et al., *Pancreatic β -Cell to β -Cell Interactions Are Required for Integrated Responses to Nutrient Stimuli*. Diabetes, 1999. **48**(7): p. 1402-1408.
78. Chowdhury, A., et al., *Functional Differences Between Aggregated and Dispersed Insulin Producing Cells*. Diabetologia, 2013. **56**(7): p. 1557-1568.
79. Yaney, G., et al., *Phosphofructokinase Isozymes in Pancreatic Islets and Clonal Beta Cells (INS-1)*. Diabetes, 1995. **44**(11): p. 1285-1289.

80. Chowdhury, A., et al., *Signalling in Insulin-Secreting MIN6 Pseudoislets and Monolayers*. Journal of Proteome Research, 2013. **12**: p. 5954-5962.
81. McCluskey, J., et al., *Development and Functional Characterization of Insulin-releasing Human Pancreatic Beta Cell Lines Produced by Electrofusion*. Journal of Biological Chemistry, 2011. **286**(25): p. 21982-21992.
82. Guo-Parke, H., et al., *Configuration of Electrofusion-Derived Human Insulin-Secreting Cell Line as Pseudoislets Enhances Functionality and Therapeutic Utility*. Journal of Endocrinology, 2012. **214**: p. 257-265.
83. Tsonkova V, S.F., Wolf X, Grunnet L, Ringgaard A, Ingvorsen C, Winkel L, Kalisz M, Dalgaard K, Bruun C, Fels J, Helgstrand C, Hastrup S, Kryh Oberg F, Vernet E, Bastner Sandrini M, Shaw A, Jessen C, Frogne T, *The EndoC- β H1 cell line is a valid model of human beta cells and applicable for screenings to identify novel drug target candidates | Elsevier Enhanced Reader*. Molecular Metabolism, 2018. **8**: p. 144 - 157.
84. Kelly, C., et al., *The role of glucagon- and somatostatin-secreting cells in the regulation of insulin release and beta-cell function in heterotypic pseudoislets*. Diabetes Metab Res Rev, 2010. **26**(7): p. 525-33.
85. Hilderink, J., et al., *Controlled aggregation of primary human pancreatic islet cells leads to glucose-responsive pseudoislets comparable to native islets*. J Cell Mol Med, 2015. **19**(8): p. 1836-46.

86. Bernard, A.B., C.C. Lin, and K.S. Anseth, *A Microwell Cell Culture Platform for the Aggregation of Pancreatic β -Cells*, in *Tissue Eng Part C Methods*. 2012. p. 583-92.
87. Lock, L.T., S.G. Laychock, and E.S. Tzanakakis, *Pseudoislets in stirred-suspension culture exhibit enhanced cell survival, propagation and insulin secretion*. *J Biotechnol*, 2011. **151**(3): p. 278-86.
88. Joo, D.J., et al., *Manufacturing of insulin-secreting spheroids with the RIN-5F cell line using a shaking culture method*. *Transplant Proc*, 2010. **42**(10): p. 4225-7.
89. Bavamian, S., et al., *Islet Cell-to-Cell Communication as Basis for Normal Insulin Secretion*. *Diabetes, Obesity and Metabolism*, 2007. **9**: p. 118-132.
90. Meda, P., *Protein-Mediated Interactions of Pancreatic Islet Cells*. *Scientifica*, 2013: p. 1-22.
91. Konstantinova, I., et al., *EphA-Ephrin-A Mediated Beta Cell Communication Regulates Insulin Secretion From Pancreatic Islets*. *Cell*, 2007. **129**: p. 359-370.
92. Rimkute L, K.T., Snipas M, Palacios-Prado N, Jotautis V, Skeberdis V, and Bukauskas F, *Modulation of Connexin-36 Gap Junction Channels by Intracellular pH and Magnesium Ions*. *Frontiers in Physiology*, 2018.
93. Goodenough, D.A. and D.L. Paul, *Gap junctions*. *Cold Spring Harb Perspect Biol*, 2009. **1**(1): p. a002576.
94. Wellershaus, K., et al., *A new conditional mouse mutant reveals specific expression and functions of connexin36 in neurons and pancreatic beta-cells*. *Exp Cell Res*, 2008. **314**(5): p. 997-1012.

95. Farnsworth, N.L. and R.K. Benninger, *New Insights into the Role of Connexins in Pancreatic Islet Function and Diabetes*. FEBS Letters, 2014: p. 1278-1287.
96. Serre-Beinier, V., et al., *Cx36 Makes Channels Coupling Human Pancreatic Beta Cells, and Correlates with Insulin Expression*. Human Molecular Genetics, 2009. **18**(3): p. 428-439.
97. Rutter, G. and D. Hodson, *Beta Cell Connectivity in Pancreatic Islets: A Type 2 Diabetes Target?* Cellular and Molecular Life Sciences, 2015. **72**: p. 453-467.
98. Squires, P., et al., *Synchronization of Ca²⁺ Signals Within Insulin-Secreting Pseudoislets: Effects of Gap-Junctional Uncouplers*. Cell Calcium, 2000. **27**(5): p. 287-296.
99. Kissler, H., et al., *Validation of Methodologies for Quantifying Isolated Human Islets: an Islet Cell Resources Study*. Clin Transplant, 2010. **24**(2): p. 236-42.
100. S, P.B.a.L. *Measurement of Oxygen Consumption Rate (OCR) and ...* Bio-Protocol 2018 [cited 2019 17/11/19]; e2850:[Available from: <https://bio-protocol.org/e2850>].
101. Luther, M.J., et al., *MIN6 beta-cell-beta-cell interactions influence insulin secretory responses to nutrients and non-nutrients*. Biochem Biophys Res Commun, 2006. **343**(1): p. 99-104.
102. Salomon, D. and P. Meda, *Heterogeneity and contact-dependent regulation of hormone secretion by individual B cells*. Exp Cell Res, 1986. **162**(2): p. 507-20.
103. Caton, D., et al., *Beta-cell crosstalk: a further dimension in the stimulus-secretion coupling of*

- glucose-induced insulin release*. Diabetes Metab, 2002. **28**(6 Pt 2): p. 3S45-53; discussion 3S108-12.
104. Green, A.D., et al., *Pseudoislet formation enhances gene expression, insulin secretion and cytoprotective mechanisms of clonal human insulin-secreting 1.1B4 cells*. Pflugers Arch, 2015. **467**(10): p. 2219-28.
 105. Lock, L., S. Laychock, and E. Tzanakis, *Pseudoislets in Stirred-Suspension Culture Exhibit Enhanced Cell Survival, Propagation and Insulin Secretion*. Journal of Biotechnology, 2011. **151**(3): p. 278-286.
 106. Cavallari, G., et al., *Rat pancreatic islet size standardization by the "hanging drop" technique*. Transplant Proc, 2007. **39**(6): p. 2018-20.
 107. Hauge-Evans, A., et al., *Pancreatic Beta-Cell-to-Beta-Cell Interactions Are Required for Integrated Responses to Nutrient Stimuli*. Diabetes, 1999. **48**: p. 1402-1408.
 108. Hilderink, J., et al., *Controlled Aggregation of Primary Human Pancreatic Islet Cells Leads to Glucose Responsive Pseudoislets Comparable to Native Islets*. Journal of Cellular and Molecular Medicine, 2015. **19**(8): p. 1836-1846.
 109. Bernard, A., C. Lin, and K. Anseth, *A Microwell Cell Culture Platform for the Aggregation of Pancreatic Beta-Cells*. Tissue Engineering: Part C, 2012. **18**: p. 583-592.
 110. Kelly, C., et al., *The Role of Glucagon and Somatostatin Secreting Cells in the Regulation of Insulin Release and Beta Cell Function in Heterotypic Pseudoislets*. Diabetes/Metabolism Research and Reviews, 2010. **26**: p. 525-533.

111. O'Driscoll, L., et al., *Phenotypic and global gene expression profile changes between low passage and high passage MIN-6 cells*. J Endocrinol, 2006. **191**(3): p. 665-76.
112. Cheng K, D.-A.V., Nolan C, TurnerN Hallahan N, Andrikopoulos S, *High Passage MIN6 Cells Have Impaired Insulin Secretion with Impaired Glucose and Lipid Oxidation*. PLoS ONE, 2012(7): p. e40868.
113. S, K., *The relative contributions of insulin resistance and beta-cell dysfunction to the pathophysiology of Type 2 diabetes | SpringerLink*. Diabetologia, 2003. **46**(1): p. 3-19.
114. Cohrs CA, P.J., Drotar D, Enos S, Kipke N, Chen C, Bozsak R, Schoniger E, Eehalt F, Distler M, Brennand A, Bornstein S, Weitz J, Solimena M and Speier S, *Dysfunction of Persisting β Cells Is a Key Feature of Early Type 2 Diabetes Pathogenesis | Elsevier Enhanced Reader*. Cell Reports, 2020. **31**: p. 107469.
115. E, F., et al., *beta-Cell function in subjects spanning the range from normal glucose tolerance to overt diabetes: a new analysis*. The Journal of clinical endocrinology and metabolism, 2005. **90**(1).
116. Weyer, C., et al., *The natural history of insulin secretory dysfunction and insulin resistance in the pathogenesis of type 2 diabetes mellitus*. J Clin Invest, 1999. **104**(6): p. 787-94.
117. Weyer C, H.R., Tataranni A, Bogardus C, *A high fasting plasma insulin concentration predicts type 2 diabetes independent of insulin resistance: evidence for a pathogenic role of relative hyperinsulinemia*. Diabetes, 2001. **49**(12): p. 2094 - 101.

118. Magale A, Ravier, M.G., Anne Charollais, Asllan Gjinovci, Dorothée Caille, Goran Söhl, Claes B. Wollheim, Klaus Willecke, Jean-Claude Henquin and Paolo Meda, *Loss of Connexin36 Channels Alters β -Cell Coupling, Islet Synchronization of Glucose-Induced Ca^{2+} and Insulin Oscillations, and Basal Insulin Release*. *diabetes*, 2005. **54**(6).
119. Morten K, P.M., Badder L, Sivathondan P, Dragovic R, Neumann A, Gavin J, Shrestha R, Reilly S, Phadwal K, Lodge T, Borzychowski A, Cookson S, Mitchell C, Morovat A, Simon A, Uusimaa J, Hynes J and Poulton J, *Insights into Pancreatic Beta Cell Energy Metabolism Using Rodent Beta Cell Models*. Wellcome Open Research, 2017. **2**(14).
120. Nicholls, D.G., et al., *Bioenergetic Profile Experiment using C2C12 Myoblast Cells*, in *J Vis Exp*. 2010.
121. Srivatsava, A.R., et al., *Assessment of the in vitro function of human stem cell-derived β cells*. 2019.
122. IR, S., et al., *Glucose-stimulated Increment in Oxygen Consumption Rate as a Standardized Test of Human Islet Quality*. *American journal of transplantation : official journal of the American Society of Transplantation and the American Society of Transplant Surgeons*, 2008. **8**(1).
123. Wilkstrom J, S.S., Stiles L, Elorza A, Allister E, Neilson A, Ferrick D, Wheeler M, Shirihai O, *A Novel High-Throughput Assay for Islet Respiration Reveals Uncoupling of Rodent and Human Islets*. *PLoS ONE*, 2013. **8**(12).
124. Cen J, S.E., Bergsten P, *Fatty acids stimulate insulin secretion from human pancreatic islets at fasting*

- glucose concentrations via mitochondria-dependent and -independent mechanisms. Nutrition & Metabolism, 2016. 13(59): p. 1-9.*
125. M, W., et al., *Multiparameter Metabolic Analysis Reveals a Close Link Between Attenuated Mitochondrial Bioenergetic Function and Enhanced Glycolysis Dependency in Human Tumor Cells. American journal of physiology. Cell physiology, 2007. 292(1).*
126. Mookerjee, S.A. and M.D. Brand, *Measurement and Analysis of Extracellular Acid Production to Determine Glycolytic Rate. J Vis Exp, 2015(106).*
127. U Kabra, K.P., A Migliorini, S Keipert, D Lamp, O Korsgren, M Gegg, S Woods, P Pfluger, H Lickert, C Affourtit, M Tschop, M Jastroch, *Direct Substrate Delivery Into Mitochondrial Fission-Deficient Pancreatic Islets Rescues Insulin Secretion. Diabetes, 2017. 66(5): p. 1247-1257.*
128. Schulz N, K.O., Jastroch M, Schurmann A, *Minor Role of Mitochondrial Respiration for Fatty-Acid Induced Insulin Secretion. Int. J. Mol. Sci. , 2013. 14: p. 18989-18998.*
129. Untereiner A, A.S., Bhattacharjee A, Gohil H, Pourasgari F, Ibeh N, Lai M, *GABA promotes β -cell proliferation, but does not overcome impaired glucose homeostasis associated with diet-induced obesity. FASEB, 2019. 33(3).*
130. Russell S, W.J., Neilson A, Gillies R, *Metabolic Profiling of healthy and cancerous tissues in 2D and 3D. Scientific Reports, 2017. 7(1): p. 1-11.*

131. *The Contributions of Respiration and Glycolysis to Extracellular Acid Production*. Biochimica et Biophysica Acta, 2015: p. 171-181.
132. P, J., et al., *Loss-of-Function Mutation in Thiamine Transporter 1 in a Family With Autosomal Dominant Diabetes*. 2019. **68**(5): p. 1084-1093.
133. Santo-Domingo J, C.C., Broenimann C, Lassueur S, Wiederkehr A, *Antibiotics induce mitonuclear protein imbalance but fail to inhibit respiration and nutrient activation in pancreatic β -cells*. Experimental Cell Research, 2017. **357**(2): p. 170-180.
134. Gerencser, A.A., *Metabolic activation-driven mitochondrial hyperpolarization predicts insulin secretion in human pancreatic beta-cells*. Biochim Biophys Acta Bioenerg, 2018. **1859**(9): p. 817-28.
135. Kloster-Jensen, K., et al., *Intracellular sirolimus concentration is reduced by tacrolimus in human pancreatic islets in vitro*. Transpl Int, 2015. **28**(10): p. 1152-61.
136. Russell, S., et al., *Metabolic Profiling of healthy and cancerous tissues in 2D and 3D*. Scientific Reports, 2017. **7**(1): p. 1-11.
137. W, S., et al., *Three-Dimensional Cell Culture-Based Screening Identifies the Anthelmintic Drug Nitazoxanide as a Candidate for Treatment of Colorectal Cancer*. Molecular cancer therapeutics, 2015. **14**(6).
138. Yamato, E., F. Tashiro, and J. Miyazaki, *Microarray analysis of novel candidate genes responsible for glucose-stimulated insulin secretion in mouse*

- pancreatic beta cell line MIN6*. PLoS One, 2013. **8**(4): p. e61211.
139. Zhou YP, C.B., Pugh W, Poloonsky K, *Basal Insulin Hypersecretion in Insulin-Resistant Zucker Diabetic and Zucker Fatty Rats: Role of Enhanced Fuel Metabolism*. Metabolism, 1999. **48**(7): p. 857-864.
140. Ravier, M.A., et al., *Loss of connexin36 channels alters beta-cell coupling, islet synchronization of glucose-induced Ca²⁺ and insulin oscillations, and basal insulin release*. Diabetes, 2005. **54**(6): p. 1798-807.
141. Xiong X, W.G., Tao, Wu P, Kono T, Li K, Ding W, Tong X, Tersay S, Harris R, Mirmira R, Evans-Molina C, DongD, *Sirtuin 6 regulates glucose-stimulated insulin secretion in mouse pancreatic beta cells | SpringerLink*. Diabetologia, 2016. **59**(1): p. 151-160.
142. González-Mariscal, I., Montoro, R.A., Doyle, M.E. et al, *Absence of cannabinoid 1 receptor in beta cells protects against high-fat/high-sugar diet-induced beta cell dysfunction and inflammation in murine islets | SpringerLink*. Diabetologia, 2018. **61**(6): p. 1470-1483.
143. Zheng, H., et al., *CNC-bZIP Protein Nrf1-Dependent Regulation of Glucose-Stimulated Insulin Secretion*. Antioxid Redox Signal, 2015. **22**(10): p. 819-31.
144. Gerber, P.A. and G.A. Rutter, *The Role of Oxidative Stress and Hypoxia in Pancreatic Beta-Cell Dysfunction in Diabetes Mellitus*, in *Antioxid Redox Signal*. 2017. p. 501-18.
145. B, T., *GLUT2, glucose sensing and glucose homeostasis | SpringerLink*. Diabetologia, 2019. **58**(2): p. 221-232.
146. Shih C, L.J., Chen H, Lin Y, Chen H, Lin Y, Kuo C, Chen Y, Wang C, *Comparison of changes in mitochondrial*

- bioenergetics between keratinocytes in human external auditory canal skin and cholesteatomas from normoxia to hypoxia*. Scientific Reports, 2018. **8**(1): p. 1-11.
147. Otonkoski T, K.N., Ustinov J, Lapatto R, Meissner T, Mayatepek E, Kere J, Sipila I, *Physical Exercise Induced Hyperinsulinemic Hypoglycemia Is an Autosomal-Dominant Trait Characterised by Abnormal Pyruvate Induced Insulin Release*. Diabetes, 2003. **52**(1): p. 199-204.
148. MacDonald, P.E., J.W. Joseph, and P. Rorsman, *Glucose-sensing mechanisms in pancreatic β -cells*, in *Philos Trans R Soc Lond B Biol Sci*. 2005. p. 2211-25.
149. Cantley, J.G., S. T. Maxwell, P. H. Withers, D. J., *The hypoxia response pathway and β -cell function*. Diabetes, Obesity and Metabolism - Wiley Online Library, 2010.
150. Gandham S, T.M., Singh A, Amiji M, *Inhibition of hexokinase-2 with targeted liposomal 3-bromopyruvate in an ovarian tumor spheroid model of aerobic glycolysis*. International Journal of Nanomedicine, 2015. **10**(1): p. 4405-4423.
151. Sato, S.I., M. Yoshizawa, T. Yamagata, K., *Moderate Hypoxia Induces β -Cell Dysfunction with HIF-1–Independent Gene Expression Changes*. plosone, 2014. **9**(12).
152. Komatsu, H., et al., *Isolated human islets require hyperoxia to maintain islet mass, metabolism, and function*. Biochem Biophys Res Commun, 2016. **470**(3): p. 534-538.

153. Thorens, B., et al., *The loss of GLUT2 expression by glucose-unresponsive beta cells of db/db mice is reversible and is induced by the diabetic environment.* J Clin Invest, 1992. **90**(1): p. 77-85.
154. Bensellam M, D.B., Rybachuk G, Laybutt D, Magnan C, Guiot Y, Pouyssegur J, Jonas J, *Glucose-Induced O₂ Consumption Activates Hypoxia Inducible Factors 1 and 2 in Rat Insulin-Secreting Pancreatic Beta-Cells.* PLoS ONE, 2012.
155. Valera, A., et al., *Expression of GLUT-2 antisense RNA in beta cells of transgenic mice leads to diabetes.* J Biol Chem, 1994. **269**(46): p. 28543-6.
156. Prentki, M. and C.J. Nolan, *Islet β cell failure in type 2 diabetes.* J Clin Invest, 2006. **116**(7): p. 1802-12.
157. Patterson J, C.K., Lou J, Manning Fox J, Macdonald P, Joseph J, *Mitochondrial Metabolism of Pyruvate is Essential for Regulating Glucose Stimulated Insulin Secretion.* Journal of Biological Chemistry, 2014. **289**: p. 13335-13346.
158. Chareyron I, W.C., Thevenet J, Santo-Domingo J, Wiederkehr A, *Cellular Stress is a Prerequisite for Glucose induced Mitochondrial Matrix Alkalinization in Pancreatic Beta Cells.* Molecular and Cellular Endocrinology, 2019. **481**: p. 71-83.
159. Cline G, L.R., Papas K, Kibbey R, Shulman G, *¹³C NMR Isotopomer Analysis of Anaplerotic Pathways in INS-1 Cells.* Journal of Biological Chemistry, 2004. **279**: p. 44370-44375.
160. Maechler, P., S. Carobbio, and B. Rubi, *In beta-cells, mitochondria integrate and generate metabolic*

- signals controlling insulin secretion*. Int J Biochem Cell Biol, 2006. **38**(5-6): p. 696-709.
161. Kelly, C., N.H. McClenaghan, and P.R. Flatt, *Role of islet structure and cellular interactions in the control of insulin secretion*. <http://dx.doi.org/10.4161/isl.3.2.14805>, 2011.
162. De Vuyst, E., et al., *Pharmacological modulation of connexin-formed channels in cardiac pathophysiology*. Br J Pharmacol, 2011. **163**(3): p. 469-83.
163. Head, W.S., et al., *Connexin-36 Gap Junctions Regulate In Vivo First- and Second-Phase Insulin Secretion Dynamics and Glucose Tolerance in the Conscious Mouse*. Diabetes, 2012. **61**(7): p. 1700-1707.
164. Bashratyan R, R.D., Rahman M, Marquardt K, Fink E, Hu W, Elder J, Binley J, Sherman L, and Dai Y, *Type 1 diabetes pathogenesis is modulated by spontaneous autoimmune responses to endogenous retrovirus antigens in NOD mice - Bashratyan - 2017 - European Journal of Immunology - Wiley Online Library*. European Journal of Immunology, 2017. **47**(3): p. 575-584.
165. Allagnat, F., et al., *Glucose represses connexin36 in insulin-secreting cells*. 2005(118): p. 5335-5344.
166. Ashcroft F, R.P., *Electrophysiology of the Pancreatic Beta Cell*. Progress in Biophysics and Molecular Biology, 1989. **54**(2): p. 87-143.
167. Curi R, N.P., Procopio J, Lagranha C, Gorjao R, Pithon-Curi T, *Glutamine, Gene Expression, and Cell Function*. Frontiers in Bioscience, 2007. **12**: p. 344-357.

168. Newsholme, P., L. Brennan, and K. Bender, *Amino Acid Metabolism, β -Cell Function, and Diabetes*. 2006: p. S39 - S47.
169. Hoy, M., et al., *Increase in cellular glutamate levels stimulates exocytosis in pancreatic beta-cells*. FEBS Lett, 2002. **531**(2): p. 199-203.
170. Straub, S. and G. Sharp, *Glucose-Stimulated Signalling Pathways in Biphasic Insulin Secretion*. Diabetes/Metabolism Research and Reviews, 2002. **18**: p. 451-463.
171. Cravedi, P., P. Ruggenti, and G. Remuzzi, *Successes and Disappointments with Clinical Islet Transplantation*, in *Islets of Langerhans*. 2015, Dordrecht : Springer. p. 1245-1274.
172. Fotino, N., C. Fotino, and A. Pileggi, *Re-engineering Islet Cell Transplantation*. Pharmacological Research, 2015. **98**: p. 76-85.
173. Wellershaus K, D.J., Deuchars J, Theis M, Charollais A, Caille D, Gauthier B, Janssen-Bienhold U, Sonntag S, Herrera P, Meda P, Willecke K, *A New Conditional Mouse Mutant Reveals Specific Expression and Functions of Connexin 36 in Neurons and Pancreatic Beta Cells*. Experimental Cell Research, 2008: p. 997-1012.
174. Cigliola V, P.C., Pierri C, Deutsch S, Haefliger J, Fadista J, Lyssenko V, Groop L, Rueedi R, Thorel F, Herrera P, Meda P, *A Variant of GJD2, Encoding for Connexin 36, Alters the Function of Insulin Producing β -Cells*. PLoS ONE, 2016. **11**(3).